	1.0		2.8	2.5
			3.2	2.2
			3.6	
			4.0	2.0
	1.1			1.8
	1.25	1.4		1.6

MICROCOPY RESOLUTION TEST CHART
NATIONAL BUREAU OF STANDARDS 1963

②

AFWAL-TR-87-3102

E X P E R I M E N T A L   A N D   A N A L Y T I C A L
S T U D Y   O F   T W O - P H A S E   F L O W
I N   Z E R O   G R A V I T Y

Davood Abdollahian

S. Levy, Incorporated
3425 South Bascom Ave.
Campbell, California 95008

Ralph Grief
Van. P. Carey
Wang Li - Ping

University of California
Berkeley, California 94720

March 1988

DTIC
ELECTE
MAY 25 1988

S   D
H

NOTICE

When Government drawings, specifications, or other data are used for any purpose
other than in connection with a definitely related Government procurement operation,
the United States Government thereby incurs no responsibility nor any obligation
whatsoever; and the fact that the government may have formulated, furnished, or in
any way supplied the said drawings, specifications, or other data, is not to be re-
garded by implication or otherwise as in any manner licensing the holder or any
other person or corporation, or conveying any rights or permission to manufacture
use, or sell any patented invention that may in any way be related thereto.

This report has been reviewed by the Office of Public Affairs (ASD/PA) and is
releasable to the National Technical Information Service (NTIS). At NTIS, it will
be available to the general public, including foreign nations.

This technical report has been reviewed and is approved for publication.

WILLIAM L. HASKIN
Project Engineer

PAUL D. LINDQUIST
Technical Manager

FOR THE COMMANDER

RICHARD C. COLCLOUGH, Jr., Chief
Vehicle Subsystems Division
Flight Dynamics Laboratory

"If your address has changed, if you wish to be removed from our mailing list, or
if the addressee is no longer employed by your organization please notify AFWAL/FIEE,
W-PAFB, OH 45433- 6553   to help us maintain a current mailing list".

Copies of this report should not be returned unless is required by security
considerations, contractual obligations, or notice on a specific document.

REPORT DOCUMENTATION PAGE

1a. REPORT SECURITY CLASSIFICATION		1b. RESTRICTIVE MARKINGS		
UNCLASSIFIED				
2a. SECURITY CLASSIFICATION AUTHORITY		3. DISTRIBUTION/AVAILABILITY OF REPORT		
		Approved for public release: distribution is unlimited		
2b. DECLASSIFICATION/DOWNGRADING SCHEDULE				
4. PERFORMING ORGANIZATION REPORT NUMBER(S)		5. MONITORING ORGANIZATION REPORT NUMBER(S)		
SLI 8707		AFWAL-TR-87-3102		
6a NAME OF PERFORMING ORGANIZATION	6b. OFFICE SYMBOL (If applicable)	7a. NAME OF MONITORING ORGANIZATION		
S. Levy, Inc		Flight Dynamics Laboratory Air Force Wright Aeronautical Laboratories		
6c. ADDRESS (City, State, and ZIP Code)		7b. ADDRESS (City, State, and ZIP Code)		
3425 S. Bascom Ave Campbell CA 95008-7006		Flight Dynamics Laboratory (AFWAL/FIEE) Wright-Patterson AFB OH 45433-6553		
8a. NAME OF FUNDING/SPONSORING ORGANIZATION	8b. OFFICE SYMBOL (If applicable)	9. PROCUREMENT INSTRUMENT IDENTIFICATION NUMBER		
		F33615-85-C-3418		

8c. ADDRESS (City, State, and ZIP Code)	10. SOURCE OF FUNDING NUMBERS			
	PROGRAM ELEMENT NO	PROJECT NO.	TASK NO.	WORK UNIT ACCESSION NO.
	65502F	3005	30	41

11. TITLE (Include Security Classification)
Experimental and Analytical Study of Two-Phase Flow in Zero Gravity

12. PERSONAL AUTHOR(S)
Davood Abdollahian, Ralph Grief, Van P. Carey, Wang Li-Ping

13a. TYPE OF REPORT	13b. TIME COVERED	14. DATE OF REPORT (Year, Month, Day)	15. PAGE COUNT
Final	FROM Sep 85 TO Oct 87	March 1988	145

16 SUPPLEMENTARY NOTATION
This is a Small Business Innovation Research (SBIR) Program Report

17	COSATI CODES		18 SUBJECT TERMS (Continue on reverse if necessary and identify by block number)
FIELD	GROUP	SUB-GROUP	Two-Phase Flow Analysis
20	04		Boiling heat transfer
20	13		Spacecraft heat transfer

19 ABSTRACT (Continue on reverse if necessary and identify by block number)

Power requirements for future space satellites are expected to increase significantly as new capabilities for communications, data processing and surveillance are implemented. More effective and efficient thermal transport techniques will be needed for heat rejection from equipment on these satellites. Circulating two-phase fluid loops have been suggested and laboratory tested for possible application in the above areas. In comparison to a single-phase loop, the two-phase system operates at considerably smaller flow rates and maintains a tighter temperature control with higher heat transfer coefficients. However, the two-phase fluid flow regimes, pressure gradients and heat transfer coefficients must be evaluated for application in the weightless environment of an orbiting satellite.

This project was funded by the Air Force Wright Aeronautical Laboratories as a Phase II SBIR program to study two-phase flow behavior under zero gravity conditions. The overall-
(over)

20. DISTRIBUTION/AVAILABILITY OF ABSTRACT	21 ABSTRACT SECURITY CLASSIFICATION	
☒ UNCLASSIFIED/UNLIMITED ☒ SAME AS RPT ☐ DTIC USERS	UNCLASSIFIED	
22a. NAME OF RESPONSIBLE INDIVIDUAL	22b TELEPHONE (Include Area Code)	22c OFFICE SYMBOL
William L. Haskin	(513) 255-6078	AFWAL/FIEE

DD FORM 1473, 84 MAR
83 APR edition may be used until exhausted
All other editions are obsolete

SECURITY CLASSIFICATION OF THIS PAGE

UNCLASSIFIED

objectives of this study were to generate a data base for two-phase pressure drop and the void-quality relationship under simulated zero gravity conditions and to develop analytical models to predict these parameters for bubbly and annular flow.

The simulation of zero gravity two-phase flow was achieved by using two immiscible liquids with equal densities to eliminate the buoyancy component. Although this approach does not eliminate the gravity effects, it provides a representation for void distribution in the absence of gravity. Water was used as one of the working fluids and simulated the gaseous phase, while the second fluid was selected to simulate the liquid phase. The property ratios of the two liquids were in the range of liquid/gas flows. The tests were performed under steady state fully developed turbulent flow conditions, since it is believed that for most practical applications the two-phase heat transfer loops operate within the turbulent flow range. The major parameters are pressure drop and cross sectional average void fraction, and the test variables consist of total flow rate, quality, and fluid properties.

The modeling effort is limited to developing relations for the two-phase friction multiplier and void-quality relation under bubbly and annular flow conditions. The bubbly flow model is based on the assumption of local homogeneous conditions between the phases but allows for void distribution in the radial direction. Separated flow conservation equations are used, and single-phase turbulent flow eddy diffusivity relations are employed. In addition, a single particle lift force model is utilized to account for radial forces on the bubbles within the shear layer. A tentative model is proposed for bubbly flow with nucleation at the wall. This aproach uses the model developed for adiabatic flow, but the boundary condition is modified to account for the presence of voids at the wall. The annular flow model is based on the triangular approach of Hewitt. The interfacial shear and entrainment relations are empirically determined from the results of the experimental effort with equal density liquids.

It should be noted that in the present analytical effort no attempt was made to model the heat transfer characteristics of two-phase flow in zero gravity. It is believed that the mechanism of heat transfer will not be affected by the absence of gravity. However, the heat transfer rates are influenced by void distribution within the two-phase flow. The earth gravity models are generally based on flow quality and therefore cannot be applied to reduced gravity conditions. If one can incorporate the differences in void-quality relation into the earth gravity correlations, they can be used under reduced gravity conditions.

TABLE OF CONTENTS

iii

LIST OF ILLUSTRATIONS

NOMENCLATURE

a	$\dfrac{\delta}{D}$
A	Cross Sectional Area
C	Constant
d	Bubble Diameter
D	Tube Diameter
e	Entrainment Fraction
f	Friction Coefficient
F_B	Body Force
F_L	Lift Force
G	Mass Flux
L	Length
$\dot{M}$	Liquid Film Flow Rate
M_L	Lift Force Per Unit Volume
N	Number of Nucleation Sites
P	Pressure
q	Volume Flow Rate
$\dot{q}$	Heat flux
r	Radial Direction
r_c	Bubble Radius at Departure
R_o	Bubble Radius at Departure
Re	Reynolds Number
S	Distance Between Bubbles, Eq. 3.48
u	Velocity in x Direction

NOMENCLATURE (Continued)

v	Velocity in y Direction
V	Specific Volume
V'm	Constant in $\overline{V'^{+2}}$ equation
W	Mass Flow Rate
x	Axial Direction
X	Quality
X_{tt}	Martinelli Parameter
y	Lateral Direction
z	Axial Direction

Greek Letters

α	Void Fraction
ρ	Density
μ	Viscosity
ϕ_f^2	Two-Phase Friction Multiplier with Liquid Flowing Alone
ϕ_{fo}^2	Two-Phase Friction Multiplier with Liquid Flowing at Total Mass Flux
σ	Stress Component
τ	Stress Component
Ω	Angular Velocity
ϵ	Eddy Diffusivity
γ	Integral in Equation 3.28
δ	Film Thickness
α_c	Ratio of Core Area to Total Area
η	$\dfrac{y}{\delta}$
ν	Kinematic Viscosity

NOMENCLATURE (Continued)

Subscripts

L, G   Liquid and Gas

sp   Single Phase

S   Silicon

D   Dowtherm

W   Water

k   Liquid or Vapor Phase

w   wall

CHF   Critical heat Flux

i   Interfacial

c   Core

Superscripts

+   Non-dimensionalized

'   Fluctuating Component

—   Mean Value

Section 1

INTRODUCTION

The power requirements for future spacecraft and satellites are expected
to increase as they grow in sophistication and capability. Due to the
new communications, data processing, and surveillance techniques, the
near future satellites are planned to operate at power levels of five to
ten kilowatts. With the future revolutionary military and surveillance
missions, this requirement is expected to grow to 100 kilowatts, (1). In
addition, a space nuclear power system concept with approximately 100
kilowatts has been defined for such uses as planetary exploration,
directed energy capabilities, surveillance, command, control and com-
munication satellites, etc. Strategic Defense Initiative (SDI) programs
have also identified a wide range of power requirements with standby
power needs of greater than 10 kilowatts and peak power loads greater
than 10 megawatts. In this context, a large array of energy sources and
power conversion concepts (thermoelectric, thermionic, photo-voltaic,
dynamic isotope power systems, etc.) have been developed and proposed.
The present thermal control methods are based on transport of heat by
solid conductors and internal radiation, heat pipes, and single-phase
liquid and gaseous loops. The high operating power for future space
applications requires more efficient thermal transport techniques. Two-
phase loops have been suggested and laboratory tested for possible
application in the above areas, Refs. (2) and (3). In comparison to a
single-phase loop, the two-phase system operates at considerably smaller
flow rates and maintains tighter temperature control with a higher heat
transfer coefficient.   However, the two-phase fluid flow regimes,
pressure gradients, and heat transfer coefficients must be evaluated for
application in the weightless environment (zero-gravity) of an orbiting
satellite. This report addresses several aspects of expected flow con-
ditions.

1.1 BACKGROUND

Design of two-phase heat transport systems for space applications requires a knowledge of heat and mass transfer under reduced gravity conditions. Many of the issues which affect system performance in space have been identified by various investigators. These include two-phase flow regime, pressure drop, void-quality relation, and two-phase heat transfer. In some instances, the technology issues identified in these studies have a detrimental effect on system performance and also pose severe restrictions on system efficiency.

A brief look at the simplified forms of the two-phase flow governing equations will reveal the need and importance of these parameters.

Void-Quality Relationship:

Generally the void-quality relation is needed to reduce the number of dependent variables in the two-phase flow conservation equations. A *simplified form of the momentum equation in the absence of gravity is* given below:

$$- \left(\frac{dP}{dx}\right) = - \left(\frac{dP}{dx}\right)_f + G^2 \frac{d}{dx} \left[\frac{x^2 V_G}{\alpha} + \frac{(1-x)^2 V_L}{1-\alpha}\right] \tag{1.1}$$

The first term in the above equation is the friction component and the second term is the inertia or acceleration component. The flow quality, x, can usually be determined from the heat input to the system, but a void-quality relation is needed to solve for the inertia and therefore the overall pressure loss.

1-2

Two-Phase Friction Multiplier:

Friction loss for a two-phase system is generally evaluated by using the single-phase relations along with a two-phase friction multiplier. The relations for the two-phase friction multiplier at reduced gravities are therefore needed for design of the spacecraft cooling systems.

The two-phase friction pressure drop can be expressed in terms of the single-phase pressure drop as follows:

$$\left(\frac{dP}{dx}\right)_f = \left(\frac{dP}{dx}\right)_{sp} \phi_{fo}^2$$

ϕ_{fo}^2 is the two-phase friction multiplier and (dP/dx) sp is the single-phase friction pressure drop when the entire flow consists of liquid alone:

$$\left(\frac{dP}{dx}\right)_{sp} = \left[\frac{2 f G^2 V_L}{D}\right]$$

where f is the single-phase friction coefficient and D is the channel diameter.

Theoretically, the friction multiplier is a function of flow quality, system pressure, and mass flux. Therefore, gravity should not have an effect on the value of the two-phase multiplier. However, the models developed for predicting the friction multiplier are mostly empirical and it is not clear if they will be valid in the absence of gravity when the phase slip and distribution of voids are expected to be different.

Forced Convective Heat Transfer Coefficient:

Prediction of the thermal performance of a boiling/condensing two-phase cycle is to a large extent dependent on the accuracy of determining the heat transfer coefficients. The most desirable mode of operation for a boiling loop is the forced convective nucleate boiling regime where the highest heat transfer coefficient is obtained. Among the existing correlations, the most successful nucleate boiling heat transfer coefficients are based on combining a forced convective single-phase and a nucleate pool boiling heat transfer coefficient. Empirical factors are then introduced to account for the influence of these two modes of heat transfer under different system conditions. Applicability of these correlations to reduced gravity conditions should be investigated.

Two-Phase Flow Regime Map:

One of the most important criteria in two-phase flow is the transition between different flow regimes. The flow regime map and the transition criteria are needed in order to operate the system under the lowest loss conditions and to avoid flow regimes which result in instabilities (slug flow). In addition, the two-phase flow regime also dictates the mode of heat transfer which will determine the thermal performance of the system.

Current knowledge of two-phase flow and heat transfer is mainly derived from terrestrial experiments. Unlike pool boiling which has been studied extensively under reduced gravity conditions, very little work has been done on understanding and modeling two-phase flow. One of the reasons for the lack of information at microgravity is the difficulty in performing such tests. A majority of low gravity fluid mechanics and heat transfer experiments have been performed in drop towers or under simulated reduced gravity conditions. As will be discussed later, studies have been recently initiated by the Air Force, NASA, and DOE to better understand the two-phase flow behavior under reduced gravity conditions.

These include experiments which simulate reduced gravity two-phase distribution, drop tower tests, and the airplane trajectory tests.

Since the field of two-phase flow in reduced gravity is fairly new, most of the research programs have aimed at developing qualitative information mainly for confirming the existence of the phenomena. The experimental results are mainly from the ground-based tests which have very short duration. Flow development and existence of steady state conditions for such a short duration is questionable. Modeling efforts are limited to determination of the flow regime transition criteria. The pressure drop, void distribution, and heat transfer characteristics have not been addressed in the existing studies.

1.2 BRIEF REVIEW OF PREVIOUS EFFORTS

The subject of two-phase flow and heat transfer has been studied extensively due to its application in chemical and nuclear industries. It has a history of over four decades and there are numerous text books which have covered different aspects of two-phase flow. A recent book on this subject, Ref. (4), contains the majority of useful data and modeling efforts. Due to the complex nature of two-phase flow, most of the problems are treated empirically and even the mechanistic approaches are augmented by empirical factors. The empirical treatment of two-phase flow makes extrapolation to other conditions e.g., reduced gravity, impractical.

The subjects of bubble formation and pool boiling under reduced gravity conditions have been studied extensively. Most of these studies have been experimental investigations which were carried out in drop towers, (5) to (9). Some tests have been performed under simulated reduced gravity conditions which were achieved by compensating for the earth's gravity by using strong magnetic force, Refs. (10) and (11). Basically the pool boiling experiments have shown negligible change in the nucleate

boiling heat transfer coefficient and considerable decrease in critical heat flux with decreasing gravities. Bubble formation and departure has been studied by resolution of gravity into components in a tilted (or horizontal) container, Ref. (12) and (13). The theory of vanishing nucleate boiling in the absence of gravity, Ref. (14), has yet to be proven in future experiments.

Unlike the areas of pool boiling, critical heat flux, and bubble growth mechanism, very little work has been done on understanding and modeling two-phase flow at reduced gravities. A review article by Siegel, Ref. (15), has covered the data available from the reduced gravity experiments prior to 1967. A summary of pre-1974 literature can also be found in Ref. (16). The most recent review of the experimental efforts in reduced gravity two-phase flow can be found in Ref.(17).

Results of an experimental study on pressure and temperature changes in forced convective boiling at zero gravity have been reported in Ref. (18). It has been shown that the system pressure and temperature increase and boiling oscillations damp out in zero gravity. Low heat flux convective boiling at zero gravity using a drop tower facility was studied in Ref. (19) and, mainly, the bubble diameter was determined. Other two-phase flow studies have reviewed the concept of two-phase flow application for spacecraft, (20) and (21). Since these efforts have basically studied the qualitative nature of two-phase flow at microgravity, it is anticipated that the most useful information will be obtained from the programs which are presently in progress. These efforts, which have been initiated by the Air Force, NASA and DOE, are expected to be completed in late 1988. A brief summary of the objectives of the major efforts in progress is given below.

AETA/Dartmouth/University of New Hampshire study, Ref. (22):

This is an experimental and analytical study of two-phase flow regime transitions under reduced gravity conditions. The outcome is expected to consist of experimental data for simulated reduced gravity conditions (equal density liquids at earth gravity) and a model for two-phase flow regime transition.

NASA & DOE Supported University Activities:

NASA and DOE have contracts with three universities to perform a series of tests with facilities ranging from drop towers to Spacelab. These efforts are:

a) University of Houston Study, Ref. (23):

This is an experimental and analytical study of two-phase flow regime transition, interfacial instabilities, and slug flow modeling. The tests are performed with air-water in the NASA drop tower facility and aboard the NASA Learjet.

b) University of Michigan Study:

This university has a program to study pool boiling (with the university drop tower) and convective boiling (aboard NASA airplane). This study will mostly concentrate on low quality regions including incipience of boiling. Tests are planned for flat surfaces and eventually inside tubes.

c) Texas A&M University:

This is an experimental program to study forced condensation and heat transfer rates. The tests are carried out in the NASA KC-135 aircraft.

Renewed interest in the space-based nuclear reactor power systems has initiated new areas in the field of reactor thermal-hydraulics and

1-7

therefore two-phase flow and heat transfer. National laboratories and private industry have started to evaluate the two-phase constitutive models which are needed in the computer codes used for steady and transient analysis of the reactors, (24) (25) (26). The Battelle study, Ref. (24), includes an experimental study of forced convective boiling which was carried out in the NASA drop tube and aboard the NASA KC-135. A total of 39 aircraft tests were completed in 1986 and the data report will be available in late 1987. In addition, the possibility of using the existing computer codes for analysis of the reactor performance under reduced gravity conditions was investigated.

A series of tests with convective boiling/condensing water, and under adiabatic conditions with nitrogen/water at atmospheric conditions were supported jointly by the Air Force Wright Aeronautical Laboratories and the Johnson Space Center aboard the NASA KC-135, Ref. (27). In addition to flow visualization which provided information on flow regime transitions, these tests provided pressure drop data for low flow rates.

NASA JSC has the responsibility for thermal management of space station equipment external to the pressurized modules. Under this program, several prototype development activities for the Thermal Bus System (TBS) were initiated. The Boeing TBS concept uses a rotary fluid management device for separation of liquid from the two-phase mixture exiting from the evaporators. The Grumman concept controls the flow into evaporators to obtain a high quality vapor at the exit. In order to gain a better understanding of the two-phase flow phenomena to ensure adequate and efficient hardware design, several ground-based studies including the university activities mentioned above and a KC-135 testing of a two-phase loop developed by Sundstrand were initiated by NASA. This loop will be used for identification of the two-phase flow regimes and measurement of pressure drops.

Design of a facility for performing a series of two-phase flow experiments aboard the shuttle vehicle has been under way for over eight

1-8

years, Refs. (28) (29). A separate study for preliminary design of a similar two-phase experiment has been initiated by NASA JSC, (30).

1.3 OBJECTIVES AND SCOPE OF EFFORT

This project was funded by the Air Force Wright Aeronautical Laboratories as a Phase II SBIR program to study two-phase flow behavior under zero gravity conditions. The overall objectives of this study were to generate a data base for two-phase pressure drop and void-quality relation under simulated zero gravity conditions and to develop analytical models to predict these parameters for bubbly and annular flow.

The simulation of zero gravity two-phase flow was achieved by using two immiscible liquids with equal densities to eliminate the buoyancy component. Although this approach does not eliminate the gravity effects, it does provide a representation for void distribution in the absence of gravity. Water was used as one of the working fluids and simulated the gaseous phase, while the second fluid was selected to simulate the liquid phase. The property ratios of the two liquids were in the range of the two-phase liquid/gas flows. The tests were performed under steady state fully developed turbulent flow conditions, since it is believed that for most practical applications the two-phase heat transfer loops operate within the turbulent flow range. The major parameters are pressure drop and cross sectional average void fraction, and the test variables consist of total flow rate, quality, and fluid properties.

The modeling effort is limited to developing relations for the two-phase friction multiplier and void-quality relation under bubbly and annular flow conditions. The bubbly flow model is based on the assumption of local homogeneous conditions between the phases but allows for void distribution in the radial direction. Separated flow conservation equations are used, and single-phase turbulent flow eddy diffusivity relations are employed. In addition, a single particle lift force model

1-9

is utilized to account for radial forces on the bubbles within the shear layer. A tentative model is proposed for bubbly flow with nucleation at the wall. This approach uses the model developed for adiabatic flow but the boundary condition is modified to account for the presence of voids at the wall. The annular flow model is based on the triangular approach of Hewitt, Ref. (31). The interfacial shear and entrainment relations are empirically determined from the results of the experimental effort with equal density liquids.

It should be noted that in the present analytical effort no attempt was made to model the heat transfer characteristics of two-phase flow in zero gravity. It is believed that the mechanism of heat transfer will not be affected by the absence of gravity. However, the heat transfer rates are influenced by void distribution within the two-phase flow. The earth gravity models are generally based on flow quality and therefore cannot be applied to reduced gravity conditions. If one can incorporate the differences in void-quality relation into the earth gravity correlations, they can be used under reduced gravity conditions.

Section 2

EXPERIMENTAL INVESTIGATIONS

The experimental program was aimed at investigating the two-phase flow behavior under zero gravity conditions. The tests were planned to simulate the phase distribution and two-phase pressure drop characteristics of gas-liquid flow in the absence of gravity. The major objective of this program was to generate a data base for the two-phase friction multiplier and void-quality relation under simulated bubbly and annular flow patterns. This was accomplished with a flow of two immiscible liquids of nearly equal densities. Although, equal density liquid-liquid flow will not eliminate the gravity effect, it should, however, be a close representation of the phase distribution. Proper scaling would also require a simulation of the viscosity and interfacial tension ratios.

The major test parameters were the void fraction (or hold-up ratio) and the pressure drop along the test section. The test variables included the total mass flow rate, relative phase content (quality), and the fluid properties.

2.1 SELECTION OF LIQUIDS

Distilled water was chosen to be one of the test fluids. Because of the low viscosity of water compared with other liquids, it was convenient to have water simulate the gas in a zero-gravity gas-liquid flow simulation. For the second fluid to properly simulate a liquid relative to water, a suitable viscosity for the fluid must be considered. The distilled water used was of density 0.997 g/ml and kinematic viscosity 0.894 cSt at atmospheric pressure and room temperature (25°C). The ratio of kinematic viscosity for water and air at the above-mentioned conditions is about 15. Based on this information, Dimethyl silicone fluid

L-45, Union Carbide Corporation and Dowtherm LF heat transfer fluid (DT-LF) were chosen to simulate the liquid respectively in different tests. The properties of the test fluids are listed below:

Fluid Properties at Room Temperature

	VISCOSITY cSt	SPECIFIC GRAVITY	SURFACE TENSION dyne/cm	RESISTIVITY ohm-cm
WATER	0.894	1.0	71.95(water-air)	2×10^4
L-45	10.0	0.938	32.31(water-L-45)	1×10^{14}
DT-LF	4.323	1.038	48.57(water-DT-LF)	6×10^{11}

Since turbulent forces dominated the buoyancy effects in this test, specific gravity values of 0.938 and 1.038 were considered to be sufficiently close to one for simulating the two-phase flow character under zero gravity condition.

2.2 TEST LOOP AND INSTRUMENTATION

The experimental apparatus used to simulate horizontal gas-liquid pipe flow under zero gravity conditions is shown in Figure 2.1

Distilled water (white arrow) and simulated liquid (L-45 or DT-LF) (black arrow) were pumped from separate storage tanks into the mixing section. Different mixing sections were designed to achieve the desired flow regimes. The flow of the two fluids (black-and-white arrow) simulating two-phase flow was produced in the mixing section and flowed into a twelve-foot-long horizontal test section. Pressure drop and void fraction measurement units were installed in this section. After the test section, the two-phase mixture flowed into a receiving tank where it was separated.
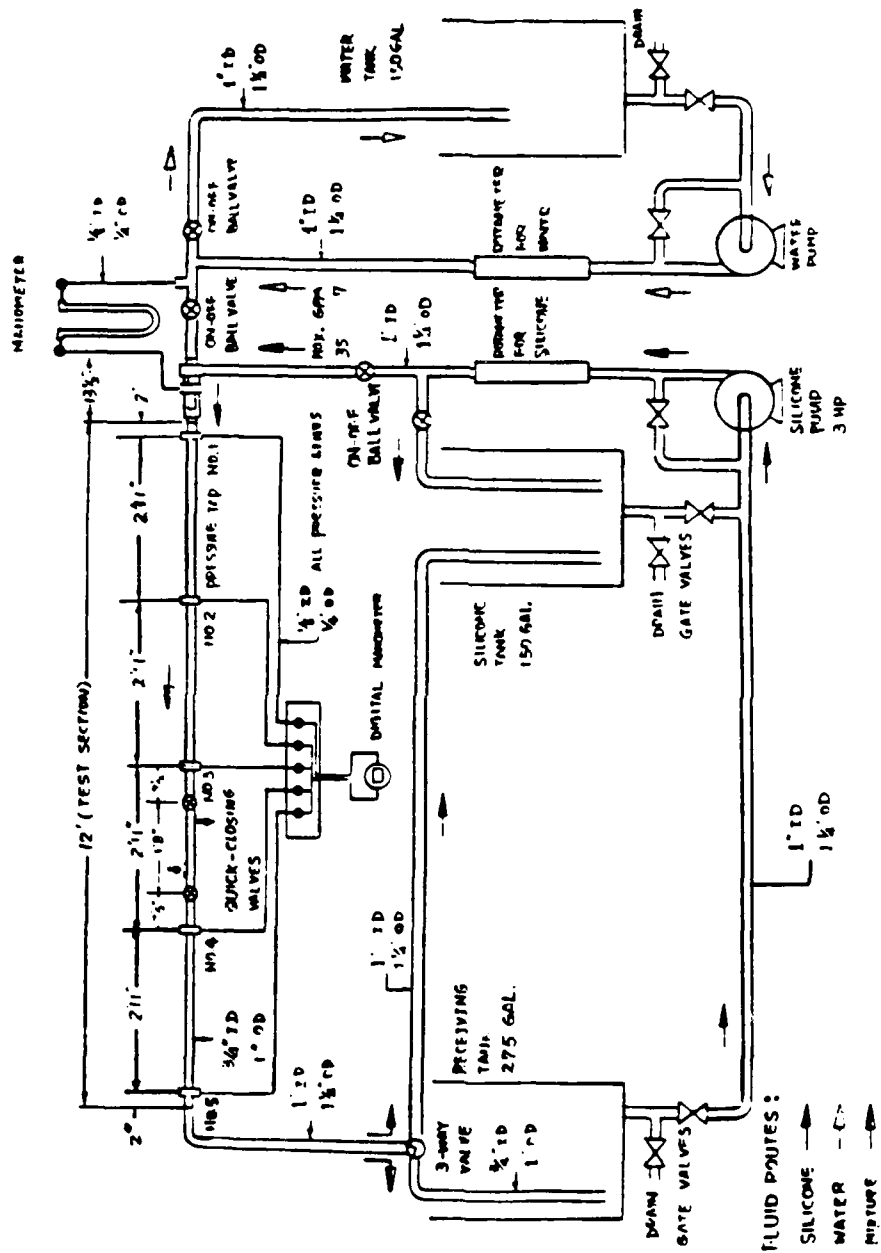
Figure 2.1 - Schematic of the Test Loop

2.2.1 Tanks

The storage tanks for the distilled water and the simulated liquid are cylindrical graduated HDPE tanks of volume 150 gallons. All tanks were from Cole-Parmer Instrument Company.

2.2.2 Pumps

The water pump is a PRICE 1.5 hp centrifugal plastic impeller, bronze body pump (PRICE model HP 75-100) with a maximum capacity of 18 gpm at 120 feet head.

2.2.3 Rotameters

The two rotameters are Fischer and Porter glass tube indicating rotameters. The rotameter used for simulated liquid had a viscosity limit of 18.5 cp and a maximum flow rate of 31.6 gpm. The rotameter used for water had a maximum capacity of 17 gpm at 70°F.

2.2.4 Mixing Sections

In order to simulate both bubbly flow and annular flow, two different sections were made to meet the purpose.

The bubbly flow mixing section is shown in Figure 2.2. Distilled water was introduced through 120 1/64 inch diameter holes on a perforated tube which was centrally located in the interior of simulated liquid flow. The distilled water emerging from the injection holes was carried away from the tube wall by the simulated liquid flow, and water bubbles were formed.

The annular flow mixing section is shown in Figure 2.3. Simulated liquid was pumped into an annular area of annulus thickness 0.075 inch to form a simulated liquid film on the inner wall of the test section. The distilled water (simulating the gas) was introduced into the core, and

2-4

Figure 2.2 – Bubbly Flow Mixing Section
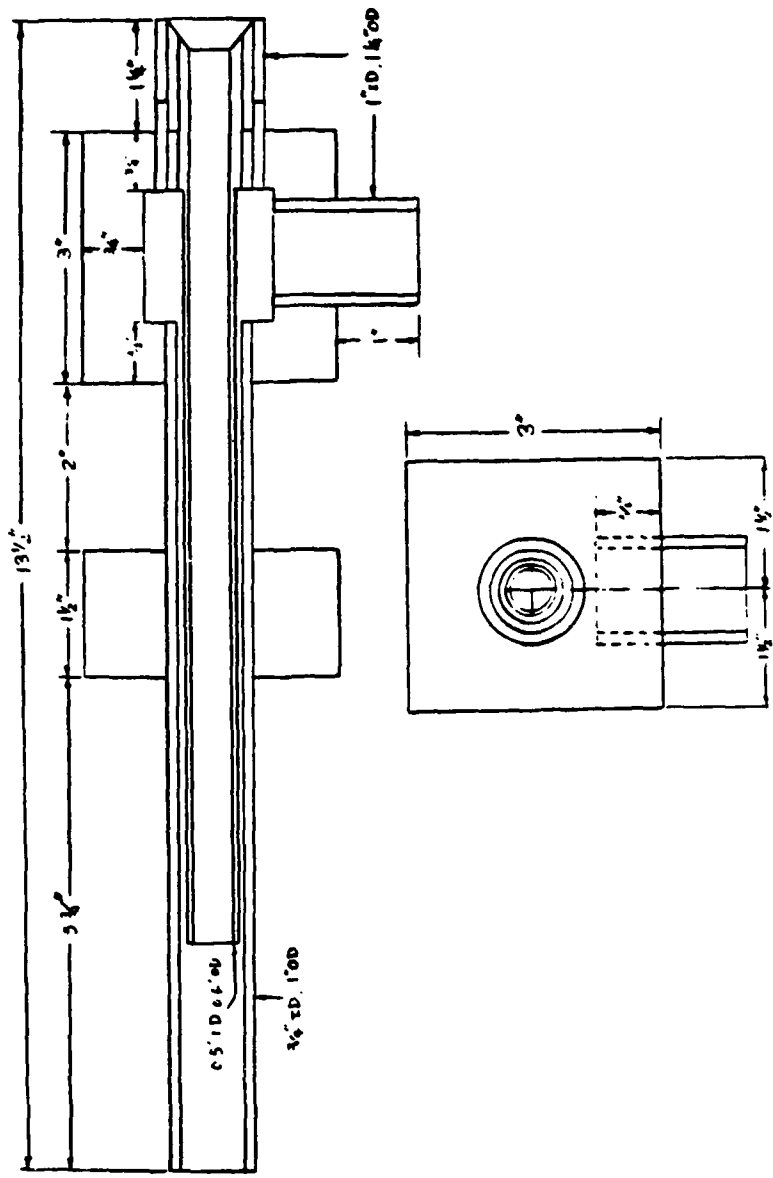
Figure 2.3 - Annular Flow Mixing Section

the result was an annular type flow, i.e. simulated liquid on the wall and gas (simulated by water) in the core. This test section was designed to make the film thickness interchangeable. The mixing section for L-45 water flow was made of plexiglass, the one for DT-LF water flow was made of pvc pipes.

2.2.5 Test Section

The test section was a twelve-foot-long, one inch outer diameter, 3/4 inch inner diameter round tube of which the axis was in the horizontal direction. For L-45 water flow, clear plexiglass tube was used, for DT-LF water flow, pc pipe was used. Pressure drop and void fraction measurements were carried out on this section. The test section was checked to be hydrodynamically smooth by a single-phase friction factor measurement.

2.2.6 Pressure Drop Measurement Unit

The pressure drop measurement unit consists of:

    (a) five pressure taps
    (b) control panel
    (c) two pressure transducers
    (d) digital transducer indicator

Five 2x2x1 inch plexiglass blocks were equally spaced along the test section to provide for the pressure taps.

These were spaced at a distance two feet and nine inches between two neighboring taps. 1/8 inch diameter holes were drilled through the wall of the test section and the plexiglass blocks to record the pressure. The five pressure taps were connected to five globe valves on the control panel to control the measurements of the pressure drops which were measured between pressure tap number one and the other four taps. The configuration of the pressure taps is shown in Figure 2.4. The circuits of the control panel are shown in Figure 2.5.

2-7

PRESSURE TAP

1"

½"D

¼"

¹⁄₁₆"D drill

FRONT VIEW

1"

¼"

1"

1"

1" D. drill

2"

TOP VIEW

½"

1"

¾"D

SIDE VIEW

¾"D
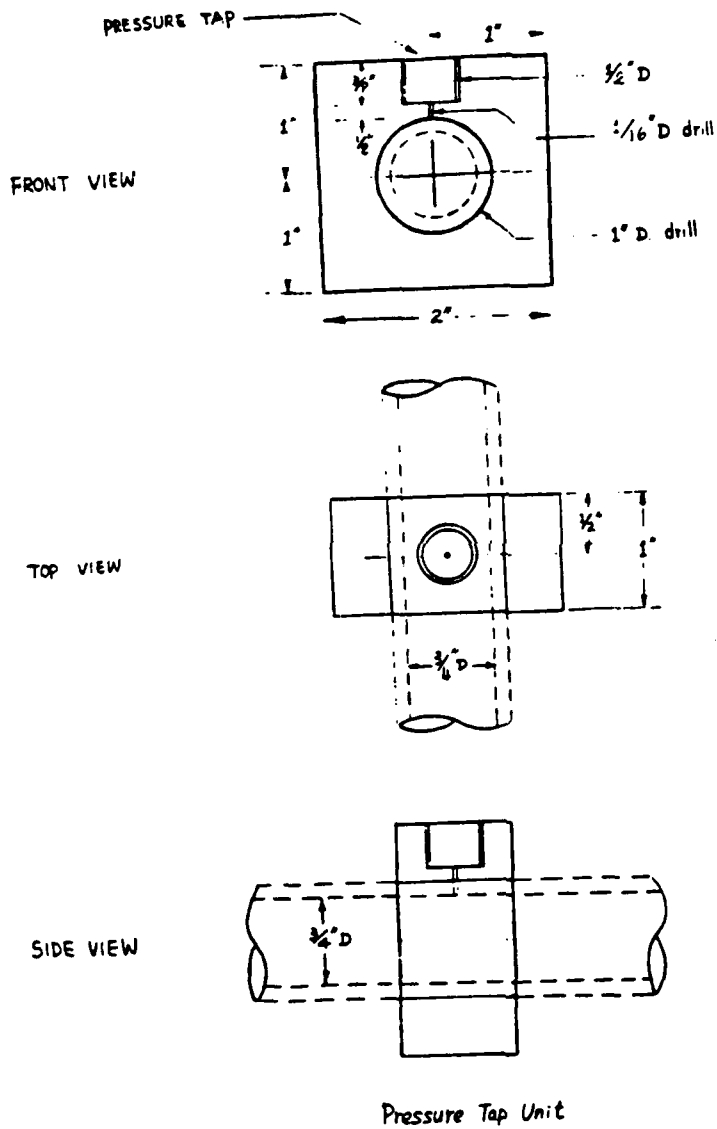
Pressure Tap Unit

Figure 2.4 - Pressure Tap Configuration

2-8
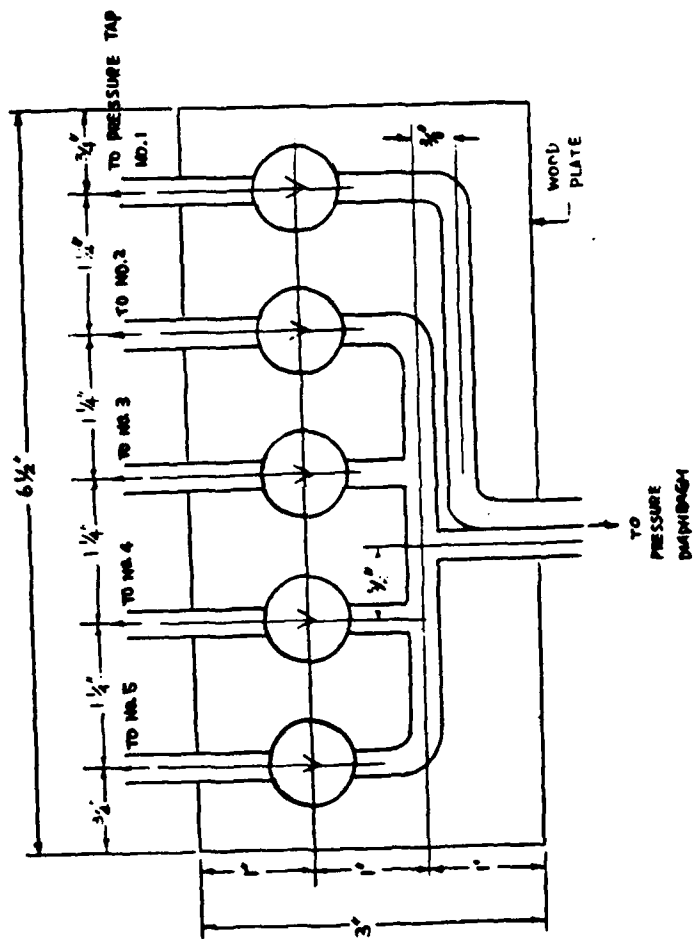
Figure 2.5 - Pressure Sensing Unit

Two Validyne DP15 variable reluctance differential pressure transducers were used to measure the pressure difference between two pressure taps. The two transducers were equipped with appropriate diaphrams for maximum pressure ranges from zero to 0.8 psid and from zero to 8.0 psid, respectively. The readings of the measured results were obtained from a Validyne model CD 223 dual channel digital transducer. A switch allowed toggling between the readings from the two transducers.

2.2.7 Void Fraction Measurement Unit

The void fraction (hold-up ratio) measurement unit consists of:

(a) two quick-closing valves and actuators

(b) two actuation gas tanks

(c) one nitrogen supply tank

(d) impedance probe

Two Worcester Controls Series 59, one inch full port ball valves with brass body and teflon seal are spaced a distance of twenty inches between pressure taps number three and number four for trapping the two-phase mixture between them. The volume of the fluid trapped by the valve was 150 ml. The two valves were actuated simultaneously by two Kinetrol model 05 vane type double acting air actuators with closing time less than one second. The two actuators were supplied with nitrogen by the two actuation gas tanks which were charged with a high pressure nitrogen supply tank. The trapped mixture could be drained out through a half-inch drain by high pressure nitrogen for the void fraction measurement.

An Auburn International Capacitance gauge model 1090 was used to provide an alternative determination of the void fraction by measuring the variation of the capacitance of the flow. The detailed working principles of this capacitance probe are given in the Appendix.

2-10

2.3 TEST MATRIX

The two-phase flow condition in the test was specified in terms of the total Reynolds number (Ret, based on simulated liquid properties) and the mean phase content or mass quality (x, water mass flow rate divided by the total mass flow rate). The selected total Reynolds numbers and mass qualities for L-45/water flow and DT-LF/water flow with bubbly and annular flow mixing sections are listed below:

Bubbly Flow Mixing Section

L-45/Water Flow

Ret	Min(x)	Max(x)	# of data points
5,500	0.13	0.80	13
7,900	0.08	0.68	20
8,800	0.11	0.51	7
10,200	0.07	0.45	5
11,600	0.11	0.37	5

DT-LF/Water Flow

Ret	Min(x)	Max(x)	# of data points
9,000	0.17	0.45	5
15,900	0.09	0.41	5
18,000	0.08	0.36	5

Annular Flow Mixing Section

L-45/Water Flow

Annulus Thickness = 0.191 cm

Ret	Min(x)	Max(x)	# of data points
6,900	0.39	0.84	6
7,900	0.38	0.74	5
8,900	0.40	0.66	5

Annulus Thickness = 0.095 cm

Ret	Min(x)	Max(x)	# of data points
5,500	0.54	0.79	5

2.4 TEST PROCEDURE

Before the test, the two actuation gas tanks in the void fraction measurement system were charged with nitrogen to sixty psig for later use. The impedance probe was calibrated by running single-phase distilled water and simulated liquid respectively through it to set the zero value (when simulated liquid was in the probe) and the full scale value (when measuring only the distilled water).

For every given total mass flow rate, the simulation started with running simulated liquid through the whole test section to build up the "liquid phase" matrix. Distilled water was then introduced into the simulated liquid flow through the mixing section to produce the desired flow pattern. The proper mass quality was obtained by adjusting the control valves for the two fluids. The pressure drops between the first pressure tap and the other four taps were measured with the pressure transducer system discussed in Section 2.2.6. The measurement of the local void fraction between the third and fourth pressure taps could be carried out

in two ways. One was by the impedance probe described in 2.2.7, and the other method was to measure the void fraction directly by removing some of the mixture from the test section. To accomplish this, the two pumps were shut off to stop the flow of the two fluids and right after this, the solenoids on the quick-closing valves were activated to close the valves. This contained the water-simulated liquid mixture between the two valves. This also terminated the test and the isolated mixture was drained for the void fraction measurement.

To completely drain the fluid between the quick-closing valves into a graduated cylinder, the drain was open and nitrogen of forty psig was introduced into the isolated section to drain the fluid into a graduated cylinder.

After the mixture sample had been drained, the system was ready for another test. The temperature of the flow was determined by measuring the temperature of the mixture in the receiving tank after the pumps had been shut off.

In order to separate the simulated liquid from the distilled water in the graduated cylinders and the receiving tank, three to four days were needed for the two liquids to be separated by gravity. After the separation had been accomplished, the distilled water was drained and discarded. The simulated liquid was pumped back through the bypass line into its storage tank for future use.

2.5 DATA REDUCTION

The test results are presented in the form of two-phase frictional multiplier (ϕ_f^2), based on the liquid phase, namely L-45 or DT-LF, and void fraction (α) as functions of Martinelli parameter (X) respectively, to describe the relations between pressure losses and flow conditions.

In order to relate these two-phase variables to the measured quantities, the following calculations were performed:

------ Two-phase Variables ------

x   :   mass quality

ϕ_f^2: two-phase frictional multiplier

X_{tt}: Martinelli parameter

------ Measured Quantities ------

ql :   simulated liquid flow rate (gpm)

qw :   distilled water flow rate (gpm)

p2,p3,p4,p5 : pressure drops between pressure tap

    number 1 and pressure taps number 2,3,4,5 (psi)

-------- Fluid Properties---------

ρ_W = 0.997 g/cm^3 Density of Water

ρ_S = 0.935 g/cm^3 Density of L-45

ρ_D = 1.035 g/cm^3 Density of DT-LF

μ_W = 0.891 cPs Viscosity of Water

μ_S = 93.50 cPs Viscosity of L-45

μ_D = 44.75 cPs Viscosity of DT-LF

2.5.1 Relation Between x and ql and q_w

Definition

$$x \equiv \frac{\text{gas mass flow rate}}{\text{total mass flow rate}} = \frac{W_w}{W}$$

Since

$$W_w = \rho_w q_w$$

$$W = \rho_w q_w + \rho_\ell q_\ell$$

Thus

$$x = \frac{\rho_w q_w}{\rho_w q_w + \rho_\ell q_\ell}$$

$$= \frac{1}{1 + \frac{\rho_\ell}{\rho_w} \frac{q_\ell}{q_w}}$$

When L-45 is used

$$x = \frac{1}{1 + 0.9378 \frac{q_S}{q_w}}$$

When DT-LF is used

$$x = \frac{1}{1 + 1.038 \frac{q_D}{q_w}}$$

2.5.2 Relation Between ϕ_f^2 and Measured Quantities

Definition

$$\phi_f^2 \equiv \frac{(\frac{dP}{dz})_F}{(\frac{dP}{dz})_f}$$

where

$(\frac{dP}{dz})_F$: two-phase frictional pressure gradient

$(\frac{dP}{dz})_f$: frictional pressure gradient for liquid

phase

$$- (\frac{dP}{dz})_F = \frac{\text{pressure drop between taps}}{\text{distance between taps}} = \frac{\Delta P}{L}$$

In order to minimize the entrance effect between pressure taps number 1 and 2 and the disturbance by the capacitance probe between pressure taps number 3 and 4, P was chosen as $P = (P3 - P2) + (P5 - P4)$, and L was taken to be twice the distance between the neighboring pressure taps, which was 66 inches.

Therefore

$$- (\frac{dP}{dz})_F = \frac{P3 + P5 - P2 - P4}{66} \quad \text{(psi/in.)}$$

The single-phase frictional pressure gradient was written in terms of friction factor as:

$$- (\frac{dP}{dz})_f = \frac{2}{D} f_\ell \rho_\ell u_\ell^2$$

where

D = the diameter of the pipe (1.905 cm)

f_ℓ = the single-phase friction factor of the simulated liquid

u_ℓ = the mean velocity of the simulated liquid when it flows alone in the pipe

By the relation

$$u_\ell = \frac{q_\ell}{A} = \frac{4q_\ell}{\pi D^2}$$

we have

$$-\left(\frac{dP}{dz}\right)_f = \frac{32}{\pi D^5} f_\ell \rho_\ell q_\ell^2$$

With

$\quad$ 1 gpm = 63.09 cm^3/sec

$\quad$ D $\quad\quad$ = 1.905 cm

$\quad$ 1 psi = 68947.6 dyne/cm^2

we obtain

$$\phi_f^2 = 0.7995 \frac{1}{f_\ell} \frac{P3 + P5 - P2 - P4}{\rho_\ell q_\ell^2}$$

For L-45-water flow

$$\phi_f^2 = 0.855 \frac{1}{f_s} \frac{P3 + P5 - P2 - P4}{q_s^2}$$

For DT-LF-water flow

$$\phi_f^2 = 0.772 \frac{1}{f_D} \frac{P3 + P5 - P2 - P4}{q_D^2}$$

2.5.3 Relation Between X_{tt} and Measured Quantities

Definition

$$X_{tt}^2 \equiv \frac{\left(\frac{dP}{dz}\right)_f}{\left(\frac{dP}{dz}\right)_g}$$

Where

$\left(\frac{dP}{dz}\right)_g$ = frictional pressure gradient for gas phase alone

$$-\left(\frac{dP}{dz}\right)_f = \frac{2}{D} f_\ell \rho_\ell u_\ell^2$$

With

$$u_\ell = \frac{q_\ell}{A} = \frac{4q_\ell}{\pi D^2}$$

$$-\left(\frac{dP}{dz}\right)_f = \frac{32}{\pi D^5} f_\ell \rho_\ell q_\ell^2$$

Similarly

$$-\left(\frac{dP}{dz}\right)_g = \frac{32}{\pi D^5} f_w \rho_w q_w^2$$

where f_w is the single-phase friction factor for water

$$X_{tt}^2 = \frac{\left(\frac{dP}{dz}\right)_f}{\left(\frac{dP}{dz}\right)_g} = \left(\frac{\rho_\ell}{\rho_w}\right) \left(\frac{f_\ell}{f_w}\right) \left(\frac{q_\ell}{q_w}\right)$$

When L-45 is used:

$$X_{tt} = 0.968 \sqrt{\frac{f_s}{f_w} \cdot \frac{q_s}{q_w}}$$

When DT-LF is used:

$$X_{tt} = 1.019 \sqrt{\frac{f_D}{f_w} \frac{q_D}{q_w}}$$

2.5.4 Calculation of Single-Phase Friction Factors, f_ℓ, f_w

The single-phase friction factor for pipe flow is usually written as a function of Reynolds number Re, defined as $Re = \rho u D / \mu$, for both laminar and fully developed turbulent flow. Because the range of the Reynolds numbers for simulated liquid and distilled water covers the transition region (for smooth pipe $2,000 < Re < 8,000$), and there is no single relation between friction factor and Reynolds number suitable to be used for the calculation of f, the experimental results (Figure 2.6) were used for this Reynolds number range. The experimental data were divided into five sections: $Re < 2,000$, $2,000 < Re < 4,000$, $4,000 < Re < 6,800$, $6,800 < Re < 8,000$, and $8,000 < Re$. The results in the middle three sections, which covered the laminar-turbulent transition region, were approximated by cubic polynomials obtained by the difference table method. The results are given as:

2-19
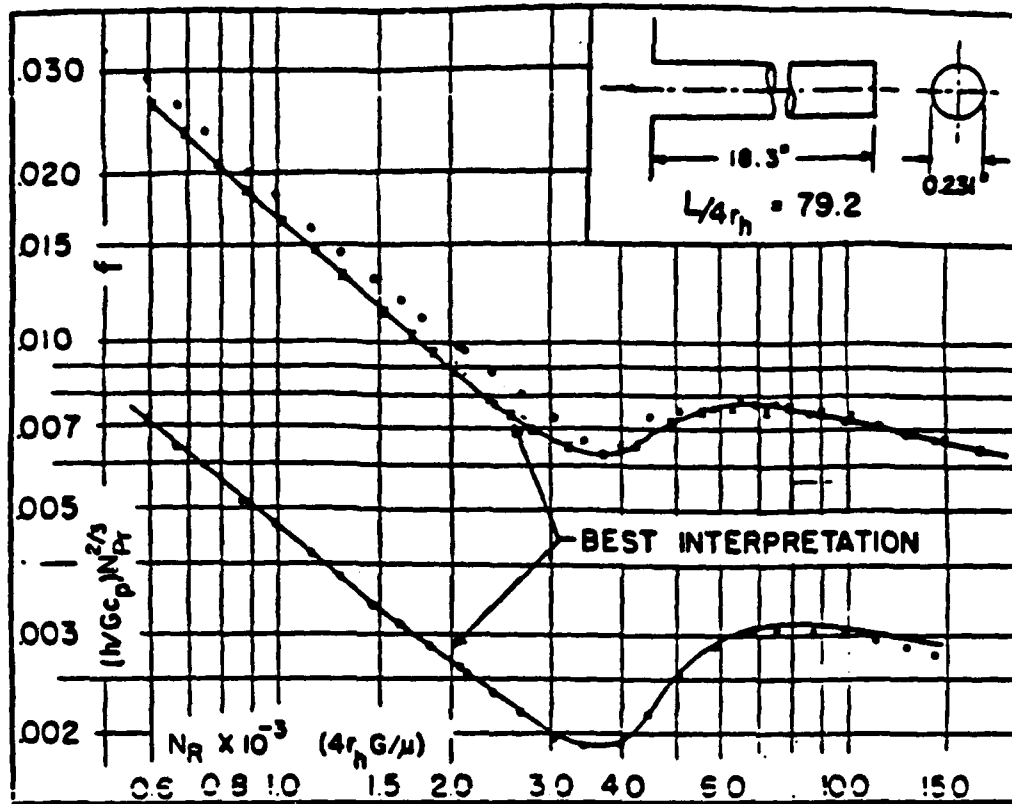
Figure 2.6 - Friction Factor for Pipe Flow in Laminar -
Turbulent Transition Region, from Compact
Heat Exchangers, W. L. Kays and A. L. London
McGraw-Hill.

Re < 2,000:

$$f = \frac{16}{Re}$$

2,000 < Re < 4,000:

$$X = \frac{Re}{1,000}$$

$$X2 = X-2$$

$$X3 = X-2.5$$

$$f = 10^{-5} \times (902-304(X2) + 148(X2)(X3) - 34.35(X2)(X3)(X-3))$$

4,000 < Re < 6,800:

$$X = \frac{Re}{1,000}$$

$$X4 = X-4$$

$$X5 = X-5$$

$$X6 = X-6$$

$$f = 10^{-5} (635 + 90(X4) - 22.5(X4)(X5) + 2.083(X4)(X5)(X6))$$

6,800 < Re < 8,000:

$$X = \frac{Re}{1,000}$$

$$X6 = X-6.8$$

$$X7 = X-7$$

$$X8 = X-7.5$$

$$f = 10^{-5} (782 + 40(X6) - 100(X6)(X7) + 83.33(X6)X7)X8))$$

8,000 < Re:

$$f = 0.05858 \times Re^{-0.2258}$$

To relate the single-phase Reynolds numbers of the test fluids to the measured quantities, start with the definition

$$Re = \frac{\rho u D}{\mu}$$

Since

$$q = uA = \frac{\pi}{4} D^2 u$$

Thus

$$Re = \frac{4\rho q}{\pi \mu D}$$

With

$$1 \text{ gpm} = 63.09 \text{ cm}^3/\text{sec}$$
$$D = 0.75 \text{ in.} = 1.905 \text{ cm}$$

We have for water flow

$$Re_w = 4718.35 \, q_w$$

For L-45 flow

$$Re_s = 421.67 \, q_s$$

For DT-LF flow

$$Re_D = 975.44 \, q_D$$

2.6 TEST RESULTS

2.6.1 Two-Phase Multiplier

The two-phase multipliers for different flow conditions are shown in the form of two-phase multiplier versus Martinelli's parameter in Figures 2.7 through 2.23 and are summarized in Table 2.1

A correlation for the two-phase multiplier as a function of Martinelli's parameter based on all the experimental data (Figure 2.23) was proposed as follows:

$$\phi_f = \sqrt{1 + \frac{2.6}{X_{tt}} + \frac{0.1}{X_{tt}^2}} \tag{2.1}$$

This relation is plotted as solid curves on the data figures. For comparison, Martinelli's correlation for air-water flow (33):

$$\phi_f = \sqrt{1 + \frac{20}{X_{tt}} + \frac{1}{X_{tt}^2}} \tag{2.2}$$

is also presented on the figures as dashed-dotted curves.

2.6.2 Void Fraction

The measured void fractions are plotted versus Martinelli's parameter for different flow conditions in Figures 2.24 to 2.36 and are summarized in Table 2.2. The recommended correlation for void fraction as a function of inverse Martinelli's parameter based on all the experimental data (Figure 2.36) is obtained as:

2-23

$$\alpha = \left(1 + \left(\frac{1}{X_{tt}}\right)^{-1.45}\right)^{-0.8} \tag{2.3}$$

and is plotted on the figures in solid curves. Martinelli's correlation for void fraction based on air-water flow ([33]) is written as:

$$\alpha = \left(1 + \left(\frac{1}{X_{tt}}\right)^{-0.8}\right)^{-0.378} \tag{2.4}$$

which is shown as dashed-dotted curves on the figures.

Table 2.1

FLOW CONDITIONS FOR TWO-PHASE MULTIPLIER FIGURES

Figure	Ret	Test Fluids	Mixing Section
2.7	All	L-45-water	Bubbly and Annular
2.8	All	L-45-water	Bubbly
2.9	All	L-45-water	Annular
2.10	5,500	L-45-water	Bubbly
2.11	7,900	L-45-water	Bubbly
2.12	8,800	L-45-water	Bubbly
2.13	10,200	L-45-water	Bubbly
2.14	11,600	L-45-water	Bubbly
2.15	6,900	L-45-water	Annular
2.16	7,900	L-45-water	Annular
2.17	8,900	L-45-water	Annular
2.18	5,500	L-45-water	Annular
2.19	All	DT-LF-water	Bubbly
2.20	9,000	DT-LF-water	Bubbly
2.21	15,900	DT-LF-water	Bubbly
2.22	18,000	DT-LF-water	Bubbly
2.23		All the data points	

Table 2.2

FLOW CONDITIONS FOR VOID FRACTION FIGURES

Figure	Ret	Test Fluids	Mixing Section
2.24	All	L-45-water	Bubbly and Annular
2.25	All	L-45-water	Bubbly
2.26	All	L-45-water	Annular
2.27	5,500	L-45-water	Bubbly
2.28	7,900	L-45-water	Bubbly
2.29	8,800	L-45-water	Bubbly
2.30	11,600	L-45-water	Bubbly
2.31	6,900	L-45-water	Annular
2.32	All	DT-LF-water	Bubbly
2.33	9,000	DT-LF-water	Bubbly
2.34	15,900	DT-LF-water	Bubbly
2.35	18,000	DT-LF-water	Bubbly
2.36		All the data points	

Figure 2.7   Two-Phase Friction Multiplier Versus Inverse Martinelli Parameter
for L-45/Water Flow with Bubbly and Annular Flow Mixing Sections
and Various Total Reynolds Numbers.
The Solid Curve corresponds to Equation 2.1 and the Dashed-Dotted
Curve to Equation 2.2.

Figure 2.8   Two-Phase Friction Multiplier Versus Inverse Martinelli Parameter for L-45/Water Flow with Bubbly Mixing Section for Various Total Reynolds Numbers.
The Solid Curve corresponds to Equation 2.1 and the Dashed-Dotted Curve to Equation 2.2.

2-28

Figure 2.9 Two-Phase Friction Multiplier Versus Inverse Martinelli Parameter for L-45/Water Flow with Annular Flow Mixing Section for Various Total Reynolds Numbers. The Solid Curve corresponds to Equation 2.1 and the Dashed-Dotted Curve to Equation 2.2.

Figure 2.10 Two-Phase Friction Multiplier Versus Inverse Martinelli Parameter for L-45/Water Flow with Bubbly Mixing Section for Total Reynolds Number of Re = 5500.
The Solid Curve corresponds to Equation 2.1 and the Dashed-Dotted Curve to Equation 2.2.

2-30

Figure 2.11 Two-Phase Friction Multiplier Versus Inverse Martinelli Para for L-45/Water Flow with Bubbly Mixing Section for Total Rey....... Number of Re = 7900.
The Solid Curve corresponds to Equation 2.1 and the Dashed-Dotted Curve to Equation 2.2.

Figure 2.12 Two-Phase Friction Multiplier Versus Inverse Martinelli Parameter for L-45/Water Flow with Bubbly Mixing Section for Total Reynolds Number of Re = 8800. The Solid Curve corresponds to Equation 2.1 and the Dashed-Dotted Curve to Equation 2.2.

Figure 2.13 Two-Phase Friction Multiplier Versus Inverse Martinelli Parameter for L-45/Water Flow with Bubbly Mixing Section for Total Reynolds Number of Re = 10200. The Solid Curve corresponds to Equation 2.1 and the Dashed-Dotted Curve to Equation 2.2.

Figure 2.14 Two-Phase Friction Multiplier Versus Inverse Martinelli Parameter
for L-45/Water Flow with Bubbly Mixing Section for Total Reynolds
Number of Re = 11600.
The Solid Curve corresponds to Equation 2.1 and the Dashed-Dotted
Curve to Equation 2.2.
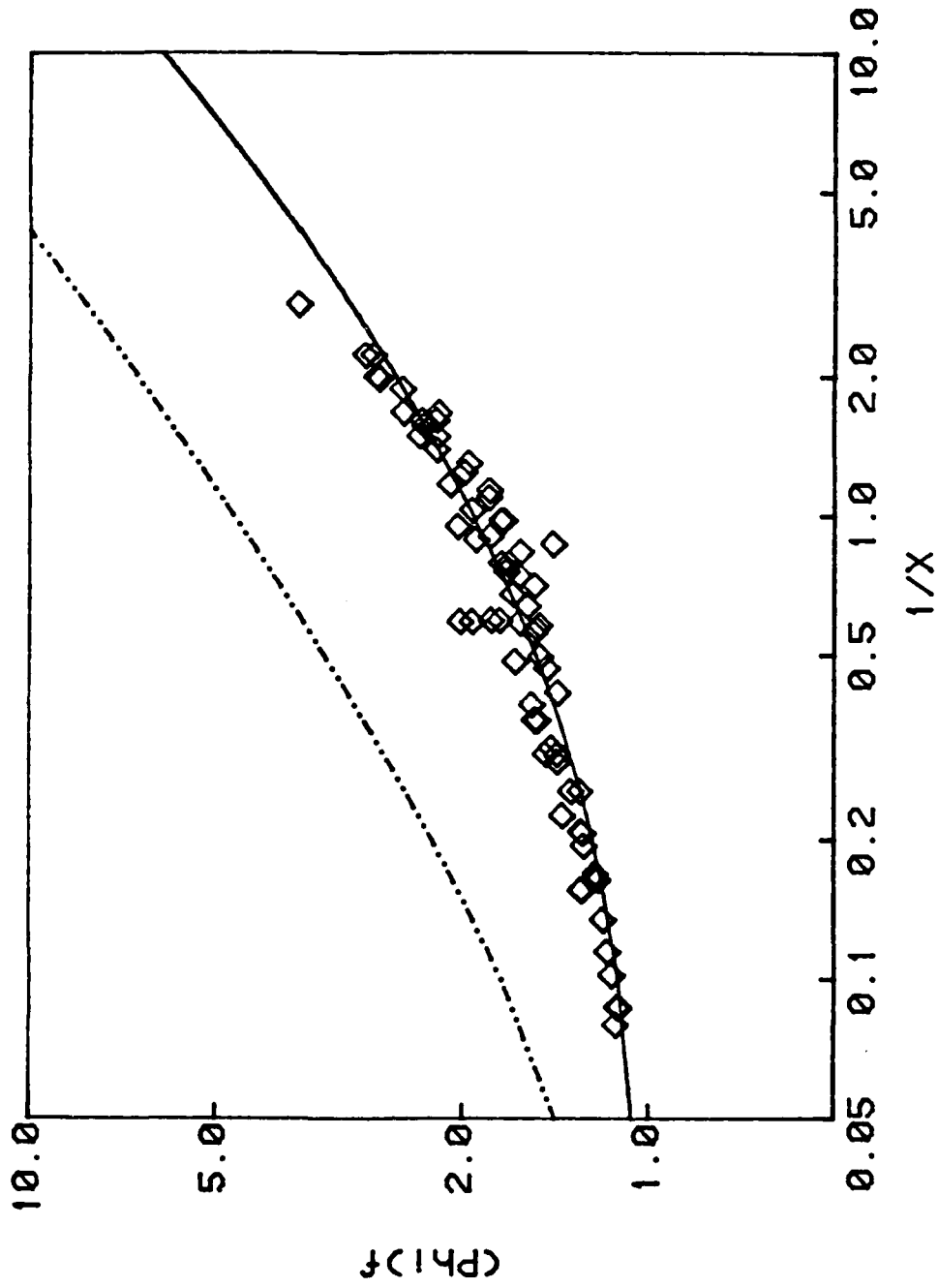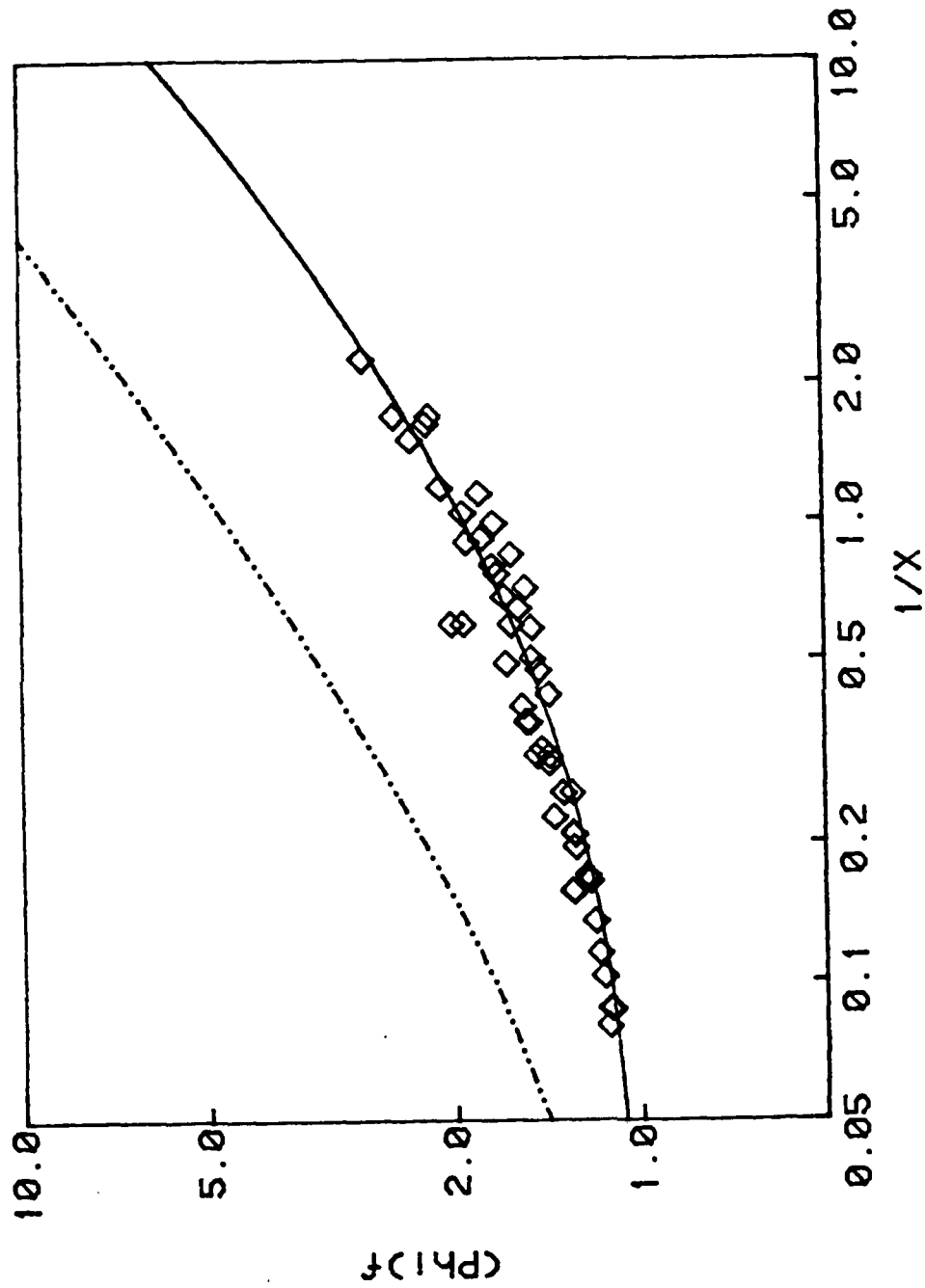
Figure 2.15   Two-Phase Friction Multiplier Versus Inverse Martinelli Parameter for L-45/Water Flow with Annular Flow Mixing Section of Annulus Thickness 0.191 cm for Total Reynolds Number of 6900. The Solid Curve corresponds to Equation 2.1 and the Dashed-Dotted Curve to Equation 2.2.

Figure 2.16 Two-Phase Friction Multiplier Versus Inverse Martinelli Parameter for L-45/Water Flow with Annular Flow Mixing Section of Annulus Thickness 0.191 cm for Total Reynolds Number of Re = 7900. The Solid Curve corresponds to Equation 2.1 and the Dashed-Dotted Curve to Equation 2.2.
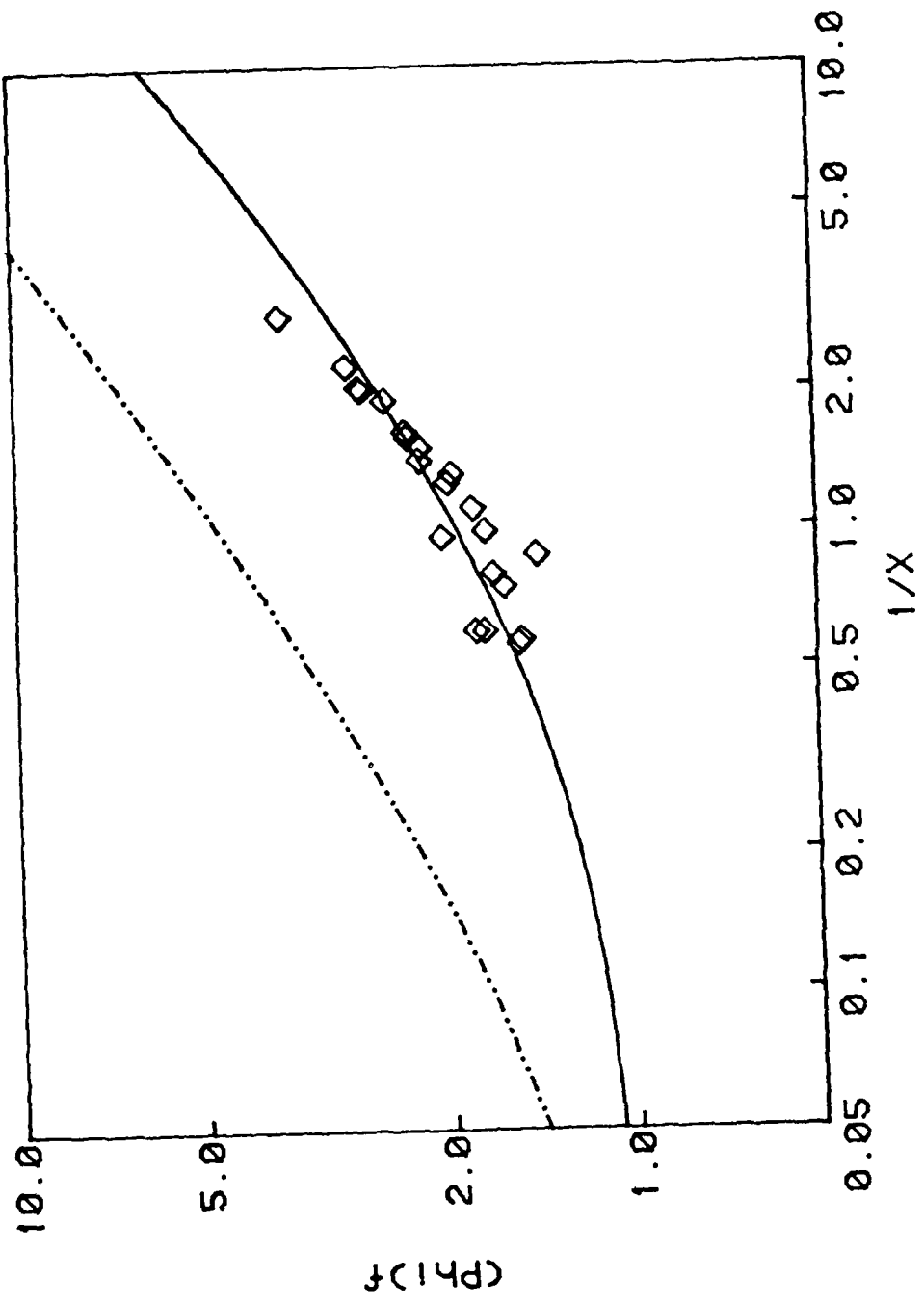
2-36

Figure 2.17 Two-Phase Friction Multiplier Versus Inverse Martinelli Parameter for L-45/Water Flow with Annular Flow Mixing Section of Annulus Thickness 0.191 cm for Total Reynolds Number of Re = 8900. The Solid Curve corresponds to Equation 2.1 and the Dashed-Dotted Curve to Equation 2.2.

Figure 2.18   Two-Phase Friction Multiplier Versus Inverse Martinelli Parameter
for L-45/Water Flow with Annular Flow Mixing Section of Annulus
Thickness 0.095 cm for Total Reynolds Number of Re = 5500.
The Solid Curve corresponds to Equation 2.1 and the Dashed-Dotted
Curve to Equation 2.2.

Figure 2.19 Two-Phase Friction Multiplier Versus Inverse Martinelli Parameter for DT-LF/Water Flow with Bubbly Mixing Section for Various Total Reynolds Numbers.
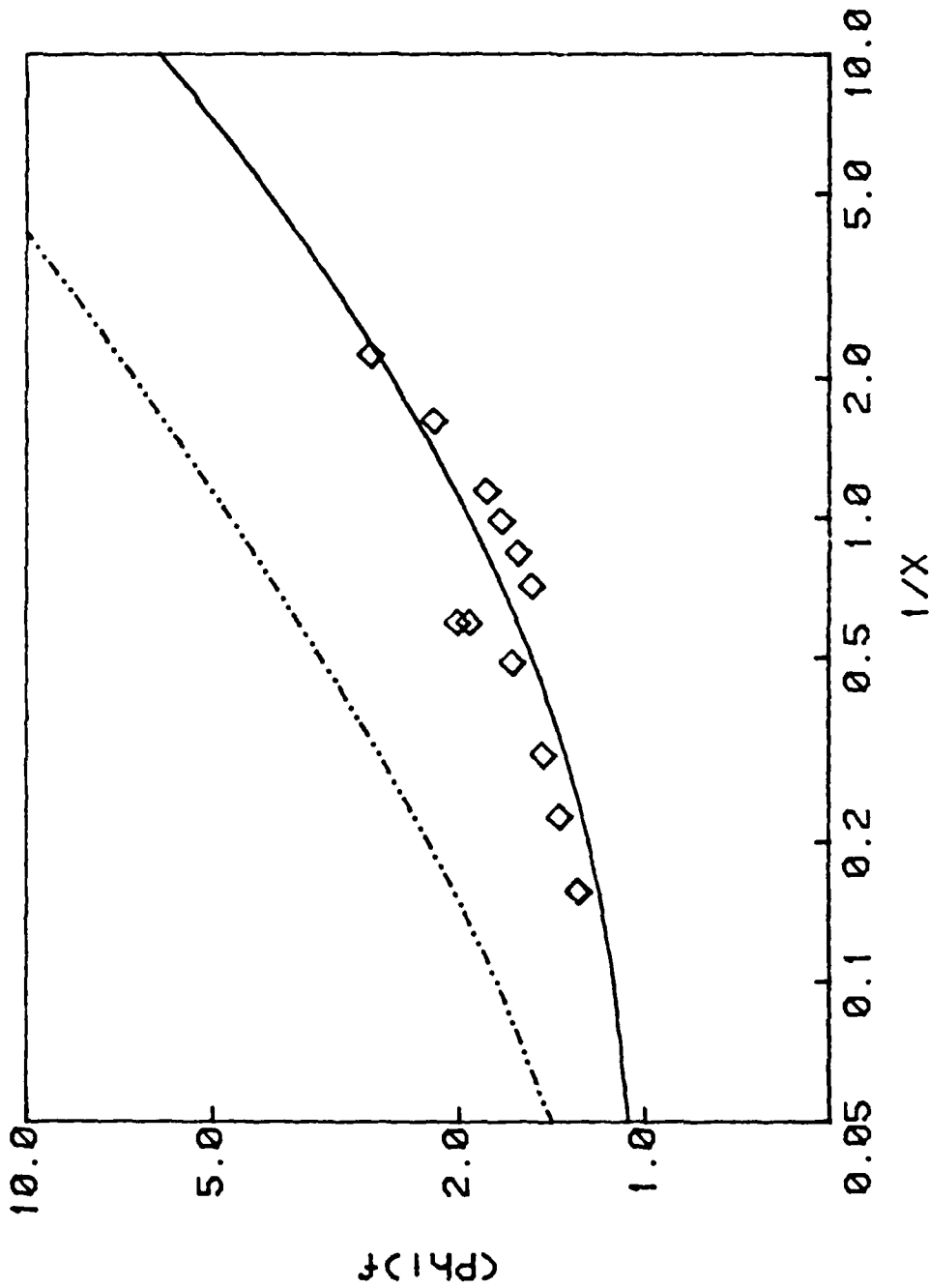The Solid Curve corresponds to Equation 2.1 and the Dashed-Dotted Curve to Equation 2.2.

2-39

Figure 2.20   Two-Phase Friction Multiplier Versus Inverse Martinelli Parameter
for DT-LF/Water Flow with Bubbly Mixing Section for Total Reynolds
Number of Re = 9000.
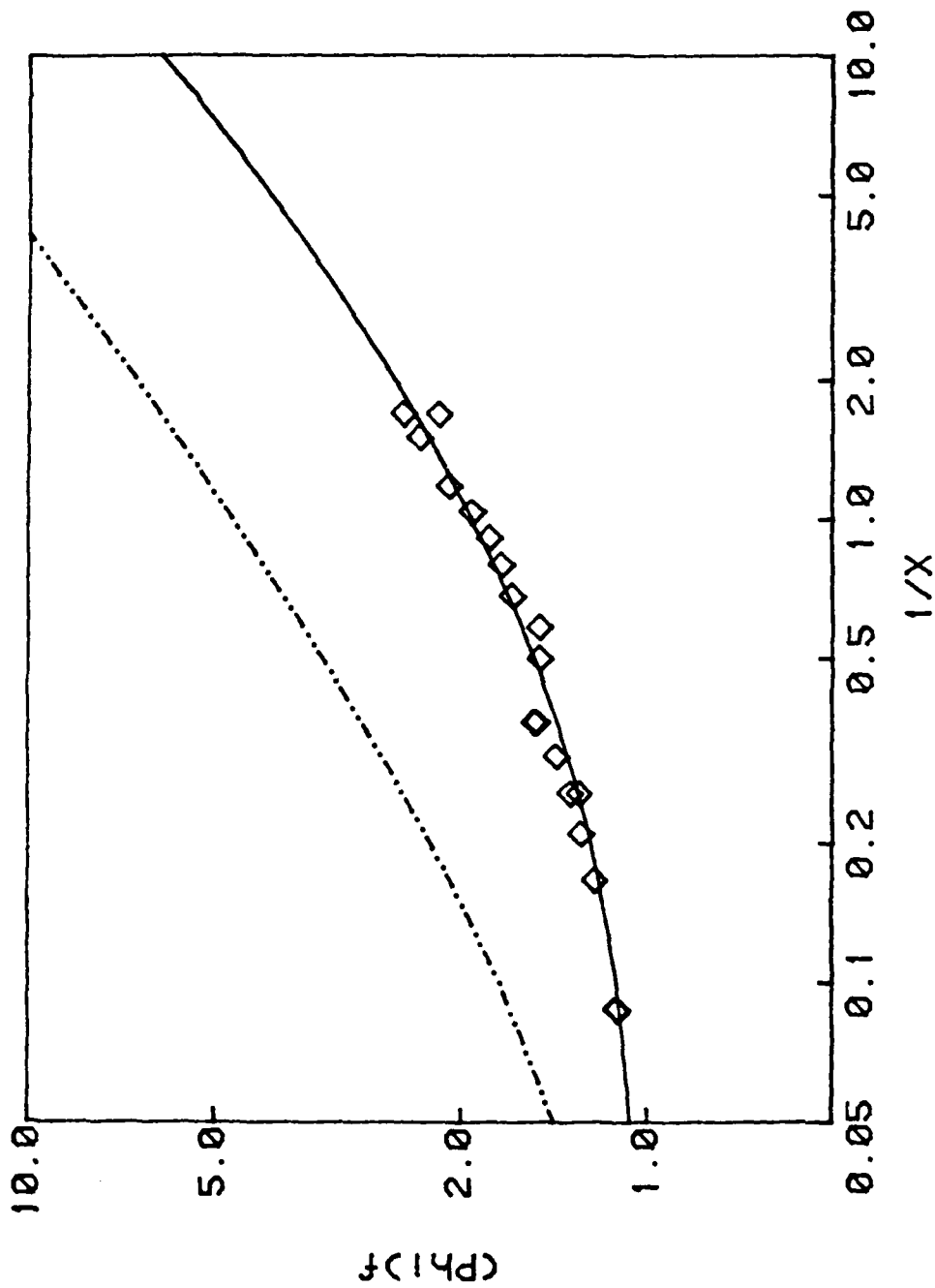The Solid Curve corresponds to Equation 2.1 and the Dashed-Dotted
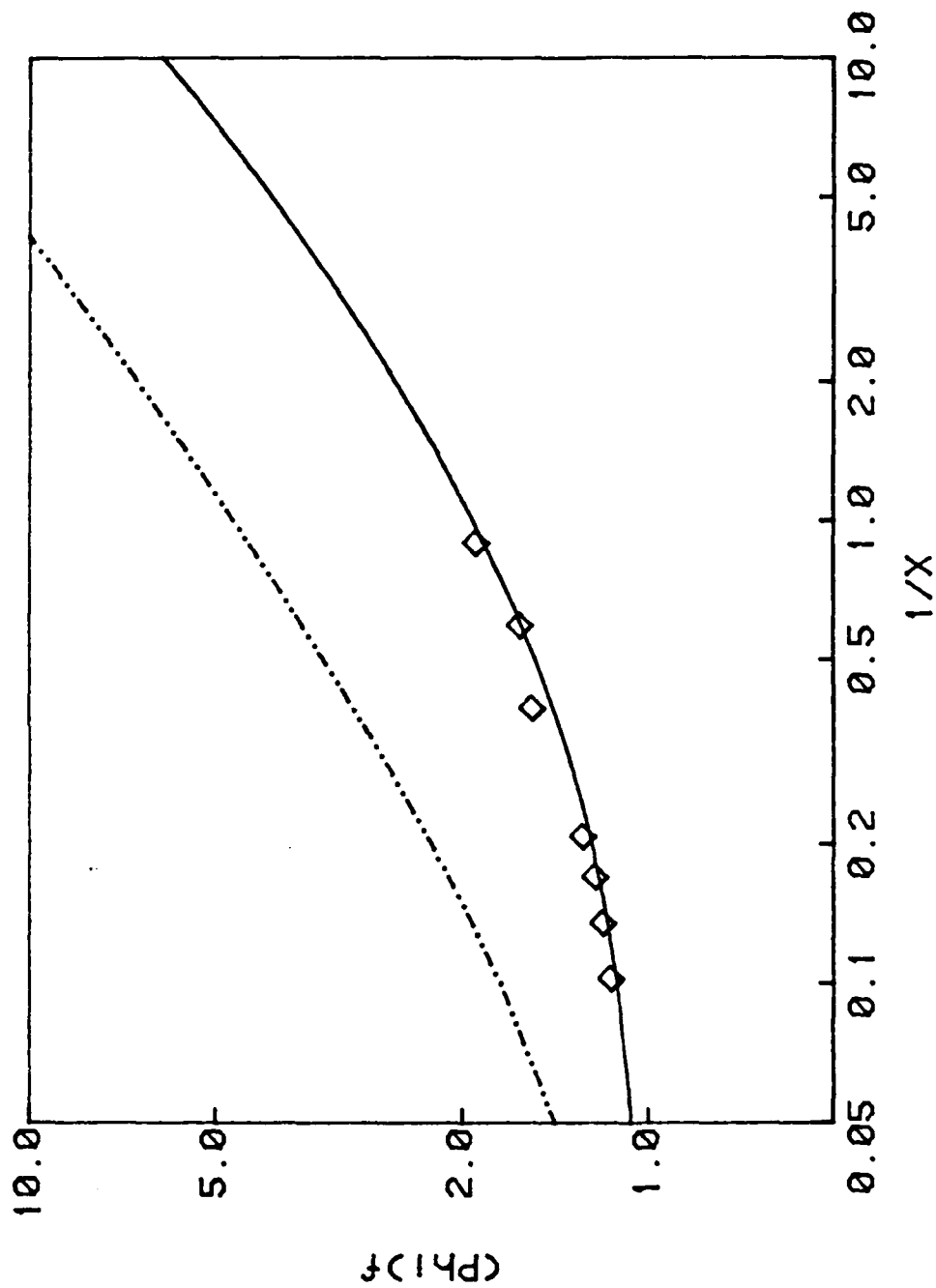Curve to Equation 2.2.

Figure 2.21   Two-Phase Friction Multiplier Versus Inverse Martinelli Parameter for DT-LF/Water Flow with Bubbly Mixing Section for Total Reynolds Number of Re = 15900. The Solid Curve corresponds to Equation 2.1 and the Dashed-Dotted Curve to Equation 2.2.

Figure 2.22   Two-Phase Friction Multiplier Versus Inverse Martinelli Parameter for DT-LF/Water Flow with Bubbly Mixing Section for Total Reynolds Number of Re = 18000.
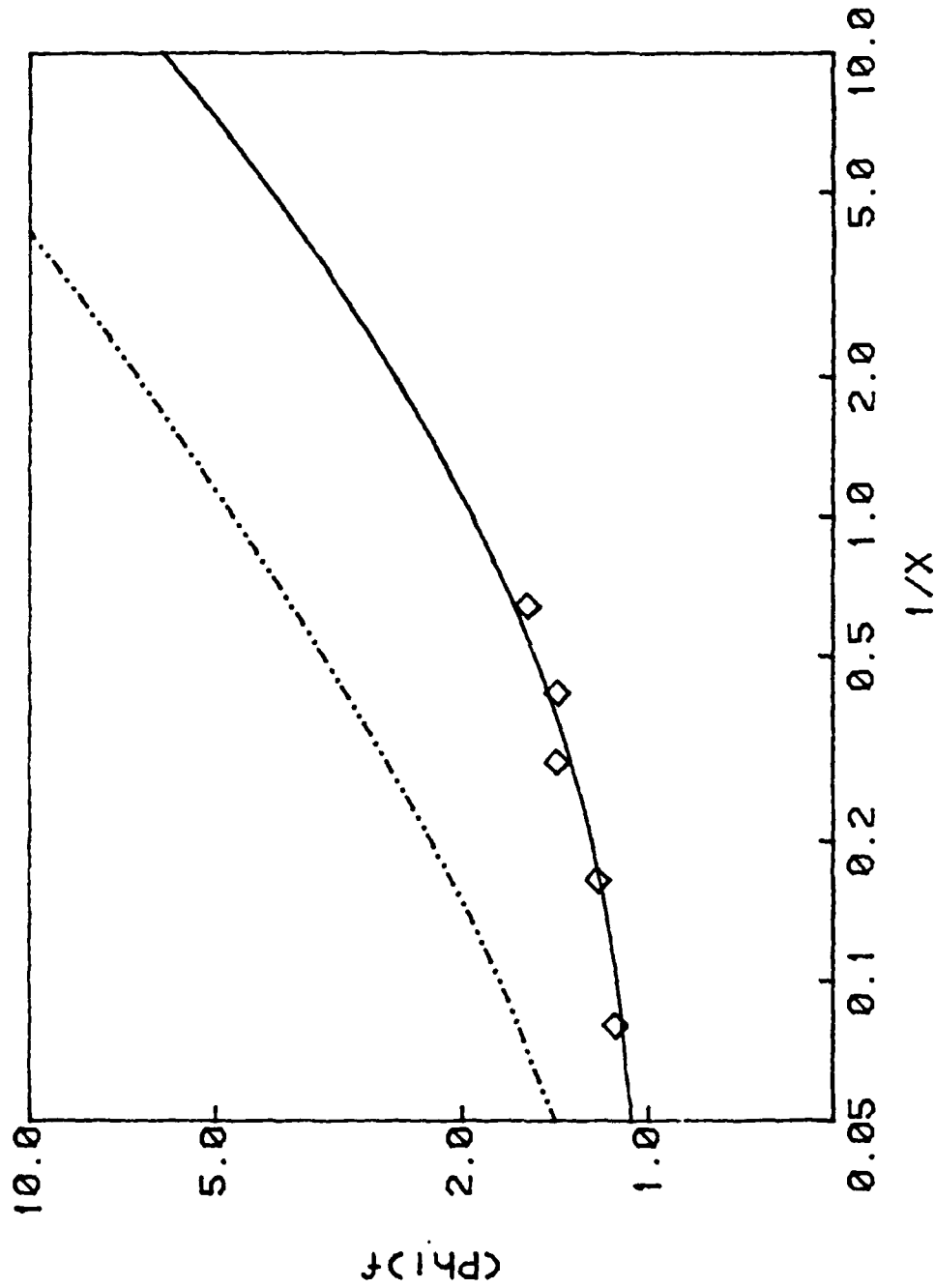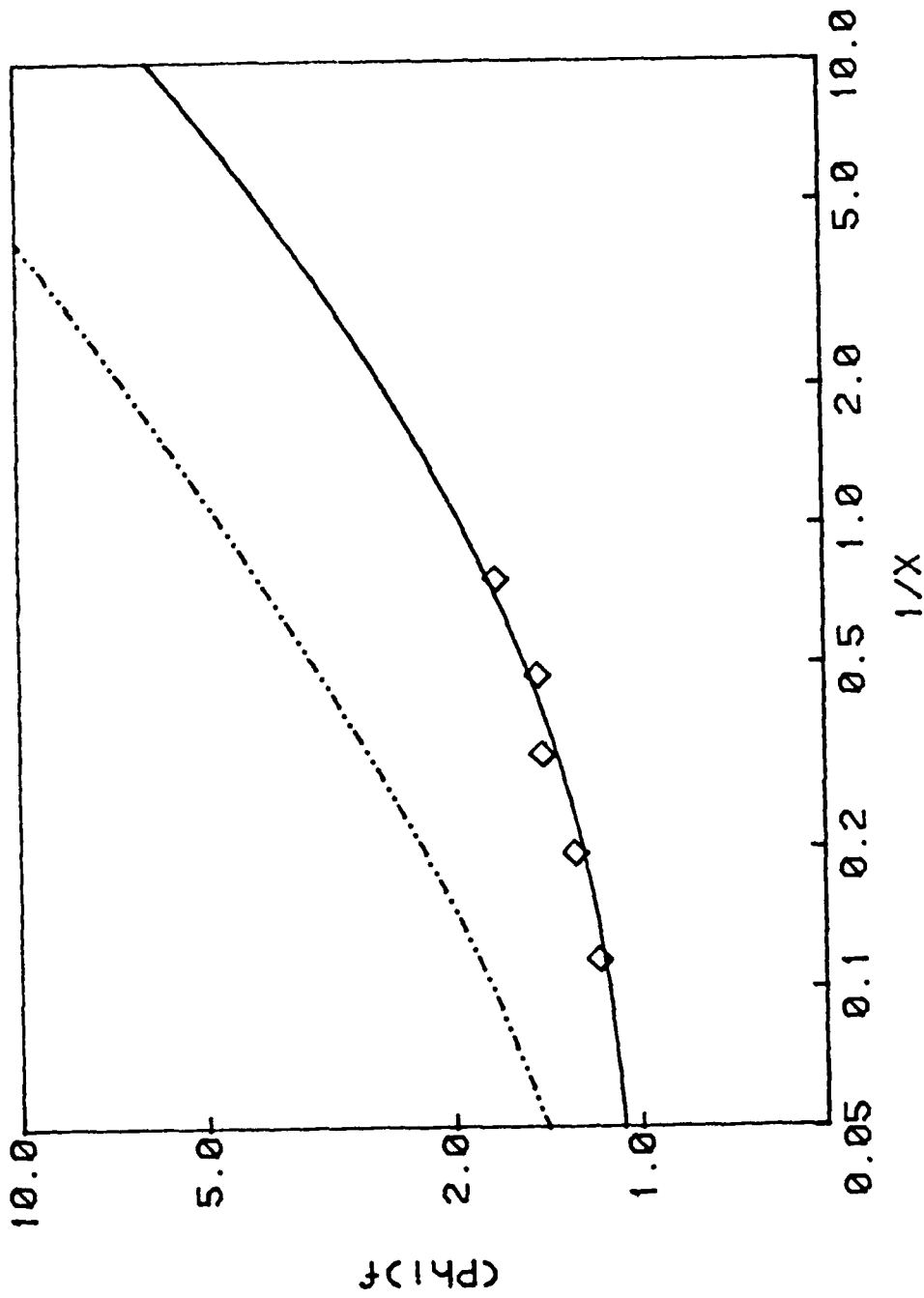The Solid Curve corresponds to Equation 2.1 and the Dashed-Dotted Curve to Equation 2.2.

Figure 2.23   Two-Phase Friction Multiplier Versus Inverse Martinelli Parameter
for All Data Points.
The Solid Curve corresponds to Equation 2.1 and the Dashed-Dotted
Curve to Equation 2.2.

2-43
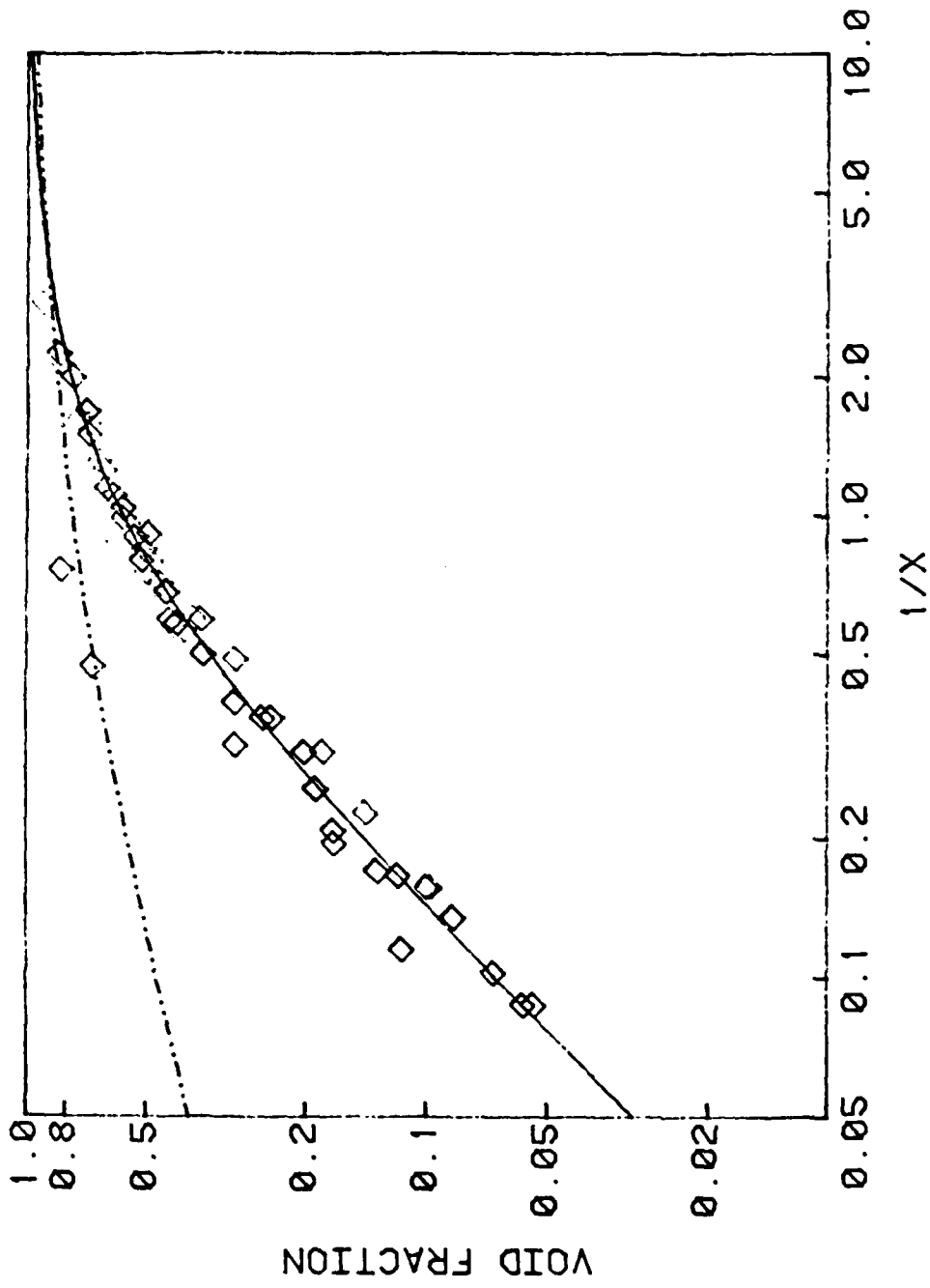
Figure 2.24 Void Fraction Versus Inverse Martinelli Parameter for L-45/Water Flow with Bubbly and Annular Flow Mixing Sections and Various Total Reynolds Numbers. The Solid Curve corresponds to Equation 2.3 and the Dashed-Dotted Curve to Equation 2.4.

Figure 2.25 Void Fraction Versus Inverse Martinelli Parameter for L-45/Water Flow with Bubbly Flow Mixing Sections and Various Total Reynolds Numbers.
The Solid Curve corresponds to Equation 2.3 and the Dashed-Dotted Curve to Equation 2.4.

Figure 2.26 Void Fraction Versus Inverse Martinelli Parameter for L-45/Water Flow with Annular Flow Mixing Sections and Various Total Reynolds Numbers.
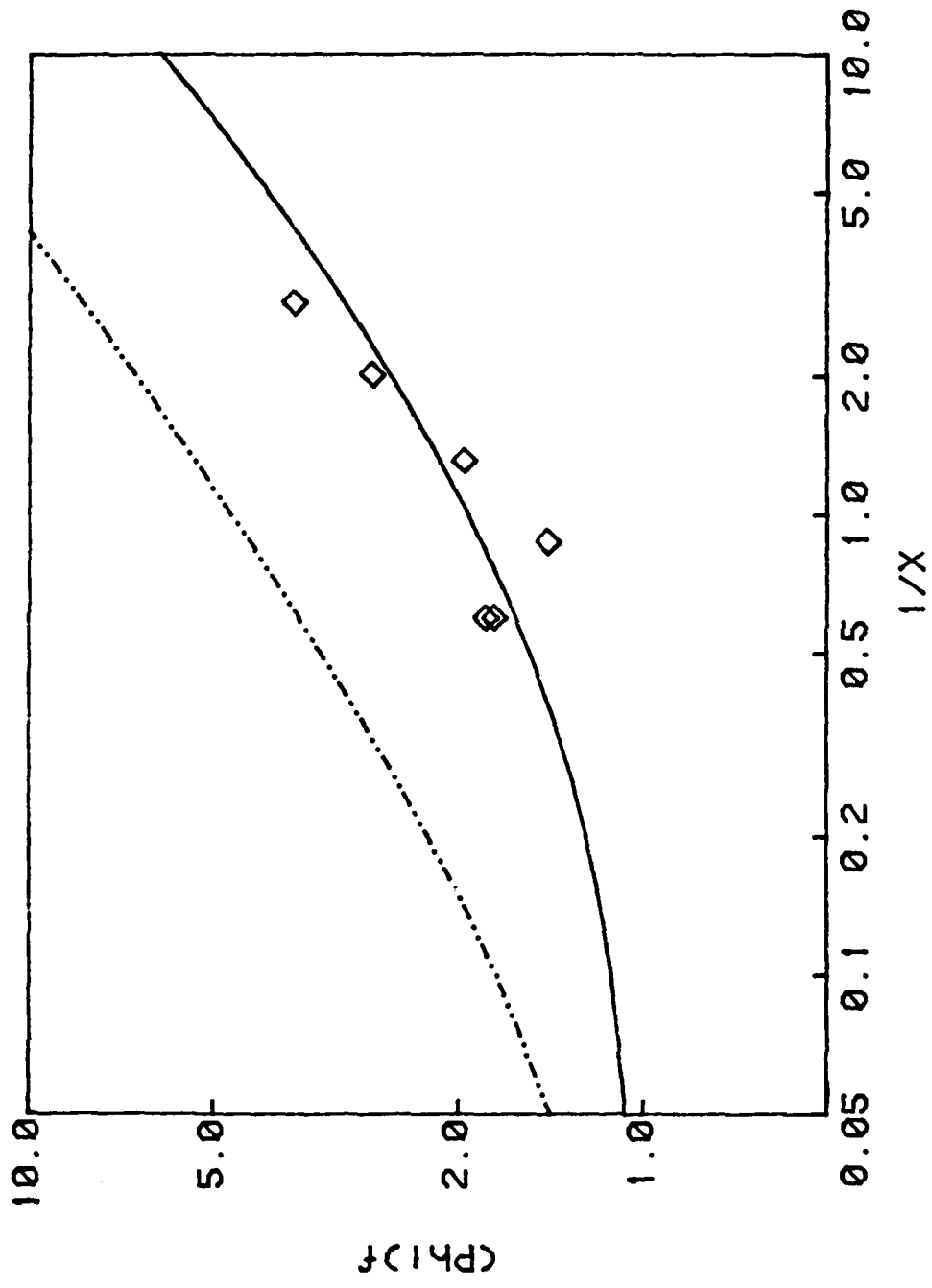The Solid Curve corresponds to Equation 2.3 and the Dashed-Dotted Curve to Equation 2.4.
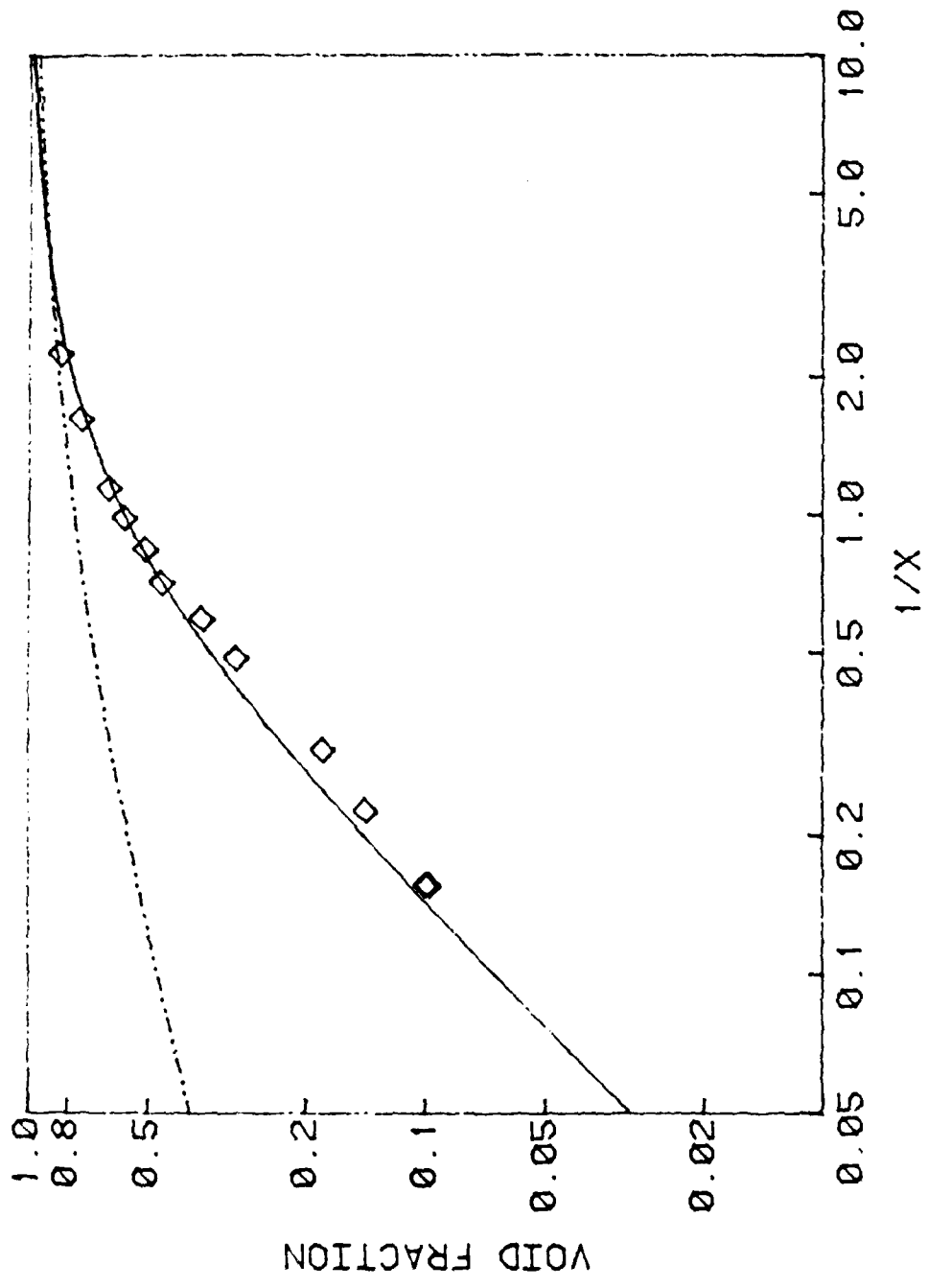
Figure 2.27 Void Fraction Versus Inverse Martinelli Parameter for L-45/Water
Flow with Bubbly Flow Mixing Section and for Total Reynolds
Number of Re = 5500.
The Solid Curve corresponds to Equation 2.3 and the Dashed-Dotted
Curve to Equation 2.4.
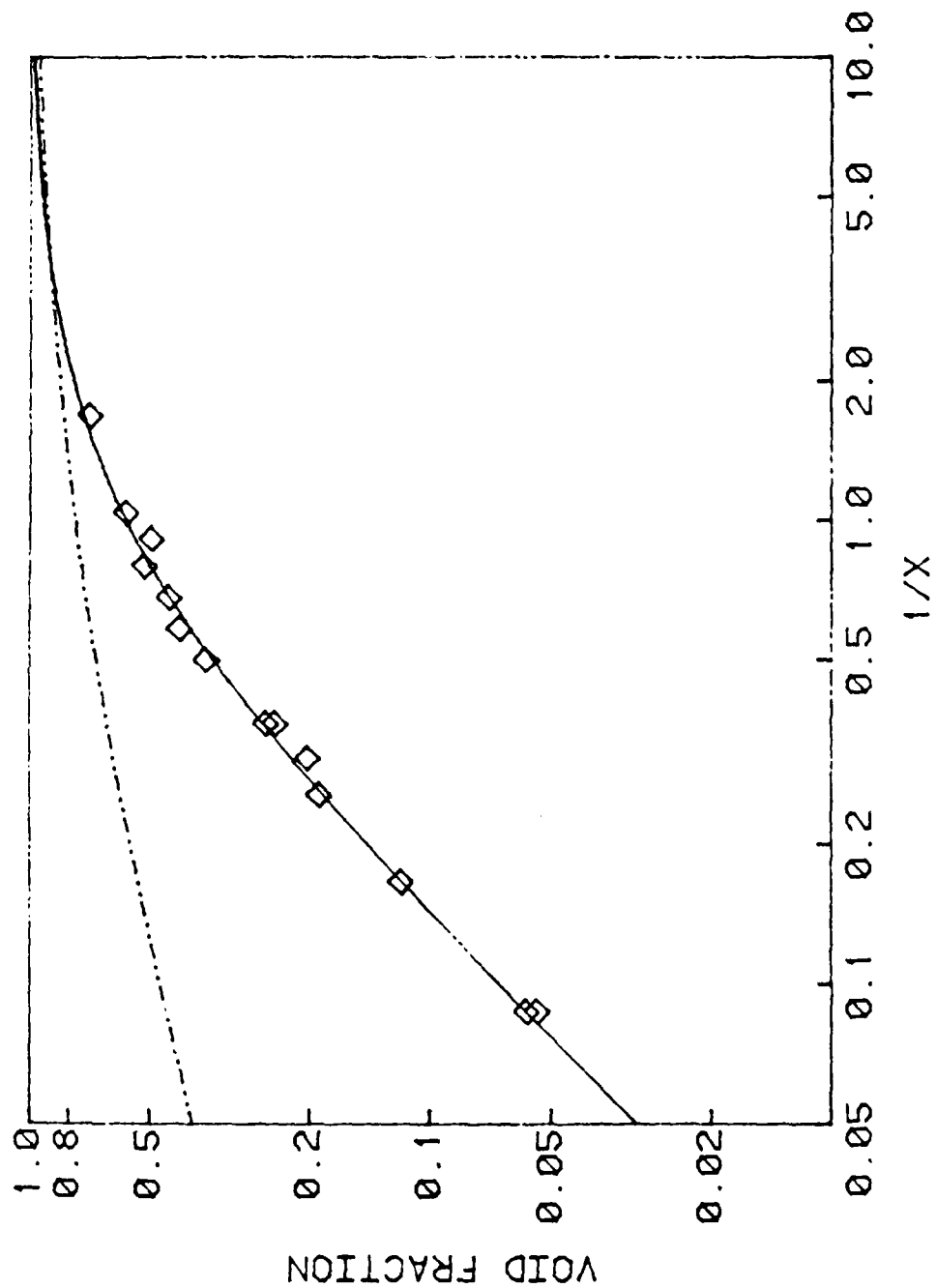
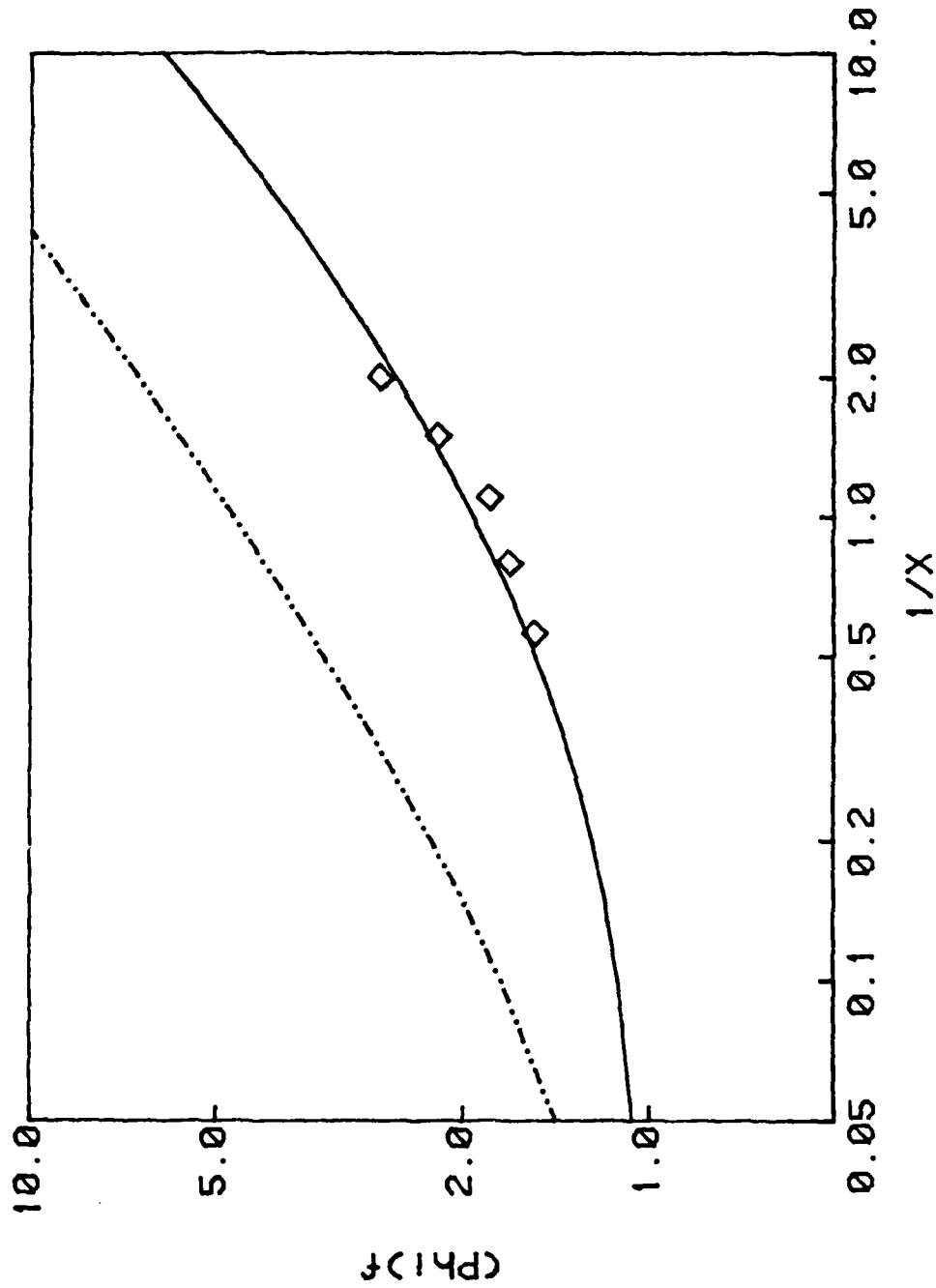Figure 2.28 Void Fraction Versus Inverse Martinelli Parameter for L-45/Water Flow with Bubbly Flow Mixing Section and for Total Reynolds Number of Re = 7900. The Solid Curve corresponds to Equation 2.3 and the Dashed-Dotted Curve to Equation 2.4.
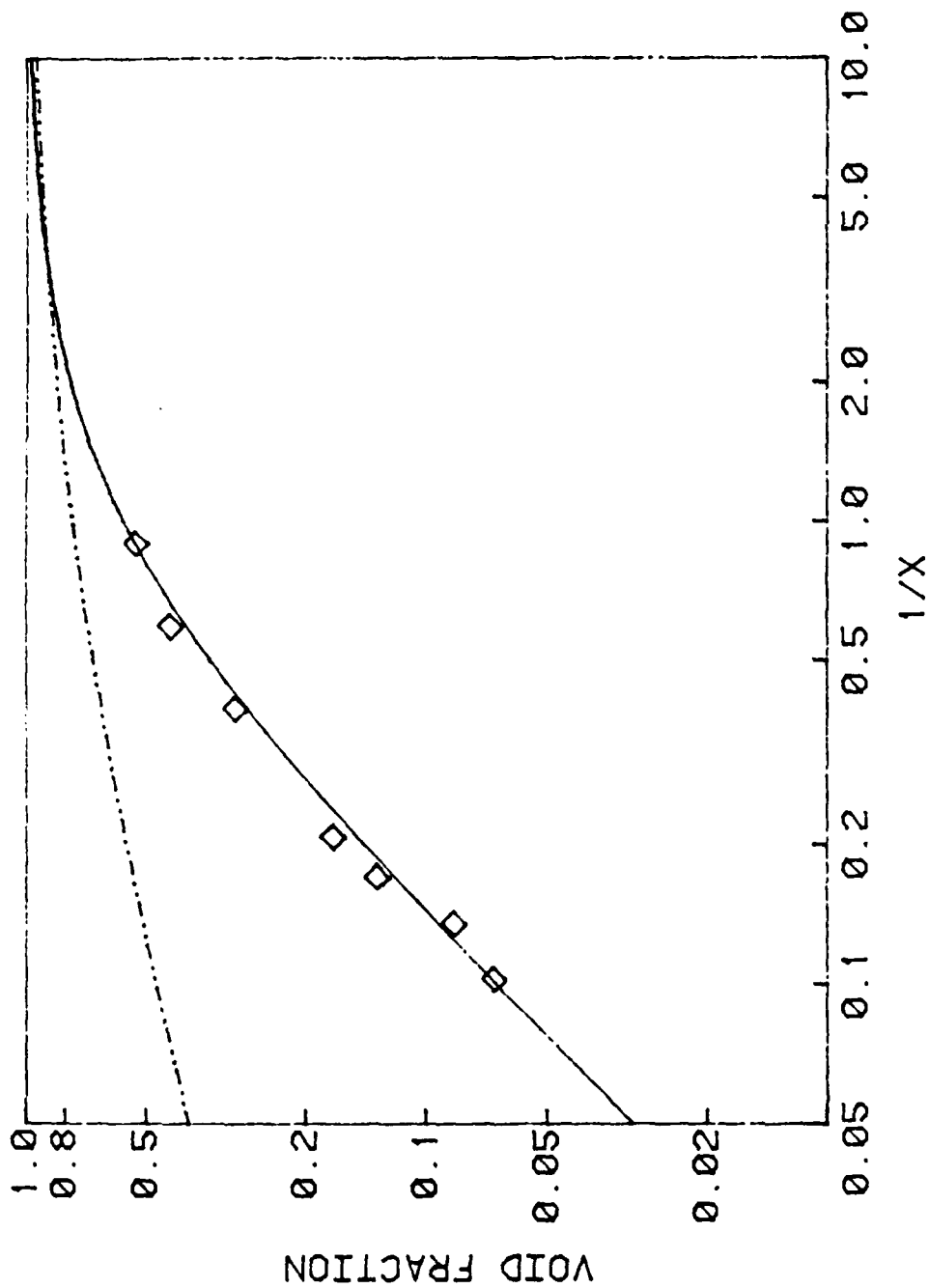
Figure 2.29 Void Fraction Versus Inverse Martinelli Parameter for L-45/Water
Flow with Bubbly Flow Mixing Section and for Total Reynolds
Number of Re = 8800.
The Solid Curve corresponds to Equation 2.3 and the Dashed-Dotted
Curve to Equation 2.4.

2-49
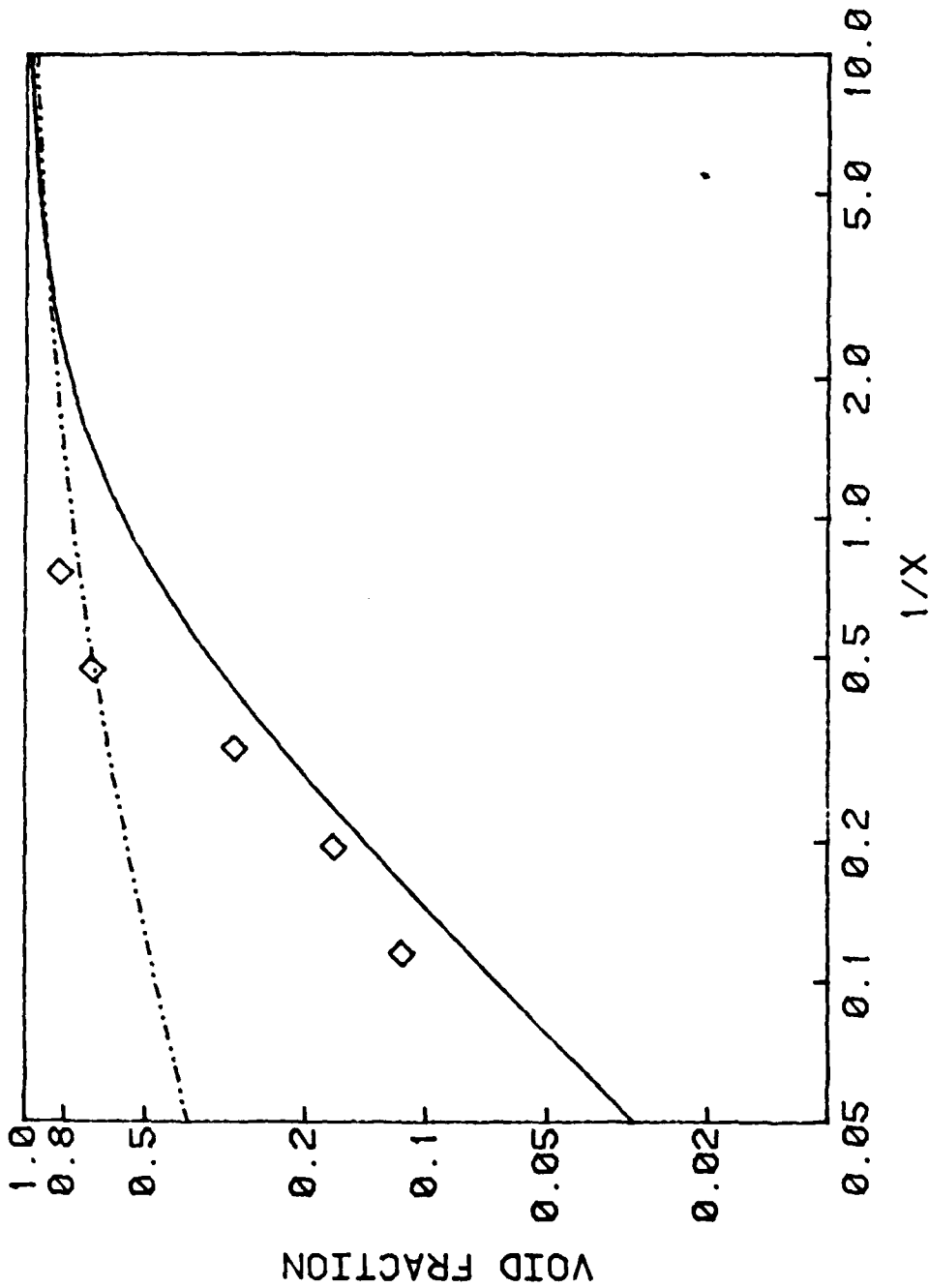
Figure 2.30   Void Fraction Versus Inverse Martinelli Parameter for L-45/Water
               Flow with Bubbly Flow Mixing Section and for Total Reynolds
               Number of Re = 11600.
               The Solid Curve corresponds to Equation 2.3 and the Dashed-Dotted
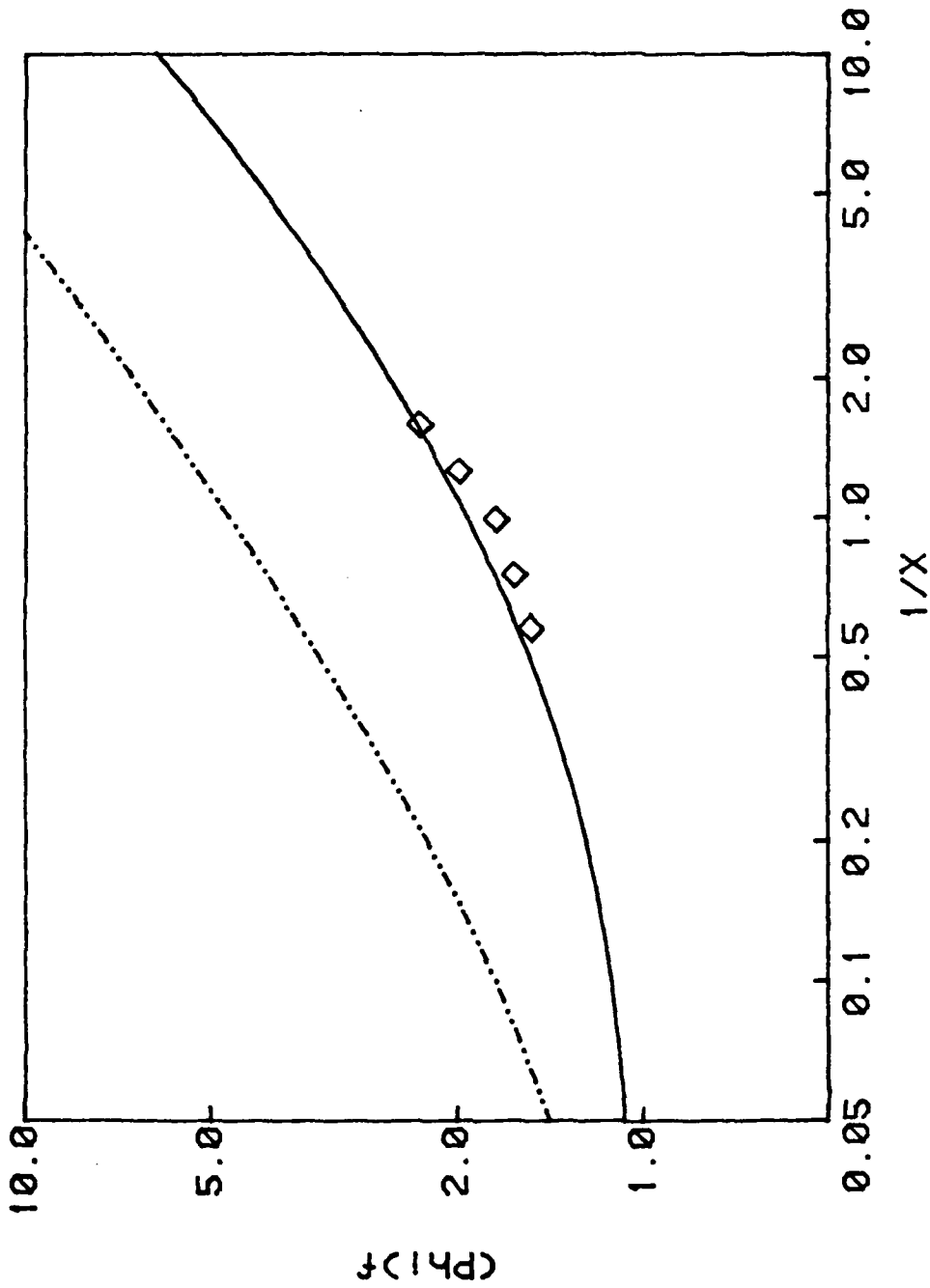   Curve to Equation 2.4.
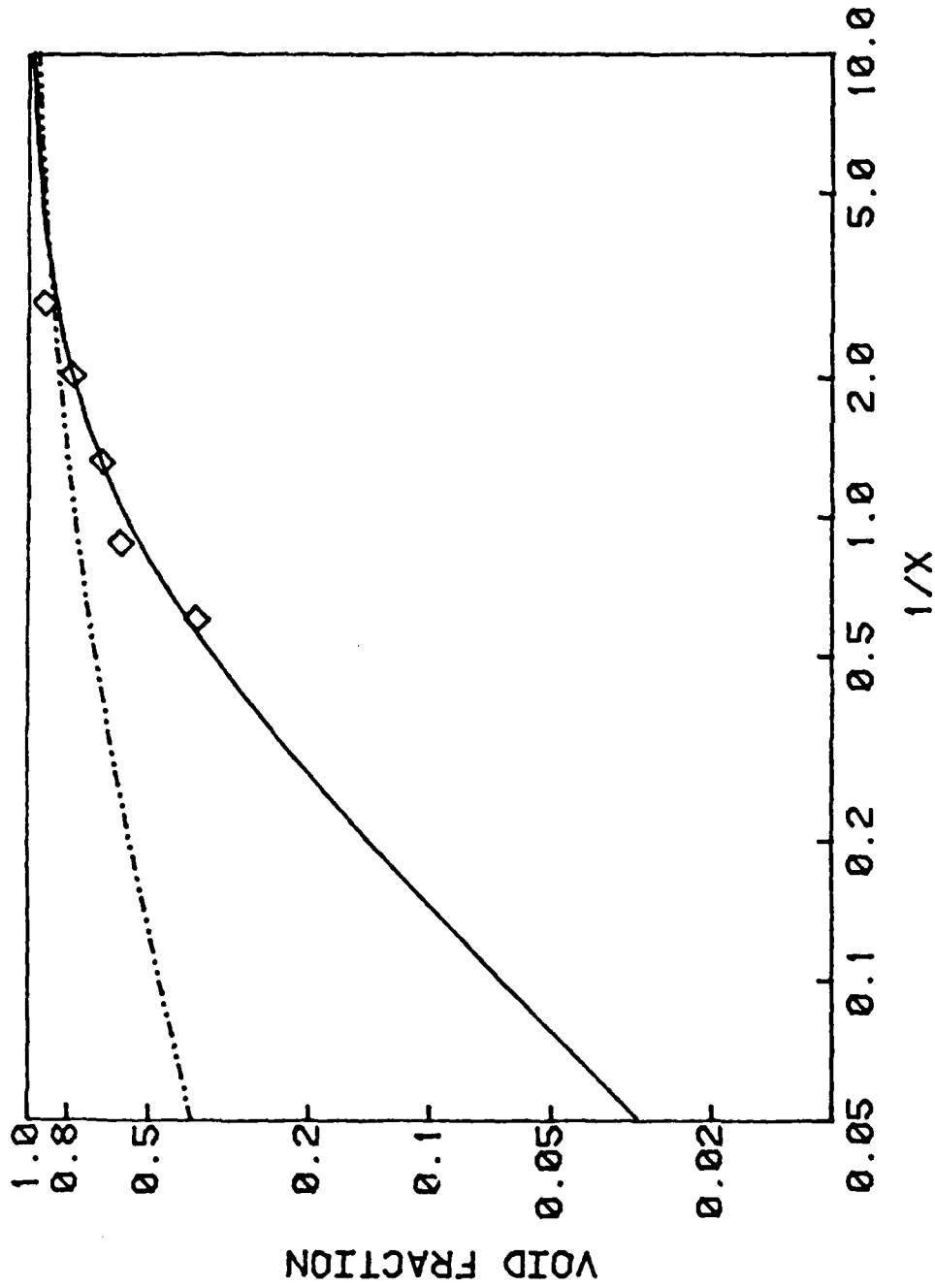
Figure 2.31 Void Fraction Versus Inverse Martinelli Parameter for L-45/Water
Flow with Annular Flow Mixing Section of Annulus Thickness 0.191
and for Total Reynolds Number of Re = 6900.
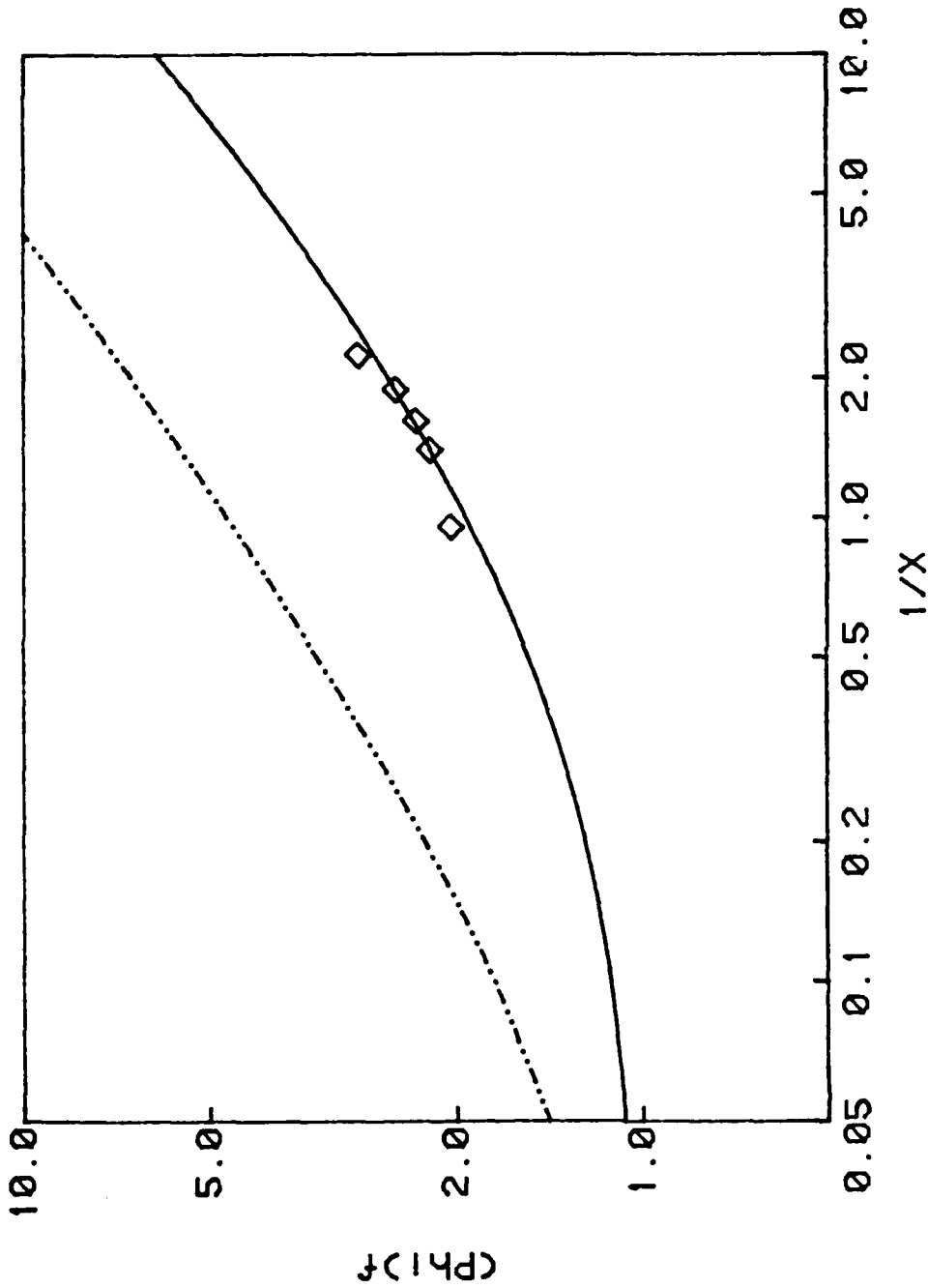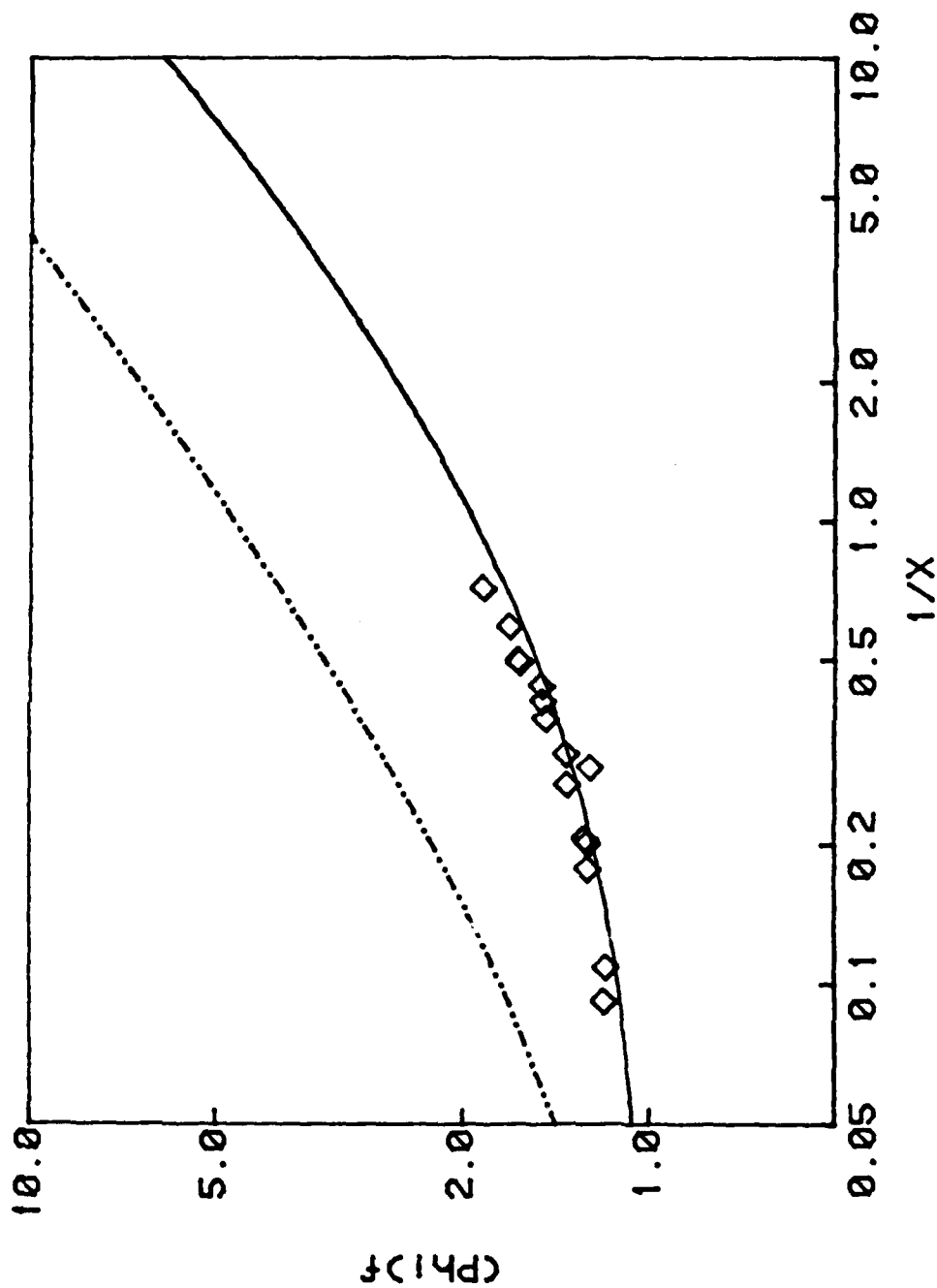The Solid Curve corresponds to Equation 2.3 and the Dashed-Dotted
Curve to Equation 2.4.

2-51
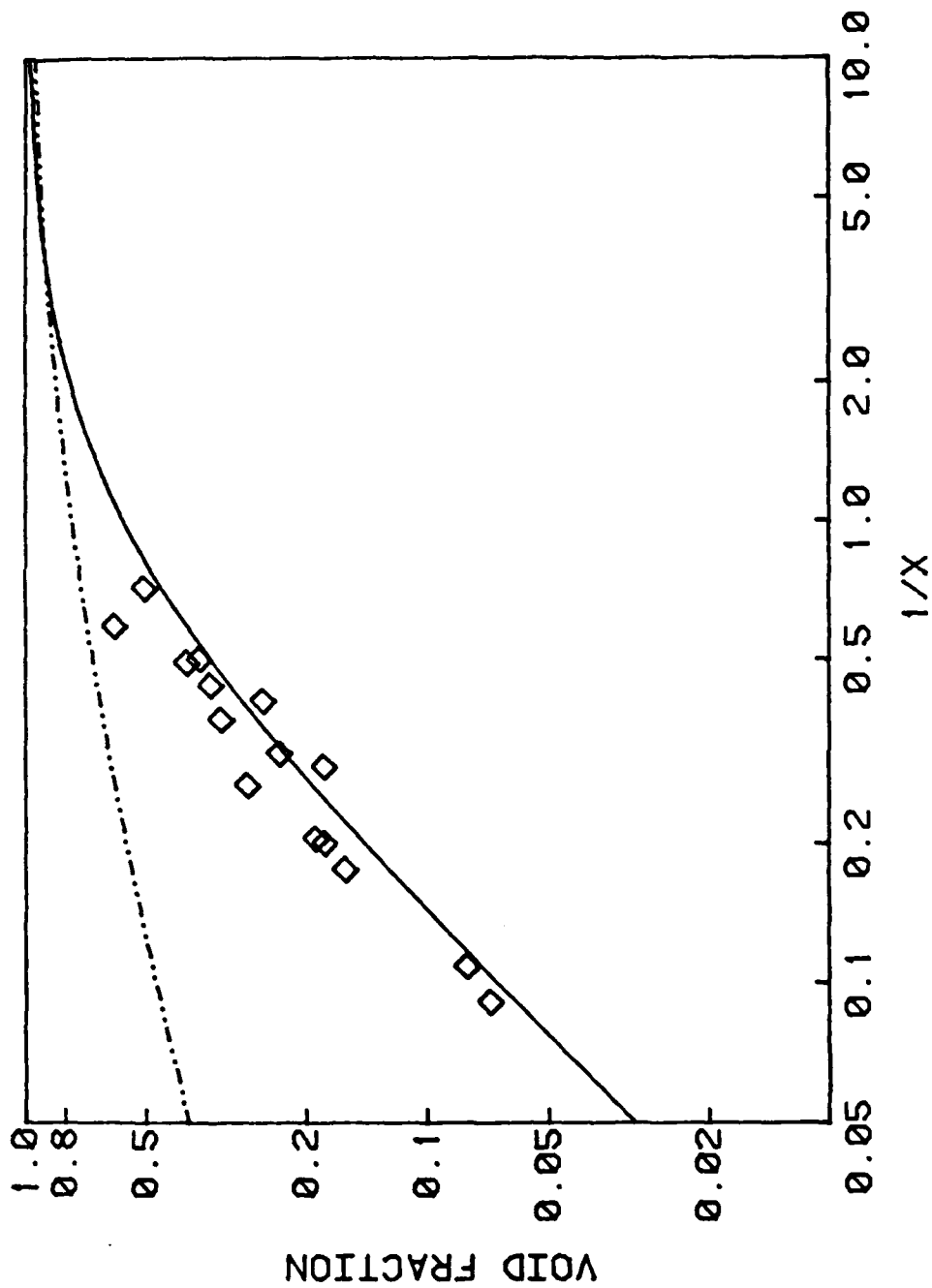
Figure 2.32   Void Fraction Versus Inverse Martinelli Parameter for DT-LF/Water Flow with Bubbly Flow Mixing Section for Various Total Reynolds Numbers.
The Solid Curve corresponds to Equation 2.3 and the Dashed-Dotted Curve to Equation 2.4.
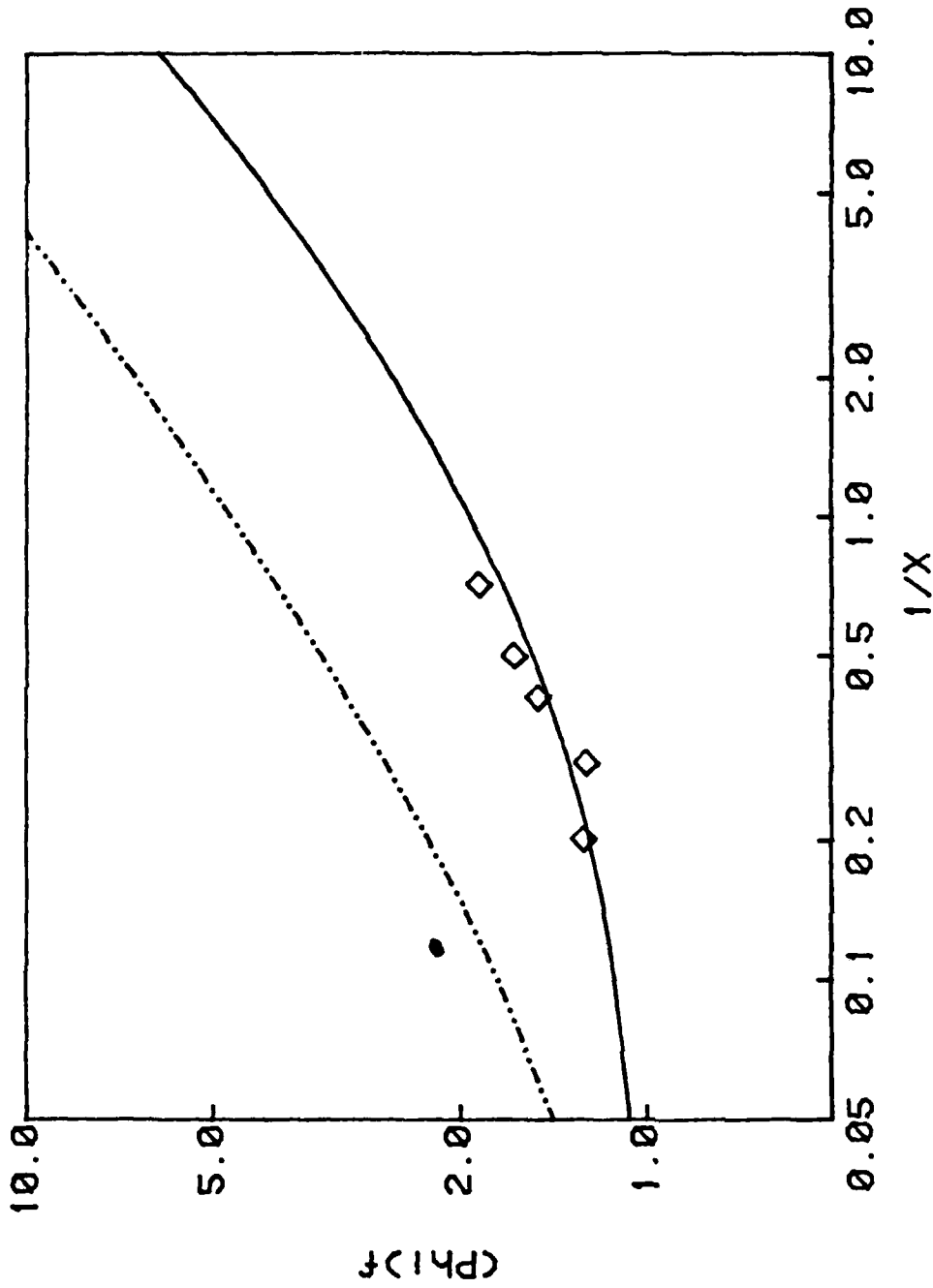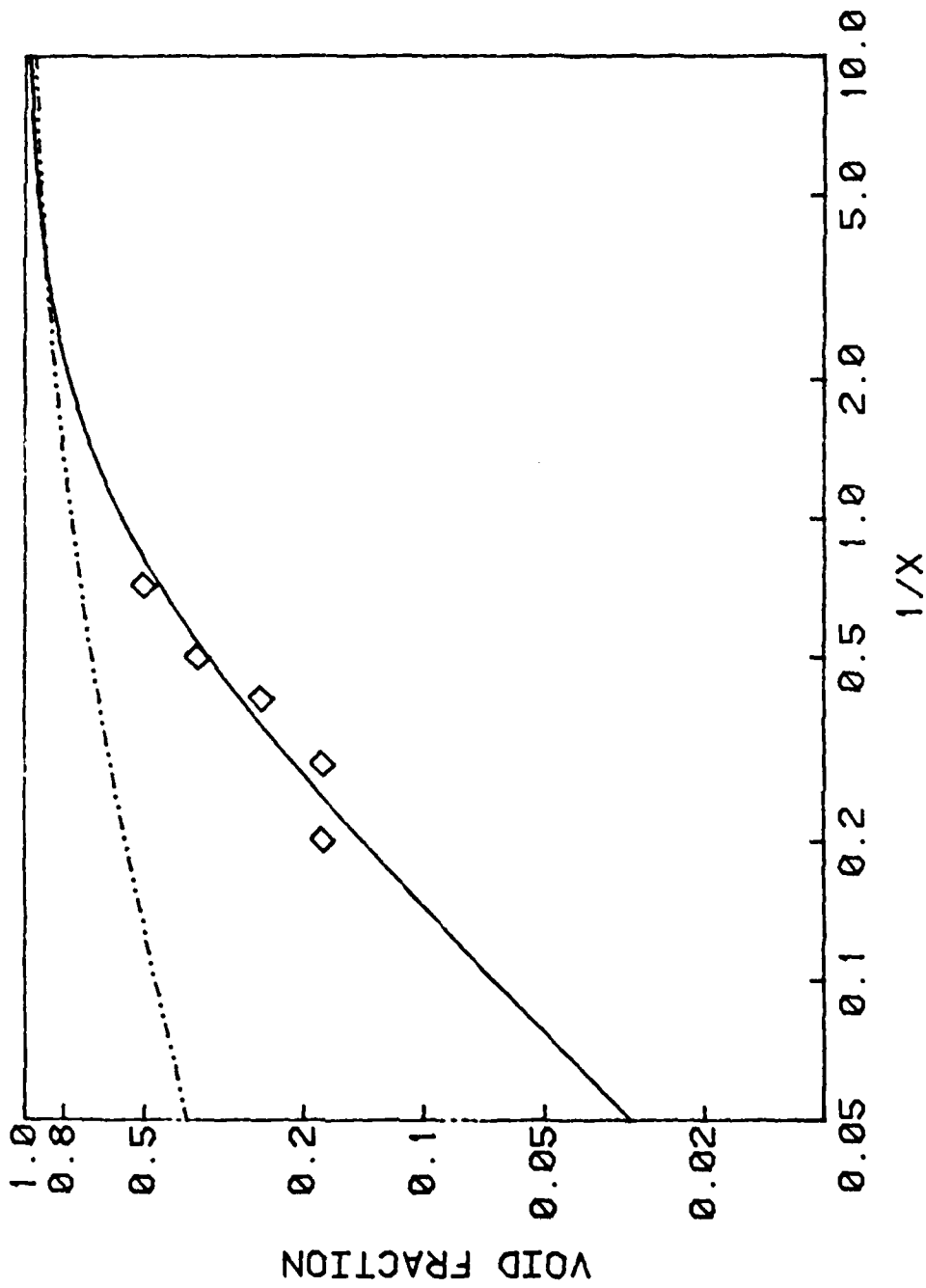
Figure 2.33 Void Fraction Versus Inverse Martinelli Parameter for DT-LF/Water Flow with Bubbly Flow Mixing Section and Total Reynolds Number of Re = 9000.
The Solid Curve corresponds to Equation 2.3 and the Dashed-Dotted Curve to Equation 2.4.
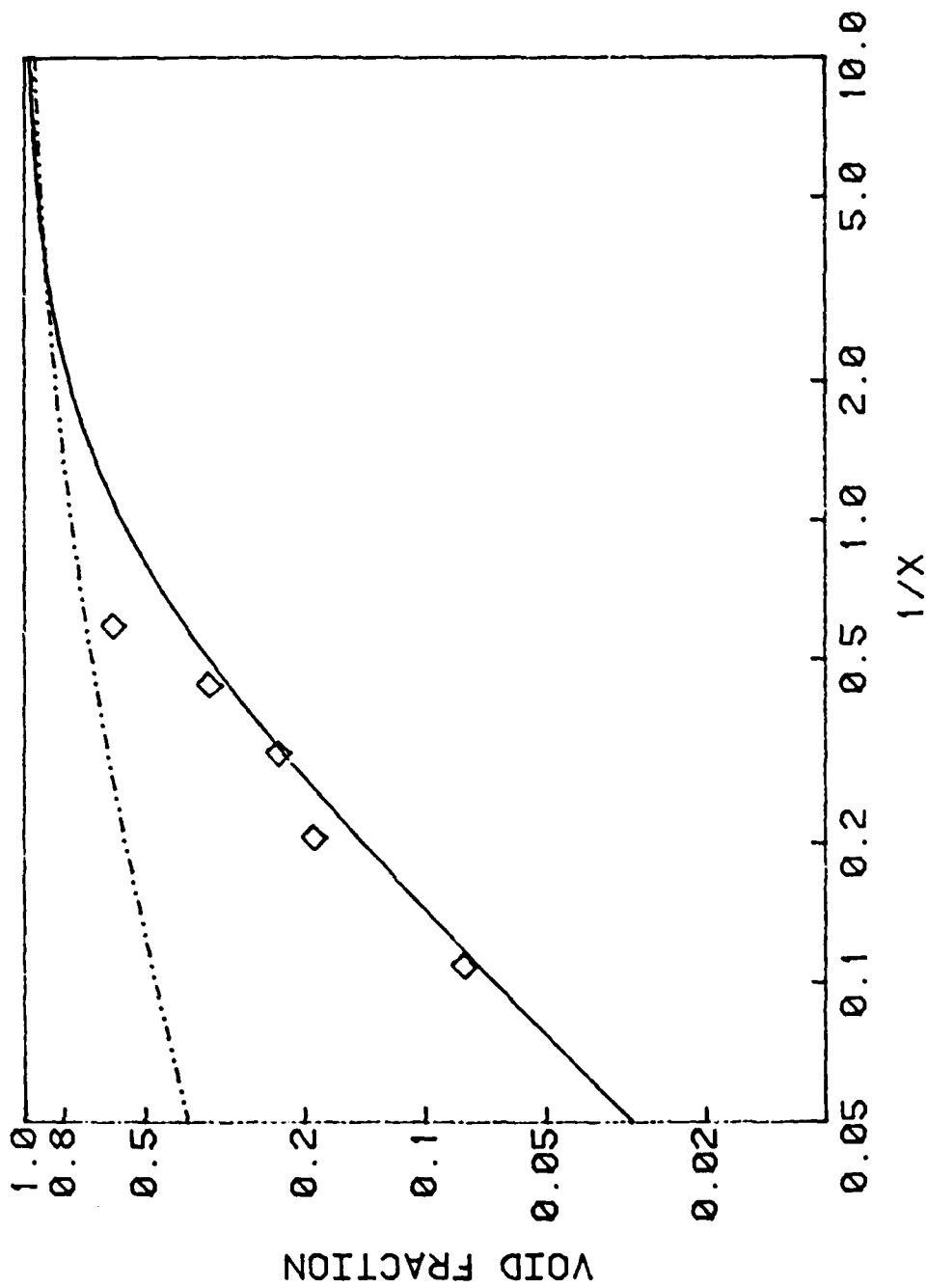
Figure 2.34   Void Fraction Versus Inverse Martinelli Parameter for DT-LF/Water Flow with Bubbly Flow Mixing Section and Total Reynolds Number of Re = 15900.
The Solid Curve corresponds to Equation 2.3 and the Dashed-Dotted Curve to Equation 2.4.
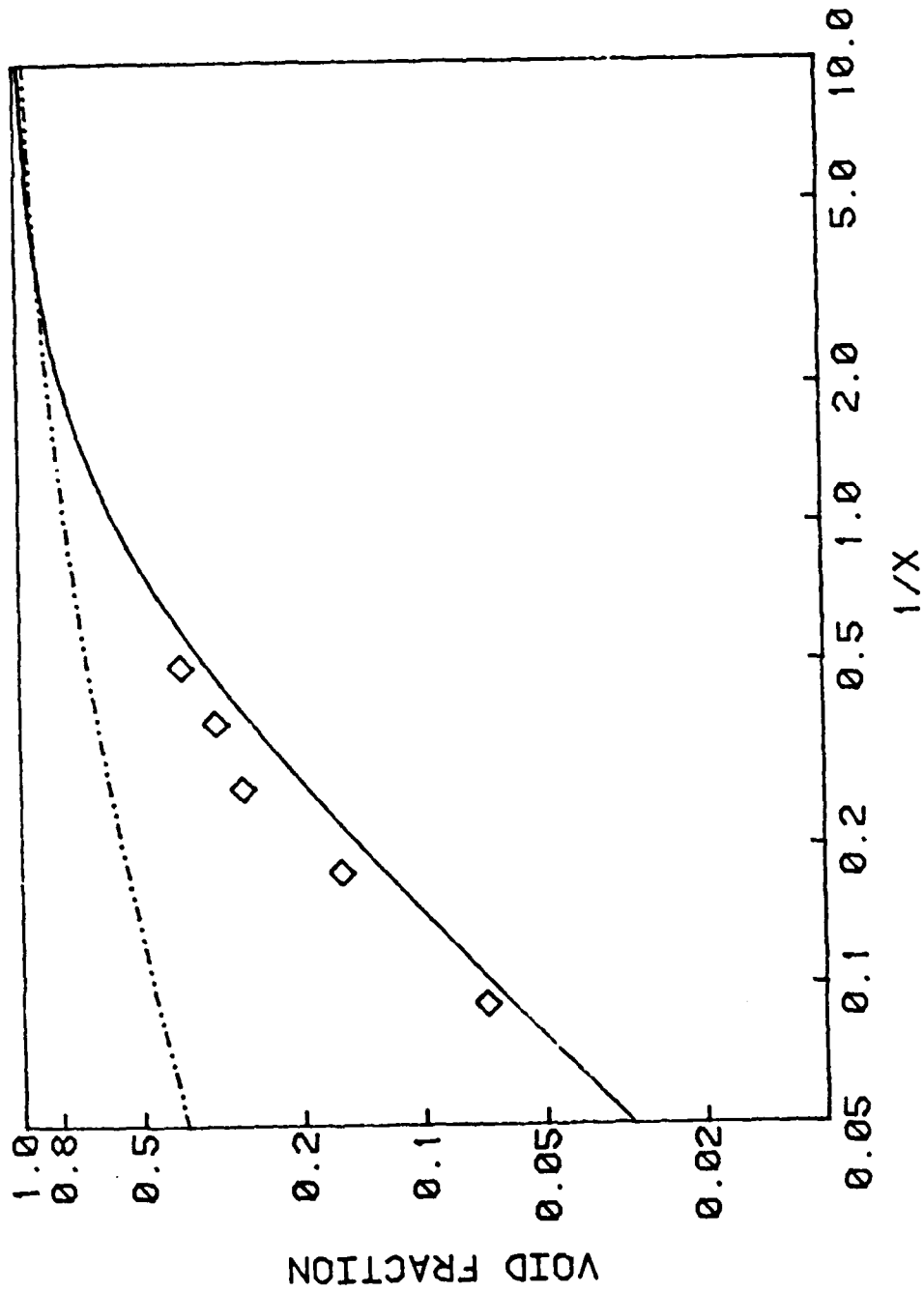
Figure 2.35 Void Fraction Versus Inverse Martinelli Parameter for DT-LF/Water Flow with Bubbly Flow Mixing Section and Total Reynolds Number of Re = 18000. The Solid Curve corresponds to Equation 2.3 and the Dashed-Dotted Curve to Equation 2.4.
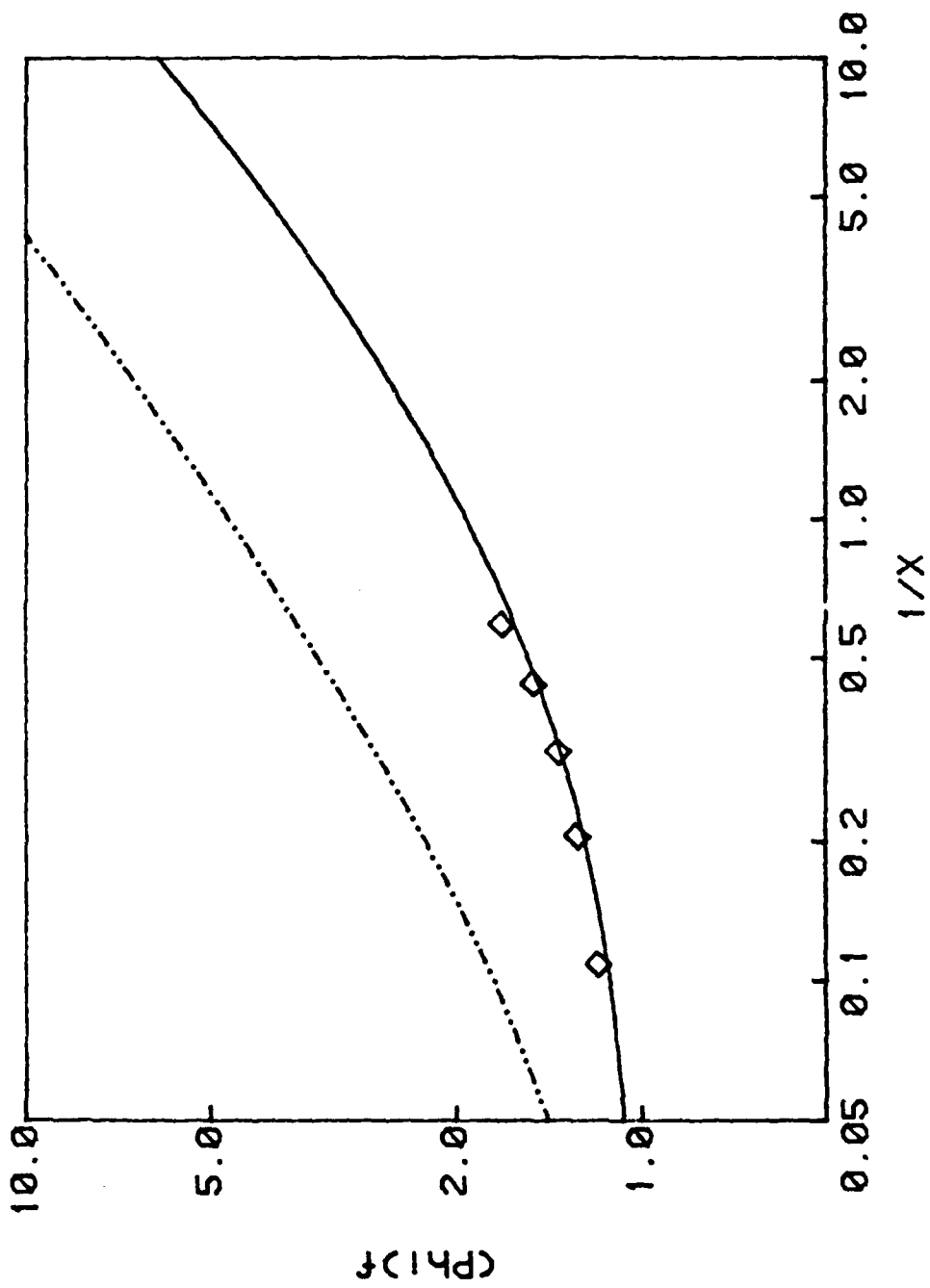
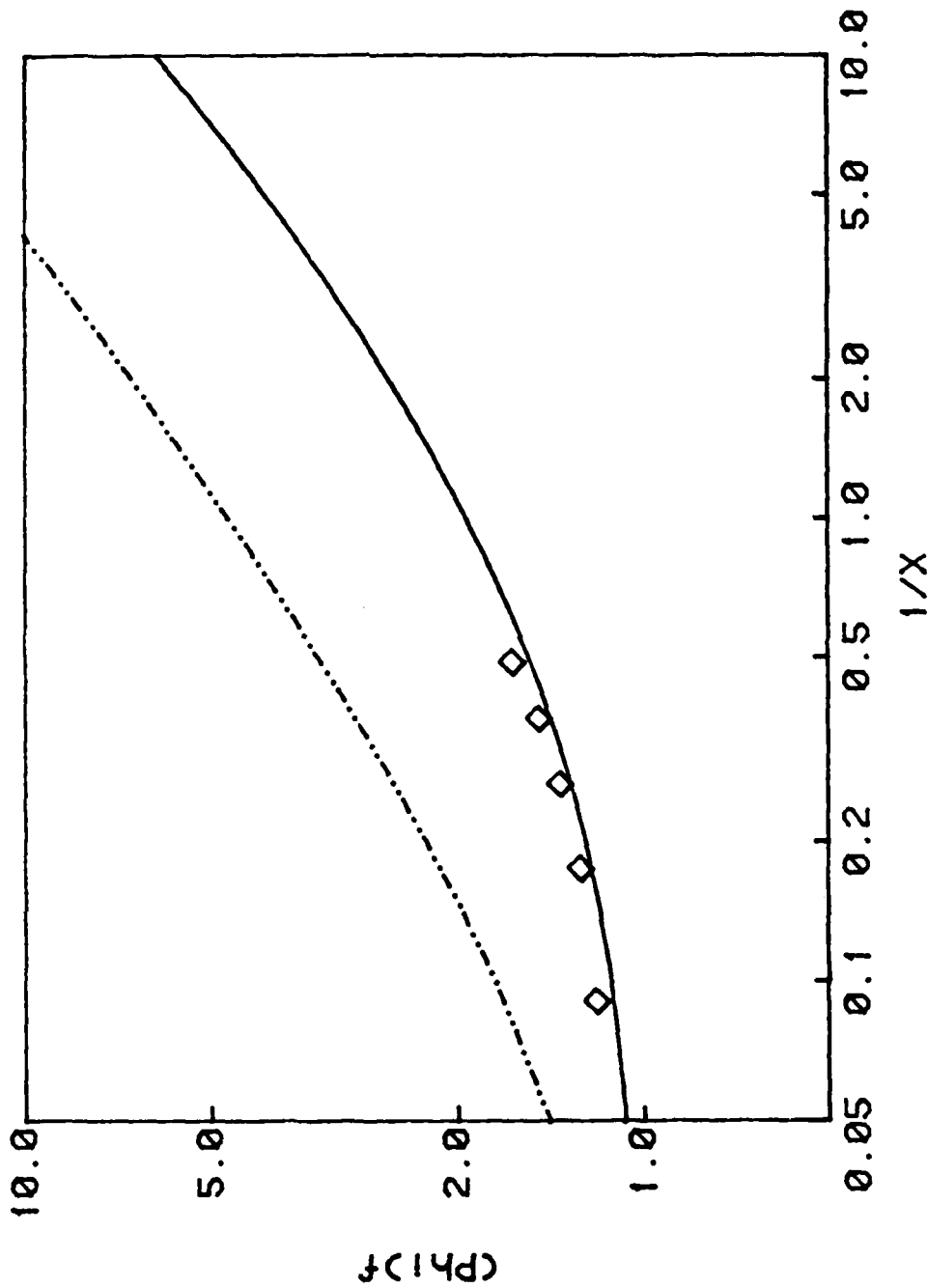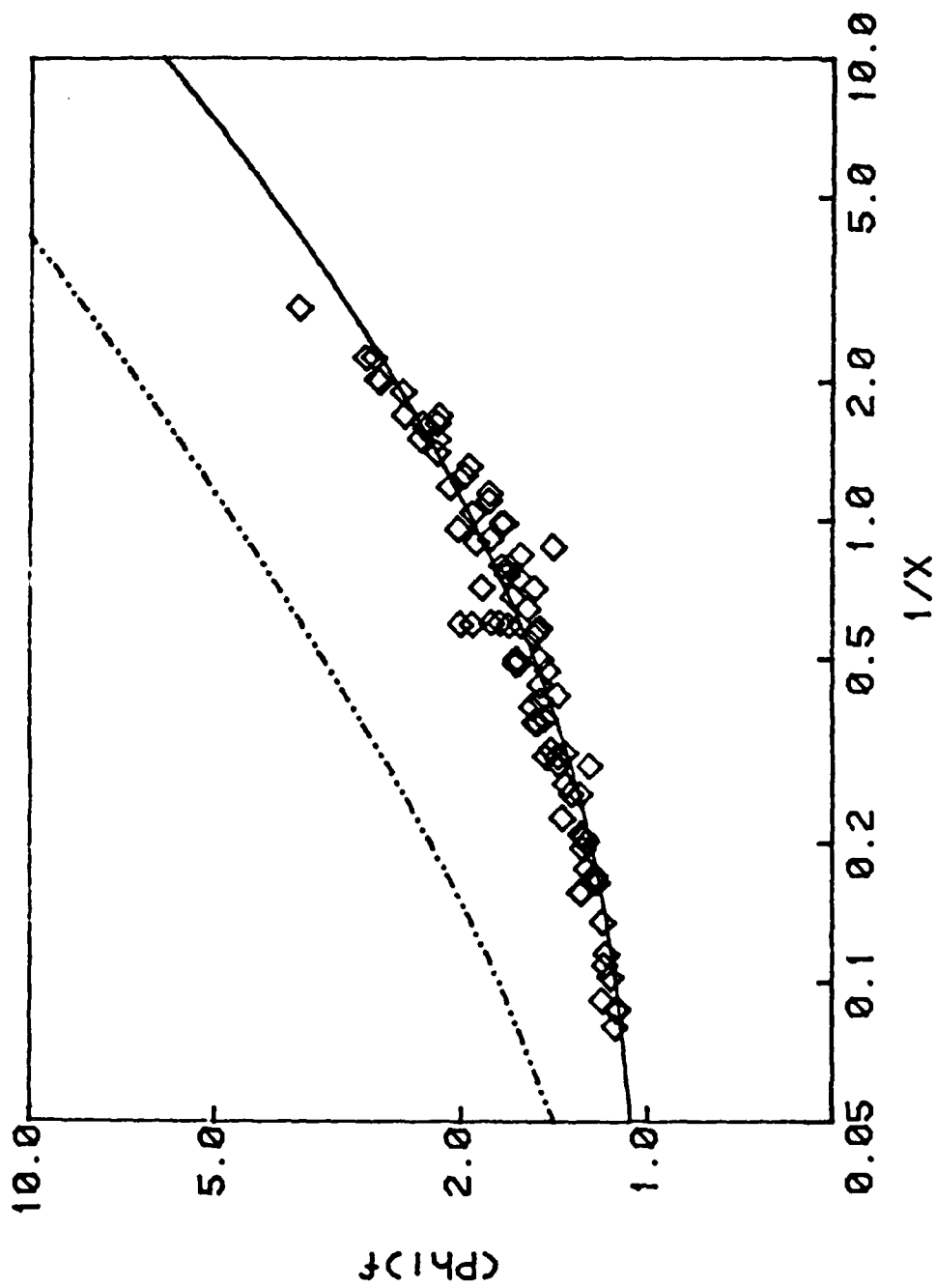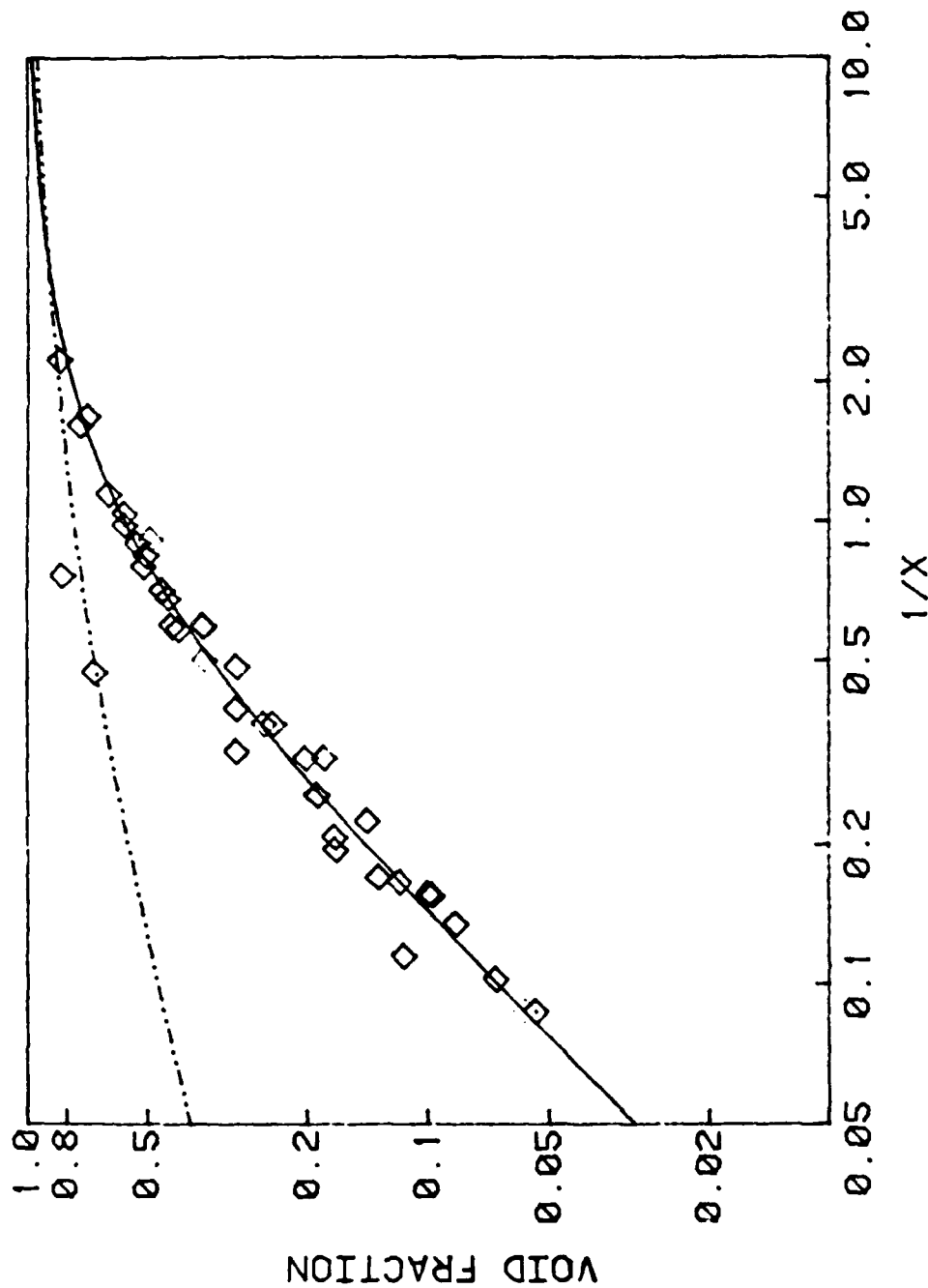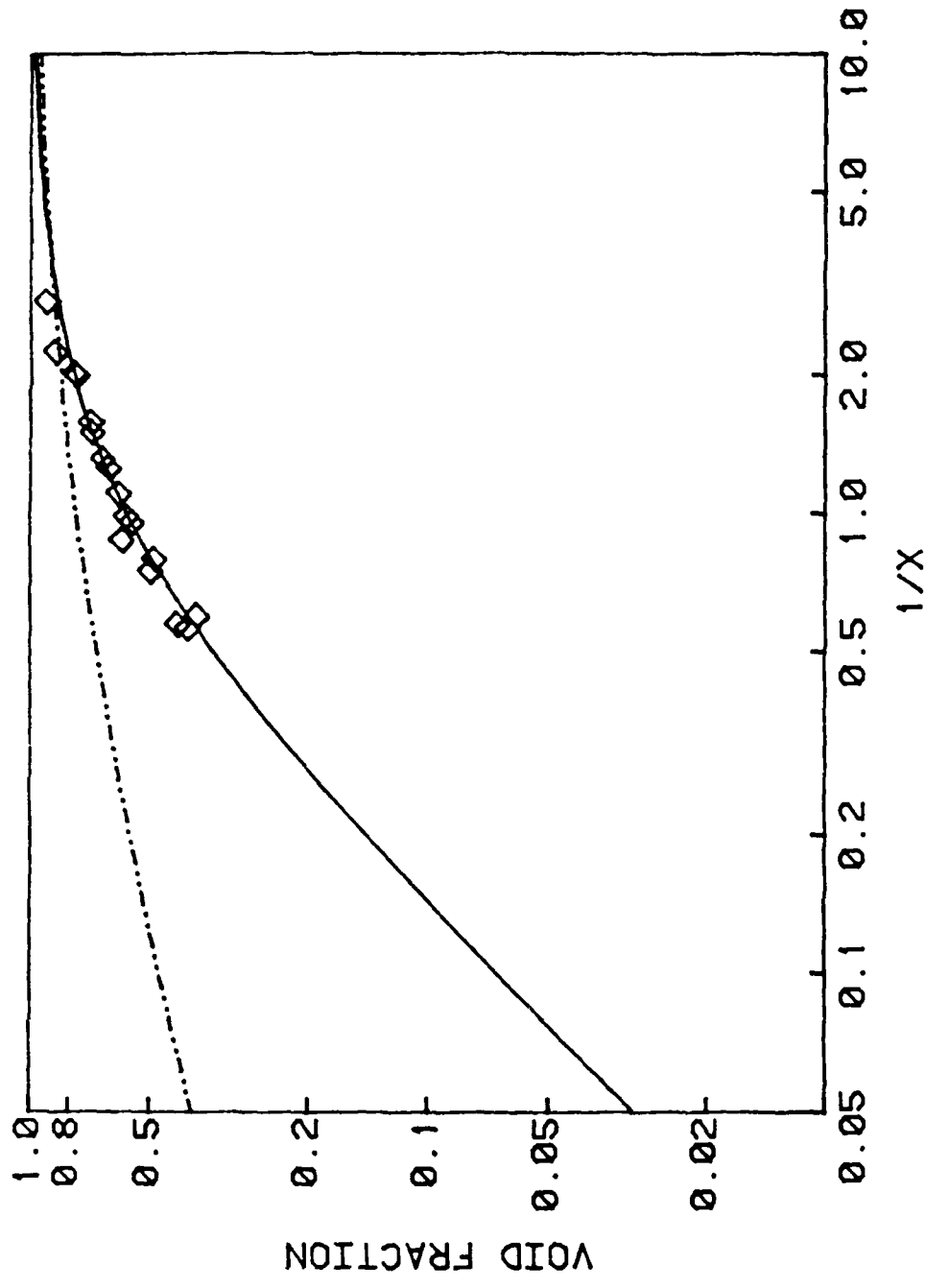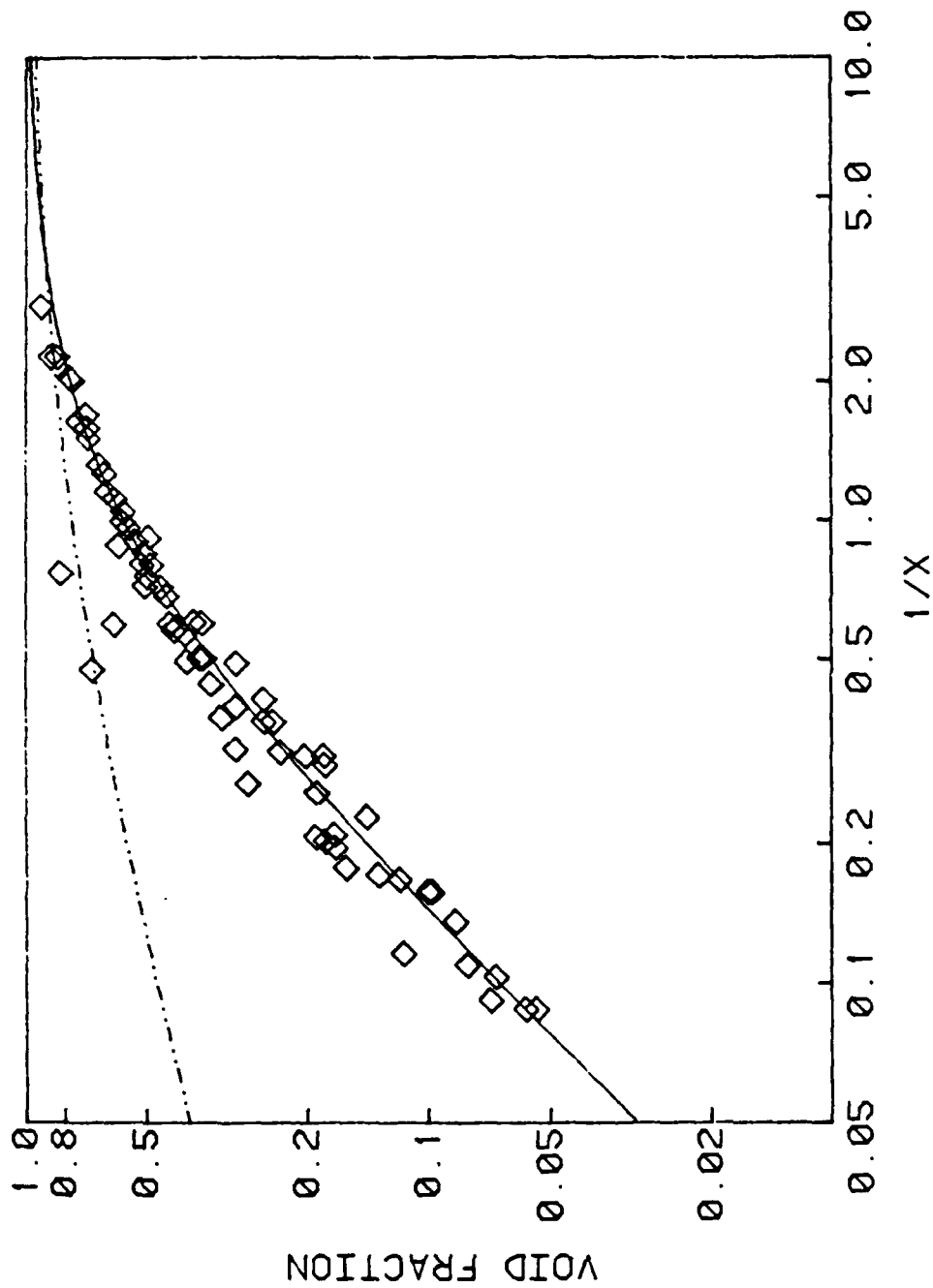Figure 2.36 Void Fraction Versus Inverse Martinelli Parameter for DT-LF/Water Flow With Bubbly Flow Mixing Section for All the Data Points. The Solid Curve Coresponds to Equation 2.3 and the Dashed-Dotted Curve to Equation 2.4.

2-56

Section 3

BUBBLY FLOW VOID DISTRIBUTION AND FRICTION MULTIPLIER

In the absence of gravity, the distribution of bubbles in a bubbly mixture within a pipe is controlled by the drag force, the lift force, and the turbulent fluctuations in the liquid phase. Since the ratio of the surface area to volume of the bubbles is large, the bubbles are expected to flow at nearly the same velocity as the liquid in the axial direction. However, since the lift force and turbulent fluctuations cause the bubbles to migrate towards the region of higher velocity (axis of the pipe), a void distribution will be established in the radial direction. Even though the flow can be assumed to be in a local homogeneous condition (due to nearly equal phase velocities), homogeneous flow assumptions cannot be made and the slip ratio would be different from unity due to the non-homogeneous void distribution in the radial direction.

Separated flow conservation equations are used to obtain a mathematical model for the flow. The governing equations which consist of the momentum conservation for the liquid and vapor phases, and mass conservation for the liquid phase are solved to develop a method for calculating the void distribution and two-phase friction multiplier for the bubbly flow under zero gravity conditions. The approach is similar to the method used by Wang, Ref. (34). However, the lift force relations used are different, and in the present study several assumptions unique to the zero gravity conditions can be made which enabled us to develop a general solution for the desired parameters.

3.1 GOVERNING EQUATIONS AND THE METHOD OF ANALYSIS

For a steady adiabatic two-phase flow with negligible interfacial mass and momentum transfer, the general form of the conservation equations in a two-dimensional cartesian coordinate is:

Mass

$$\frac{\partial(\rho_k\alpha_k u_k)}{\partial x} + \frac{\partial(\rho_k\alpha_k v_k)}{\partial y} = 0 \qquad (3.1)$$

Momentum

x dir.
$$\frac{\partial}{\partial x}(\rho_k\alpha_k u_k^2) + \frac{\partial}{\partial y}(\rho_k\alpha_k u_k v_k) = -\alpha_k\frac{\partial P}{\partial x} + \frac{\partial}{\partial x}(\alpha_k\sigma_{xx}) \qquad (3.2)$$

$$+ \frac{\partial}{\partial y}(\alpha_k\tau_{xy}) + F_{Bx}$$

y dir.
$$\frac{\partial}{\partial x}(\rho_k\alpha_k v_k u_k) + \frac{\partial}{\partial y}(\rho_k\alpha_k v_k^2) = -\alpha_k\frac{\partial P}{\partial y} + \frac{\partial}{\partial x}(\alpha_k\tau_{xy}) \qquad (3.3)$$

$$+ \frac{\partial}{\partial y}(\alpha_k\sigma_{yy}) + F_{By}$$

where u and v are the phasic velocities in the x and y direction, respectively, σ and τ are components of the total stress tensor, F_B is the body force, and the subscript k refers to the liquid (L) or vapor (G) phases. Therefore $\alpha_L = 1-\alpha$ and $\alpha_v = \alpha$.

For a bubbly flow in a pipe where x is the axial direction and y is transverse or lateral direction measured from the wall, the conservation equations for the continuous phase, liquid, become

Mass

$$\frac{\partial}{\partial x} [(1-\alpha) u_L] + \frac{\partial}{\partial y} [(1-\alpha) v_L] = 0 \qquad (3.4)$$

Momentum

x dir.:

$$\frac{\partial}{\partial x} [(1-\alpha) u_L^2] + \frac{\partial}{\partial y} [(1-\alpha) u_L v_L] = -\frac{1}{\rho_L} (1-\alpha) \frac{\partial P}{\partial x} + \frac{1}{\rho_L} \frac{\partial}{\partial x} [(1-\alpha)\sigma_{xx}]$$

$$+ \frac{1}{\rho_L} \frac{\partial}{\partial y} [(1-\alpha) \tau_{xy}] \qquad (3.5)$$

y dir.:

$$\frac{\partial}{\partial x} [(1-\alpha)v_L u_L] + \frac{\partial}{\partial y} [(1-\alpha)v_L^2] \approx -\frac{1}{\rho_L} (1-\alpha) \frac{\partial P}{\partial y} + \frac{1}{\rho_L} \frac{\partial}{\partial x} [(1-\alpha) \tau_{xy}]$$

$$+ \frac{1}{\rho_L} \frac{\partial}{\partial y} [(1-\alpha) \sigma_{yy}] - \frac{M_L}{\rho_L} \qquad (3.6)$$

where M_L in the above equation is the lift force on the bubbles which is the only body force in the absence of buoyancy.

For a steady fully developed flow $\partial/\partial x = 0$. Using the conservation of mass, equation (3.4), it can be shown that $v_L = 0$ and therefore the inertial terms in equation (3.6) are neglected. Considering that the velocities in turbulent flow consist of a mean and fluctuating component as

$$u = \overline{u} + u' \qquad v = \overline{v} + v'$$

The total stress tensor is broken down into viscous or laminar and turbulent stresses as given below.

$$\underline{\tau} = \begin{pmatrix} \sigma_{xx} & \tau_{xy} \\ \tau_{yx} & \sigma_{yy} \end{pmatrix}$$

$$= \begin{pmatrix} 2\mu \dfrac{\partial \overline{u}}{\partial x} - 2/3\, \mu\theta - \rho\overline{u'}^2 & \mu \left(\dfrac{\partial \overline{u}}{\partial y} + \dfrac{\partial \overline{v}}{\partial x}\right) - \rho\overline{u'v'} \\[3ex] \mu \left(\dfrac{\partial \overline{u}}{\partial y} + \dfrac{\partial \overline{v}}{\partial x}\right) - \rho\overline{u'v'} & 2\mu \dfrac{\partial \overline{v}}{\partial y} - 2/3\, \mu\theta - \rho\overline{v'}^2 \end{pmatrix} \qquad (3.7)$$

$$\theta = \frac{\partial \overline{u}}{\partial x} + \frac{\partial \overline{v}}{\partial y}$$

In transverse, y direction, the viscous stresses can be neglected and equation (3.6) reduces to

$$- (1-\alpha) \frac{\partial P}{\partial y} - (1-\alpha) \frac{\partial}{\partial y} \left(\rho_L \overline{v'^2}\right) - \rho_L \overline{v'^2} \frac{\partial}{\partial y} (1-\alpha) - M_L = 0 \qquad (3.8)$$

The conservation of momentum for the discontinuous phase, vapor, reduces to the balance between the pressure and lift forces.

$$- \alpha \frac{\partial P}{\partial y} + M_L = 0 \qquad (3.9)$$

eliminating $\partial P/\partial y$ from equations (3.8) and (3.9) results in the following equation for the void distribution in y direction.

$$\frac{\partial (1-\alpha)}{\partial y} + \frac{1-\alpha}{\overline{v'^2}} \frac{d\overline{v'^2}}{dy} + \frac{1}{\rho_L \overline{v'^2}} \frac{M_L}{\alpha} = 0 \qquad (3.10)$$

In order to solve for the velocity distribution which is needed for evaluating the lift force and calculating the pressure drop, the relation for the total shear stress is employed:

$$\tau = \mu_L \frac{d\overline{u}_L}{dy} - \rho_L \overline{u'v'} \qquad (3.11)$$

The turbulent stress in the above equation can be expressed in terms of the eddy diffusivity, non-dimensionalized and solved for the liquid velocity, if the eddy diffusivity relation in two-phase flow can be specified. However, the experimental results of Refs. (34) and (35) have shown that the turbulent stresses are strongly affected by the presence of bubbles. Therefore, the single-phase relations for the eddy diffusivity have to be modified to account for the turbulence induced by bubbles.

3.1.1 Lift Force

The lift force acts on a particle within the fluid shear layer or on a rotating particle in the absence of shear. At high relative velocities, a rotating particle may experience a large lift force which is called the Magnus effect (36). This force acts perpendicular to the direction of the flow and in the case of pipe flow drives the particle to regions of higher velocity, center of the tube. This force is normally neglected in earth gravity conditions where the drag and buoyancy forces are dominant. At small relative velocities, the lift force due to free particle rotation was given by Rubinow and Keller (37) as

$$F_L = \frac{\pi}{8} d^3 \rho \, \Omega \, u \tag{3.12}$$

where Ω is the angular velocity which for a freely rotating particle is given by

$$\Omega = 1/2 \frac{du}{dy}$$

d is the particle diameter, and ρ is the density of the fluid around the particle.

Saffman (38), (39) has shown that when the relative velocity between the particle and the liquid is small and the fluid Reynolds number is large, lift force due to particle rotation is less by an order of magnitude than that due to shear. The lift force due to shear is given by

$$F_L = 6.46 \, \mu^{1/2} \, \rho^{1/2} \, (u_L - u_v)^2 \left(\frac{du_L}{dy}\right)^{1/2} \tag{3.13}$$

where μ is the fluid viscosity.

Lift force per unit volume of total flow becomes

$$M_L = 1.4 \, \alpha \, \mu_L^{1/2} \, \rho_L^{1/2} \, (u_L - u_v) \, d^2 \left(\frac{du_L}{dy}\right)^{1/2} \tag{3.14}$$

In the absence of gravity, the bubbles will travel at the same velocity as the local fluid. However, if the center of mass of bubble travels at the velocity u_L, the velocity of the liquid at the surface of the bubble would be

$$u_L \pm \frac{1}{2} \frac{du_L}{dy} d$$

3-6

This means that the relative velocity is proportional to $1/2 \ du_L/dy \ d$. Assuming that the Saffman relation, equation (3.14), can be used for the lift force on the bubbles, the force per unit volume becomes

$$M_L = 0.7 \ \alpha \ \mu_L^{1/2} \ \rho_L^{1/2} \ (\frac{du_L}{dy})^{3/2} \tag{3.15}$$

Since the bubble is actually surrounded by a two-phase mixture of vapor and liquid, an effective viscosity, Ref. (40), is used in the present analysis to account for the existence of the neighboring bubbles.

$$M_L = 0.7 \ \alpha \ \mu_{eff}^{1/2} \ \rho_L^{1/2} \ (\frac{du_L}{dy})^{3/2} \tag{3.16}$$

$$\mu_{eff} = \frac{x \ \rho_L \ \mu_G + (1-\alpha) \ \rho_G \ \mu_L}{x \ \rho_L + (1-x) \ \rho_G}$$

3.1.2 Turbulent Eddy Diffusivity

Early efforts for analyzing the velocity distribution in bubbly two-phase flow treated the mixture as a continuous medium. Turbulent exchanges of momentum and density were introduced to evaluate the velocity and density (or void) distributions. Levy (41) used this approach with the single-phase turbulent mixing length relations to calculate the pressure drop and void distribution. Bankoff (42) assumed uniform stress distribution and employed the single-phase mixing length relation.

Starting with the original studies of Serizawa et al. (35) and Sullivan et al. (43) on the turbulence structure of bubbly two-phase mixtures, a series of efforts followed which concentrated on the effect of bubbles on the liquid phase turbulence and the void distribution in bubbly flow (44, 45, 34). These studies have shown that the turbulence intensity increases when bubbles are introduced in the flow and in comparison to

single-phase flow it becomes flatter within the core. For moderate liquid velocities, the turbulent stresses increase with increasing superficial velocity of vapor, J_G.

In order to account for the effect of bubbles on the turbulent stresses, Ref. (46) suggests an eddy diffusivity due to bubble agitation. Equation (3.11) for the total shear stress becomes

$$\tau = \mu_L \frac{d\overline{u}_L}{dy} - \rho_L \overline{u'v'} - \rho_L \overline{u''v''} \tag{3.17}$$

The second term in the above equation is the single-phase turbulent stress component and a single-phase eddy diffusivity relation can be used for the purpose of the present study. The third term on the right hand side is the enhancement due to the presence of bubbles. Based on the analysis of potential flow over a sphere, a relation for $\overline{u''v''}$ is developed in Ref. (46) as follows:

$$\overline{u''v''} = - C \, \alpha \, \frac{d\overline{u}_L}{dy}$$

where C depends on the average size and velocity of the bubbles. Equation (3.17) will therefore become

$$\tau = \mu_L \frac{d\overline{u}_L}{dy} + \rho_L \, \epsilon' \, \frac{d\overline{u}_L}{dy} + \rho_L \, C \, \alpha \, \frac{d\overline{u}_L}{dy} \tag{3.18}$$

For the single-phase eddy diffusivity, Spalding's relation, Ref. (47),

$$\epsilon' = \frac{\mu_L}{\rho_L} (0.044) \left[e^{0.4u^+} - 1 - 0.4u^+ - 0.08u^{+2} \right] \qquad (3.19)$$

which is continuous from the sublayer into the core is used. Since this diffusivity results in a non-zero velocity gradient at the center of the pipe, Reichardt's relation, Ref. (48), which is proposed for the center regions of the pipe can be used in the turbulent core. This relation is given as

$$\epsilon' = \frac{\mu_L}{\rho_L} (0.067) \left[1 - (1 - \frac{y}{R_0})^2 \right] \left] 1 + 2 (1 - \frac{y}{R_0})^2 \right] \qquad (3.20)$$

where R_0 is the radius of the tube.

3.2 NON-DIMENSIONAL EQUATIONS AND METHOD OF SOLUTION

Substituting the relation for lift force from equation (3.16) in equation (3.10) results in

$$\frac{\partial (1-\alpha)}{\partial y} + \frac{1-\alpha}{\overline{v'^2}} \frac{d\overline{v'^2}}{dy} + 0.7 \frac{\mu_{eff}^{1/2} \rho_L^{-1/2}}{\overline{v'^2}} (\frac{du_L}{dy})^{3/2} = 0 \qquad (3.21)$$

Considering that

$$\tau = \tau_w (1 - \frac{y}{R_0})$$

equation (18) becomes

$$\frac{du_L}{dy} = \frac{\tau_w (1 - \frac{y}{R_0})}{\mu_L + \rho_L \epsilon' + \rho_L C \alpha} \qquad (3.22)$$

Equations (3.21) and (3.22) are non-dimensionalized in terms of the following variables

$$y^+ = y \ \frac{\sqrt{\dfrac{\tau_w}{\rho_L}}}{\mu_L} \ \rho_L$$

$$u^+ = \frac{u}{\sqrt{\dfrac{\tau_w}{\rho_L}}} \tag{3.23}$$

to result in

$$\frac{d(1-\alpha)}{dy^+} + \frac{1-\alpha}{\overline{v'^{+2}}} \ \frac{d\overline{v'^{+2}}}{dy^+} + \frac{0.7}{\overline{v'^{+2}}} \ \left(\frac{du^+}{dy^+}\right)^{3/2} = 0 \tag{3.24}$$

$$\frac{du^+}{dy^+} = \frac{1 - \dfrac{y^+}{R^+}}{1 + C\,\alpha + 0.044 \ [e^{0.4u^+} -1 -0.4u^+ -0.08u^{+2}]} \tag{3.25}$$

In the above equation u^+ is the non-dimensional mean liquid velocity, $\overline{u_L^+}$, and the bar and subscript L are dropped from now on. The above differential equations can be solved simultaneously for α and u^+ if $\overline{v'^{+2}}$ variation is known.

Comprehensive measurements of single-phase turbulence structure including velocity profile, turbulent fluctuations, and Reynold stresses have been reported by Laufer (46). Variation of $\sqrt{\overline{v'^{+2}}}$ for different Reynolds numbers is shown in Figure 3.1. It is apparent that $\overline{v'^{+2}}$ peaks near the wall and then decreases toward the center of the tube and the peak value is a function of the Reynolds number. For a bubbly two-phase

3-10
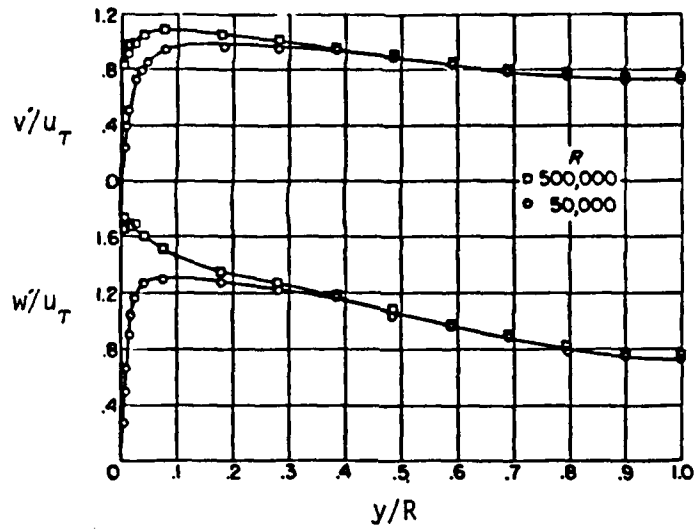
Figure 3.1 - Distribution of v'/u and w'/u

$$v' = \sqrt{\overline{v'^2}} \qquad u_\tau = \sqrt{\frac{\tau_w}{\rho}}$$

flow, the variation of $\overline{v'^{+2}}$ is similar to Figure 3.1, in that it peaks
to a maximum near the wall and levels off at positions also close to the
wall, Refs. (34, 35). However, measurements of Wang (34) and Serizawa
(35) have shown that:

1. $\overline{v'^{+2}}$ peaks closer to the wall in comparison to single-phase flow.

2. $\overline{v'^{+2}}$ is considerably flatter for two-phase bubbly flow.

3. The maximum value is a function of Reynolds number and quality.

Although the general trend of $\overline{v'^{+2}}$ can be obtained from the data of
Refs. (34) and (35), systematic measurement near the wall is not
available. Closer look at the data has shown that detailed variation of
$\overline{v'^{+2}}$ is not necessary for the present analysis, and only the variation
of maximum $\overline{v'^{+2}}$ with Reynolds number and quality, along with an approxi-
mate shape representing the peaking and flattening of this parameter
over the tube cross section, is sufficient.

From equation (3.24) it can be seen that peaking of $\overline{v'^{+2}}$ will result in
a void fraction peak near the wall. Detailed cross sectional void
measurements have shown such a void peaking for vertical upward bubbly
flow at earth gravity, Refs. (34, 45, 50).

Due to lack of sufficient data on the variation of $\overline{v'^{+2}}$ in a bubbly flow
and the diffuculty in measuring the turbulent fluctuations near the
wall, an approximate shape for $\overline{v'^{+2}}$ is used in the present analysis.

It is assumed that $\overline{v'^{+2}}$ rises exponentially near the wall. It is
further assumed that the peak v'^{+2} occurs at $y/R \approx 0.08$. The following
relations are used to specify an exponentially rising and falling shape
for the parameter $\overline{v'^{+2}}$.

$$\overline{v'^{+2}} = \frac{v'_m}{120}\left[-0.54 + \frac{e^{30\left(\frac{y^+}{R^+}+0.02\right)} - e^{-30\left(\frac{y^+}{R^+}+0.02\right)}}{e^{30\left(\frac{y^+}{R^+}+0.02\right)} + e^{-30\left(\frac{y^+}{R^+}+0.02\right)}}\right] \quad \text{for } \frac{y^+}{R^+} < 0.08$$

$$\overline{v'^{+2}} = \frac{-1}{6} e^{-300\left(\frac{y^+}{R^+}-0.08\right)^2} \quad\quad\quad \text{for } \frac{y^+}{R^+} > 0.08 \quad\quad (3.26)$$

It should be emphasized that, although the relations given in equation (3.26) are arbitrarily developed but seem to be very specific, the exact form of the equation is not important. These equations are written in the above form to show an exponentially rising $\overline{v'^{+2}}$ to a maximum value at y/R = 0.08 and an exponentially falling v'^{+2}. Since the value of v'_m is correlated from our experimental data, different shapes can be used and v'_m correlation will vary. The only difference may be that the peaking of void may occur at a different radial location.

Equation (3.26) in differential form becomes

$$\frac{d\overline{v'^{+2}}}{dy^+} = \frac{v'_m}{\left[e^{30\left(\frac{y^+}{R^+}+0.02\right)} + e^{-30\left(\frac{y^+}{R^+}-0.08\right)}\right]^2} \quad\quad \frac{y^+}{R^+} < 0.08$$

$$\quad\quad (3.27)$$

$$\frac{d\overline{v'^{+2}}}{dy^+} = -100\left(\frac{y^+}{R^+}-0.08\right) e^{-300\left(\frac{y^+}{R^+}-0.08\right)^2} \quad\quad \frac{y^+}{R^+} > 0.08$$

Differential equations (3.24), (3.25), and (3.27) can be solved for α and u^+ for a given value of parameter C.

For a pipe with radius R, the average mass flux is defined as

$$G = \frac{\int \rho u \; dA}{A}$$

where

$$A = \pi R^2 \; ; \; dA = 2\pi \; rdr$$

$$G = \frac{2 \int_0^R \rho u \; rdr}{R^2}$$

Assuming that liquid and vapor travel at nearly equal velocities (local homogeneous condition), the relation for mass flux will become

$$G = \frac{2 \int_0^R [\alpha \rho_V + (1-\alpha) \; \rho_L] \; u \; rdr}{R^2}$$

Non-dimensionalizing the above equation results in

$$\frac{G}{\rho_L \sqrt{\frac{\tau_w}{\rho_L}}} = \frac{2}{R^{+2} \rho_L} \int_0^{R^+} [\alpha \rho_V + (1-\alpha) \; \rho_L] \; u^+ \; (R^+ - y^+) \; dy^+ = \gamma \quad (3.28)$$

The two-phase Reynolds number is defined as

$$Re = \frac{G(2R)}{\mu_L} = 2R^+ \; \gamma \tag{3.29}$$

The two-phase friction multiplier is defined as

$$\phi_0^2 = \frac{-\frac{(dp)}{dx}}{-\frac{(dp)}{dx}_\ell} \tag{3.30}$$

3-14

where the denominator in the above equation is the frictional pressure gradient if the total flow is assumed to flow as liquid, e.g.,

$$- \left(\frac{dp}{dx}\right)_\ell = f_0 \frac{G^2}{4\rho_L R} \tag{3.31}$$

where f_0 is the single-phase liquid friction coefficient given by the following relations:

$$f_0 = \frac{64}{Re} \qquad\qquad Re < 2300 \tag{3.32}$$

$$f_0 = 1.84 \times 10^{-4} \, Re^{0.646} \qquad 2300 < Re < 4000$$

$$f_0 = 0.316 \, Re^{-0.25} \qquad\qquad Re > 4000$$

The wall shear is given by

$$\tau_w = - \left(\frac{dp}{dx}\right) \frac{P_h}{A} = \frac{1}{8} \, \phi_0{}^2 f_0 \rho_L \left(\frac{G}{\rho_L}\right)^2 \tag{3.33}$$

Therefore, the two-phase friction multiplier becomes

$$\phi_0{}^2 = \frac{8}{\gamma^2 f_0} \tag{3.34}$$

The flow quality is defined as

$$x = \frac{w_G}{w} = \frac{w_G}{G_A} \tag{3.35}$$

$$\frac{w_G}{A} = \frac{\int \alpha u \rho_G \, dA}{A} = \frac{2\rho_G \int_0^R \alpha u \, r dr}{R^2}$$

$$= \frac{2\rho_G \int_0^R \alpha \, u \, (R-y) \, dy}{R^2}$$

The above equation in non-dimensional form becomes

$$\frac{W_G}{A} = \frac{2\rho_G \sqrt{\frac{\tau_w}{\rho_L}}}{R^{+2}} \int_0^{R^+} \alpha \, u^+ \, (R^+ - y^+) \, dy^+ \tag{3.36}$$

Using equations (3.28) and (3.36) in (3.35) results in the following relation for flow quality.

$$x = \frac{2\rho_G \int_0^{R^+} \alpha \, u^+ \, (R^+ - y^+) \, dy^+}{\rho_L \, R^{+2} \, \gamma} \tag{3.37}$$

The cross sectional average void fraction is defined as

$$\bar{\alpha} = \frac{\int \alpha \, dA}{A} = \frac{2 \int_0^R \alpha \, r \, dr}{R^2}$$

in non-dimensional form this equation becomes

$$\bar{\alpha} = \frac{2 \int_0^{R^+} \alpha \, (R^+ - y^+) \, dy^+}{R^{+2}} \tag{3.38}$$

Equations (3.28), (3.37), and (3.38) can be expressed in differential form as follows:

$$\frac{d\gamma'}{dy^+} = \frac{2}{\rho_L \, R^+} \, [\alpha \, \rho_v + (1-\alpha) \, \rho_L] \, u^+ \, (1 - \frac{y^+}{R^+}) \tag{3.39}$$

3-16

$$\gamma = \frac{2\gamma'}{\rho_L R^+}$$

$$\frac{dx'}{dy^+} = \alpha \, u^+ \left(1 - \frac{y^+}{R^+}\right) \tag{3.40}$$

$$x = \frac{2 \, x' \, \rho_G}{\rho_L \, R^+ \, \gamma}$$

$$\frac{d\alpha}{dy^+} = \frac{2 \, \alpha \left(1 - \frac{y^+}{R+}\right)}{R^+} \tag{3.41}$$

For a given value of the parameters C and R^+, the differential equations (3.24), (3.25), (3.27), (3.39), (3.40), and (3.41) can be solved simultaneously from the wall to R^+ to get values for α, x, ϕ_o^2 and Re (or G for known R). For given fluid properties and pipe diameter, there is only one combination of C and R^+ that results in the desired G and x combination. Therefore, for every G (or Re) and x combination, the solution for void fraction and two-phase friction multiplier can be obtained.

3.2.1 Boundary Conditions

In order to solve the above differential equations, the boundary conditions at the wall should be known. Since the non-dimensional turbulent fluctuation, v'^2 is zero at the wall, equation (3.24) is not defined at the wall. The integration starts from a point very close to the wall where all liquid conditions can be assumed and the state variables can be defined. $y^+ = 0.1$ is within the laminar sublayer and sufficiently close to the wall where a zero void assumption can be made. Therefore, at $y^+ = 0.1$

$$\alpha = 0.0$$
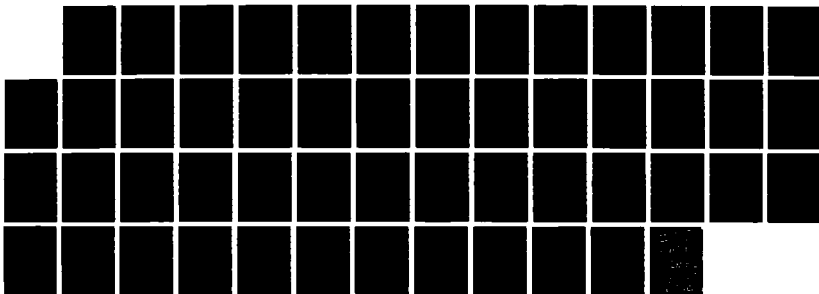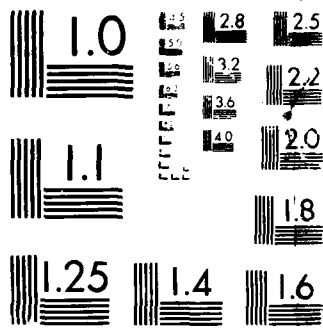
MICROCOPY RESOLUTION TEST CHART
NATIONAL BUREAU OF STANDARDS 1963

$$u^+ = 0.1$$

$$\gamma = \frac{2}{R^+} \left[\frac{(0.1)^2}{2} - \frac{(0.1)^3}{3R^+} \right] \approx \frac{0.01}{R^+} \qquad (3.42)$$

$$x = 0$$

$$\overline{\alpha} = 0$$

3.2.2 Method of Solution

A computer program, ZGBUB, was developed to solve the six differential equations, (3.24), (3.25), (3.27), (3.39), (3.40), and (3.41) from the boundary condition given above up to a specified R^+. This program uses the SFODE integration algorithm which solves a system of ordinary differential equations using Adams Predictor-Corrector method. ZGBUB was written in FORTRAN, and the calculations were performed on an IBM-PC/XT (with MS-DOS operating system) and a MicroVax-II (with VMS operating system). All the routines were written in double precision to reduce the round-off errors.

In order to solve the differential equations for α, x, ϕ_0^2, and G the values of v'_m in equation (3.26) and parameter C in equation (3.25) should be known. The experimental data for silicone-water and Dowtherm-water experiments described in Section 2 was used to obtain the values of C and v'_m. As will be discussed later, only a correlation for v'_m in terms of Re and x is needed to close the problem. For a given set of fluid properties and pipe diameter, there are only unique values of C and R^+ which can result in a desired G and x combination. Therefore, iteration on different values of C and R^+ can be performed to give the needed G and x which will also provide ϕ_0^2 and α values.

3-18

3.3 RESULTS AND DISCUSSION

The empirical parameters in the present analysis are v'_m which is the maximum value for the turbulent intensity (v'^{+2}) and C which is the coefficient for the eddy diffusivity due to the presence of bubbles. As mentioned earlier, the data from Refs. (34), (44), (45) and (46) show that the turbulent intensity peaks to a maximum value near the wall (y/R between 0.05 to 0.1) and unlike the single-phase flow, it decreases rapidly and flattens out for y/R > 0.1. In addition, the value of v'_m is a function of liquid Reynolds number and the vapor phase content. The parameter C depends on the average bubble size and velocity.

The experimental program and results for silicon-water and Dowtherm-water tests were discussed in the previous sections. The reduced data consisted of cross sectional average void fraction and two-phase friction multiplier for the given mass flux (G) and quality (x). As mentioned earlier, due to high phase velocities, photographic methods for visual determination of flow regimes were not possible in the present experiments. However, the differential pressure measurements and the Auburn meter measurement gave an indication of departure from bubbly flow. Generally, this occured around void fraction of 0.3. Therefore, the tests where we had a bubbly flow simulation could be identified and used in the present analysis.

Silicon-water and Dowtherm-water properties were used in the ZGBUB program to find the measured two-phase friction multiplier for the given combination of mass flux and flow quality. Only the bubbly flow tests were used for this purpose and the test conditions are given in Table 3.1. Only one combination of R^+, v'_m, and C could be found to match the data. The predicted values of v'_m and C are given in Table 3.2.

A computer program which obtains a weighted least square fit of a user specified function to data values by means of stepwise Gauss-Newton

3-19

Table 3.1

TEST CONDITIONS FOR BUBBLY FLOW SIMULATION TESTS

TEST #	Volume Flow (GPM)		Total Mass Flux (Lbm/ft2/s)	Quality	Reynolds Number
	Silicon	Water			
10	16.59	1.41	767.1	0.083	7630
14	12.76	5.00	767.0	0.295	7630
15	13.40	4.40	767.0	0.259	7630
16	14.67	3.20	766.6	0.189	7626
17	15.31	2.60	766.6	0.153	7626
19	16.59	1.41	767.1	0.083	7630
20	12.76	5.00	767.0	0.295	7630
44	17.55	2.40	852.6	0.127	8481
45	16.27	3.59	852.1	0.190	8476
46	13.72	5.99	852.5	0.318	8480
47	18.20	1.80	853.0	0.095	8485
48	16.91	3.00	852.5	0.159	8480
51	22.33	1.70	1023.6	0.075	10182
52	17.86	5.90	1023.9	0.260	10185
54	20.42	3.50	1024.0	0.155	10186
56	23.60	2.70	1122.6	0.109	11167
58	21.69	4.50	1123.0	0.181	11171
60	19.14	6.90	1123.4	0.278	11175
81	17.55	1.41	899.8	0.072	18398
82	16.27	2.70	898.7	0.139	18376
83	14.99	3.99	897.6	0.205	18353
86	15.31	1.48	796.9	0.086	16293
87	14.04	2.77	795.7	0.161	16270
88	12.76	4.06	794.6	0.236	16247
91	7.98	1.53	449.8	0.157	9197

Table 3.2

VALUES OF v' AND C FOR BUBBLY FLOW SIMULATION TESTS

TEST #	Total Mass Flux (Lbm/ft2/s)	Quality	v'	C
10	767.1	0.083	5460	-18.40
14	767.0	0.295	19000	-3.39
15	767.0	0.259	14100	-5.79
16	766.6	0.189	7900	-6.15
17	766.6	0.153	6700	-8.60
19	767.1	0.083	5310	- 14.00
20	767.0	0.295	18000	-2.70
44	852.6	0.127	4775	-5.70
45	852.1	0.190	5730	-3.00
46	852.5	0.318	12950	-1.10
47	853.0	0.095	4629	-10.20
48	852.5	0.159	5158	-3.90
51	1023.6	0.075	3184	-3.45
52	1023.9	0.260	4775	1.00
54	1024.0	0.155	3811	-1.80
56	1122.6	0.109	2994	-0.50
58	1123.0	0.181	3280	1.55
60	1123.4	0.278	4224	2.10
81	899.8	0.072	1776	12.00
82	898.7	0.139	2027	9.55
83	897.6	0.205	2305	7.10
86	796.9	0.086	2107	6.30
87	795.7	0.161	2412	3.50
88	794.6	0.236	2940	1.00
91	449.8	0.157	4730	-3.80

iterations was used to correlate v'_m and C. This nonlinear least squares regression program, BMD07R, is part of the SIGSTAT statistical package, Ref. (51), and can have as many as 10000/n variables, where n is the number of observations. For our purposes there are two independent variables namely, Reynolds number defined as

$$Re = \frac{GD}{\mu_L}$$

and quality x.

The predicted values for v'_m and C, given in Table 3.2, were used to find the functions of independent variables which represent the variations of v'_m and C. These functions were then used in BMD07R to find the parameters which would fit the predicted values. The best fit for v'_m values is given below.

$$v'_m = 34.71\ e^{-5.0[x^{-0.387} -7.7(Re\ 10^{-3})^{-0.499}]} + 345.95(10^{-5}Re)^{-1.038}$$

$$(3.43)$$

Comparison of the predicted values of v'_m from Table 3.2 and those obtained from the above relation is shown in Figure 3.2. The deviation is within ±20%. A fit for the parameter C in terms of the Reynolds number and quality was also found. It should be noted that since C depends on the average bubble size and velocity, this type of fit will not be useful to define its variation and a third independent parameter may be needed. This parameter should depend on the fluid properties including interfacial tension. However, data from a range of fluids with varying properties is needed to establish such a parameter.

As mentioned earlier, for a given combination of G and x there is a unique solution which can be obtained with specific values of C and R^+.
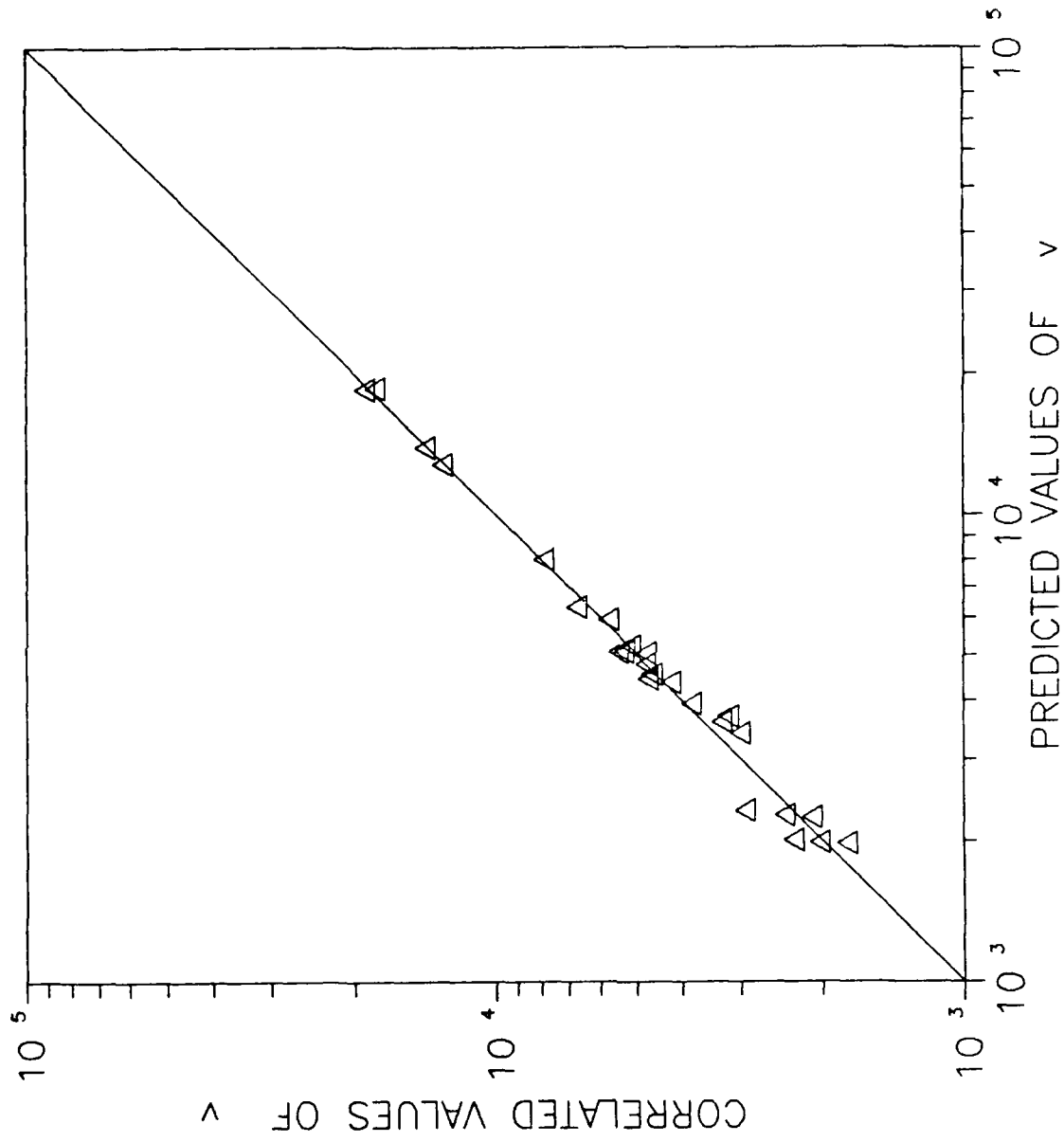
Figure 3.2 — Comparison of Correlated and Fitted Values
of the parameter v

Therefore, functional variation of the parameter C is not necessary for obtaining the predictions for the two-phase friction multiplier and void fraction. However, knowledge of such a correlation will eliminate the need for iteration on C and R^+ values in order to match the G and x combination.

Obviously, the two-phase friction multiplier predicted by the present method would fit the silicon-water and Dowtherm-water data fairly well since it was based on those results. A comparison of the predicted and measured two-phase multipliers is shown in Figure 3.3. It should be noted that the data and predictions for void fraction and friction pressure drop are very close to the results of the Homogeneous Equilibrium Model (HEM). The two-phase friction multiplier and void-quality relation from HEM are:

$$\phi_o^2 = 1 + \frac{\rho_L - \rho_G}{\rho_G} x \tag{3.44}$$

$$\alpha = \frac{x}{x + \frac{\rho_G}{\rho_L}(1-x)} \tag{3.45}$$

The present model assumes a local homogeneous condition but allows for void distribution within the cross section. This results in void peaking near the wall but nearly a flat void distribution a small distance away from the wall. The reason for homogeneous behavior of the data is believed to be the equal density of fluids rather than an inherent condition in the absence of buoyancy. If the model developed based on the above data is mechanistically based and represents the physical phenomenon, it should account for different fluid conditions and will not necessarily predict close to HEM at all times. Actually, it will be shown later that the proposed model predicts considerably different pressure drop behavior than HEM for gas-liquid flow at zero gravity.
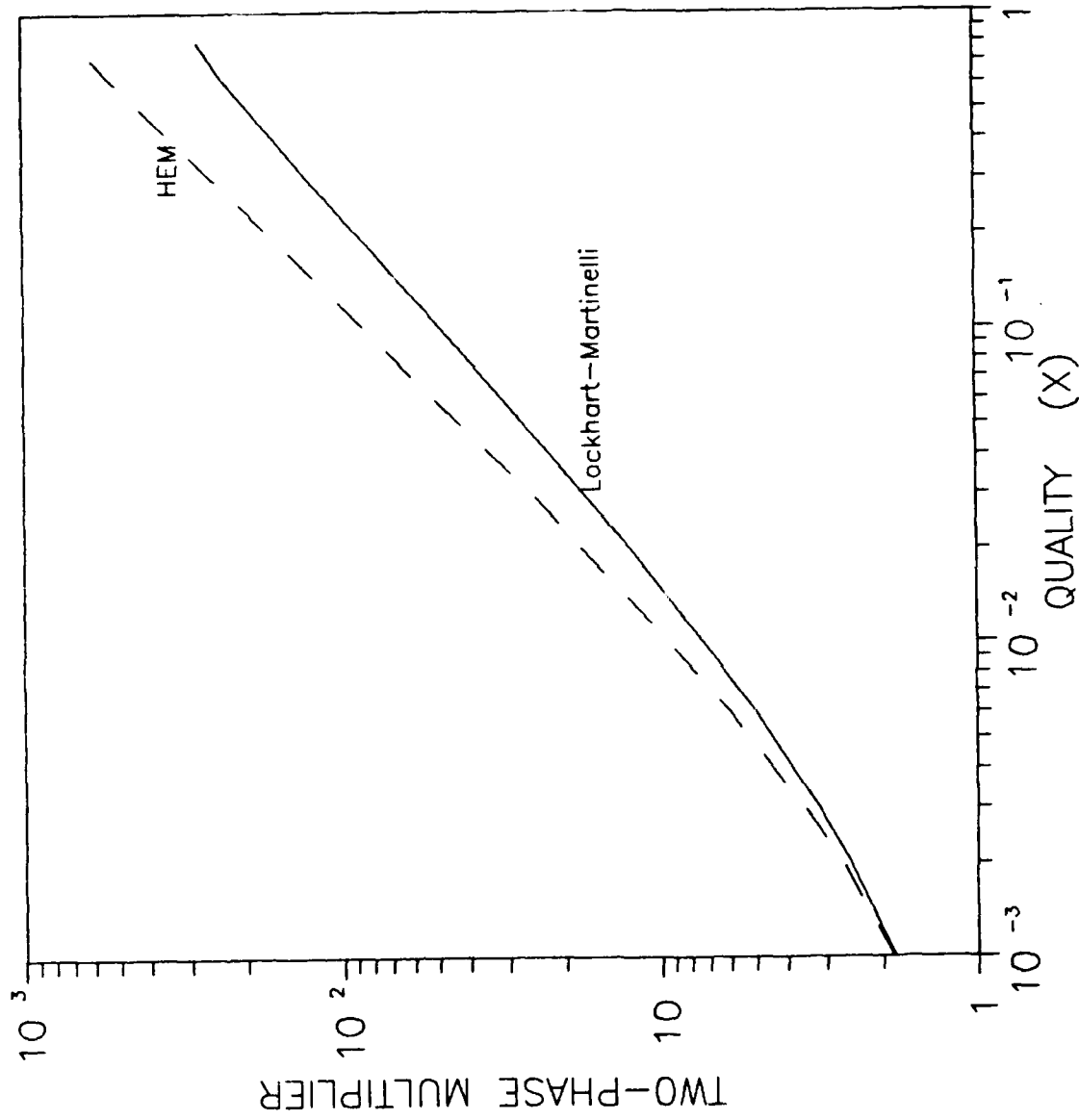
Figure 3.3– Two-Phase Friction Multiplier Using HEM
and Lockhart–Martinelli for Air/Water at 14.7 psi

3-25

However, the predicted cross sectional average void fractions are essentially the same as HEM. Apparently, the void peaking near the wall and the absence of phase slip results in much larger two-phase pressure drop.

In order to evaluate the predictive capability of this model, it should be compared with the true zero gravity adiabatic gas-liquid data. As discussed earlier, there is practically no zero gravity bubbly flow data which can be used for our purpose. Results of a series of adiabatic two-phase flow tests aboard a KC-135 aircraft flying in a parabolic trajectory have been reported in Ref. (52). These tests were mostly performed in slug and annular flow regimes, and in addition to the flow regime transitions, have qualitatively shown that in comparison to earth gravity conditions, the pressure drop significantly increases. As discussed earlier, the majority of two-phase flow studies at zero gravity are presently in progress and the results should be available by early 1988. Among these, only the results of a series of tests by Battelle Laboratories, Ref. (53), have been made available to us. These tests consisted of a set of convective boiling tests with water and a set of adiabatic nitrogen/water tests at atmospheric conditions. Unfortunately, these tests did not cover the whole range of flow regimes and only two sets of conditions may have been in the bubble regime. Close examination of these tests showed that the flow was laminar and the present model can not be used to predict the results. However, it was generally concluded that, (27), the pressure drop was higher than expected under earth gravity conditions. The air/water tests performed by the University of Houston, Ref. (54), aboard the NASA learjet covered the entire range of flow regimes. These tests were mainly aimed at flow regime identification and the pressure drop results have not been published yet.

Since the present model does not have a closed form solution and contains an iterative approach, solutions can only be developed for specific fluid

conditions and test section geometry. In order to provide predictions which can be used in design of spacecraft thermal management systems, a series of results for selected fluids are presented here. In addition, the predictions for the test conditions of the zero gravity experimental efforts in progress are presented and compared to earth gravity models. These predictions can be compared with the test results when published.

A majority of the separated flow models for two-phase friction pressure drop under earth gravity conditions are empirical and only a few have physical basis. These models do not differentiate between different flow regimes, boiling or adiabatic conditions, and the test section orientation. The most widely used model is the Lockhart-Martinelli-Nelson correlations. The Lockhart-Martinelli model was developed for adiabatic flow of low pressure air-water mixtures in horizontal tubes. The two-phase friction multiplier was correlated as a function of the Martinelli parameter defined as

$$x_{tt}^2 = \frac{(\frac{dP}{dz})_L}{(\frac{dP}{dz})_G}$$

The general form of the two-phase friction multiplier (based on the single-phase component of pressure drop calculated for liquid flowing alone in the channel) is

$$\phi_L^2 = 1 + \frac{C}{x_{tt}} + \frac{1}{x_{tt}^2} \tag{3.46}$$

where the values of parameter C are given for Laminar/turbulent combinations of gas and liquid phases. For the case of turbulent flow in both gas and liquid, C=20 and Martinelli parameter can be approximated by

$$x_{tt}^2 = (\frac{\rho_G}{\rho_L}) (\frac{\mu_L}{\mu_G})^{0.25} (\frac{1-x}{x})^{1.75} \tag{3.47}$$

Although, this correlation was developed for air-water flow, the results were presented in general form to be used for steam-water mixtures.

This model was extended by Martinelli-Nelson (66) to forced convective boiling of water as follows. It was assumed that the flow of gas and liquid will be turbulent. It was further assumed that the air-water results of Lockhart-Martinelli can be used for steam-water at atmospheric conditions. A relation for ϕ_L^2 at critical pressure was developed by assuming equal densities and viscosities for both phases. Two-phase multipliers for intermediate pressures were then interpolated from atmospheric and critical values. For steam-water mixtures at high pressures, two-phase multipliers are generally enveloped between Martinelli-Nelson and HEM predictions and approach HEM as mass flow rates are increased. Unlike the high pressure conditions, HEM could result in higher two-phase multipliers at low pressures. The predictions by Lockhart-Martinelli and HEM for air-water mixtures at atmospheric conditions are given in Figure 3.3. Other correlations include Thom, (55), which is applicable to steam-water, and Baroczy, (56), which is applicable to a wide range of boiling liquids.

For steam-water mixtures at 1000 psi, predictions by the present model for G=358 Lbm/ft2-s (1750 Kgm/m2-s) are compared to predictions by HEM, Thom, and Martinelli-Nelson along with the earth gravity data in Figure 3.4. The effect of mass flux on the zero gravity model in this range is small. In general it was found that, unlike the earth gravity conditions where the two-phase friction multiplier decreases with increasing mass flux, at zero gravity the multiplier may increase or decrease with mass flux depending on the fluid condition. It is believed that decreasing ϕ_0^2 with increasing mass flux at 1 g conditions is due to phase slip which does not exist at zero gravity.
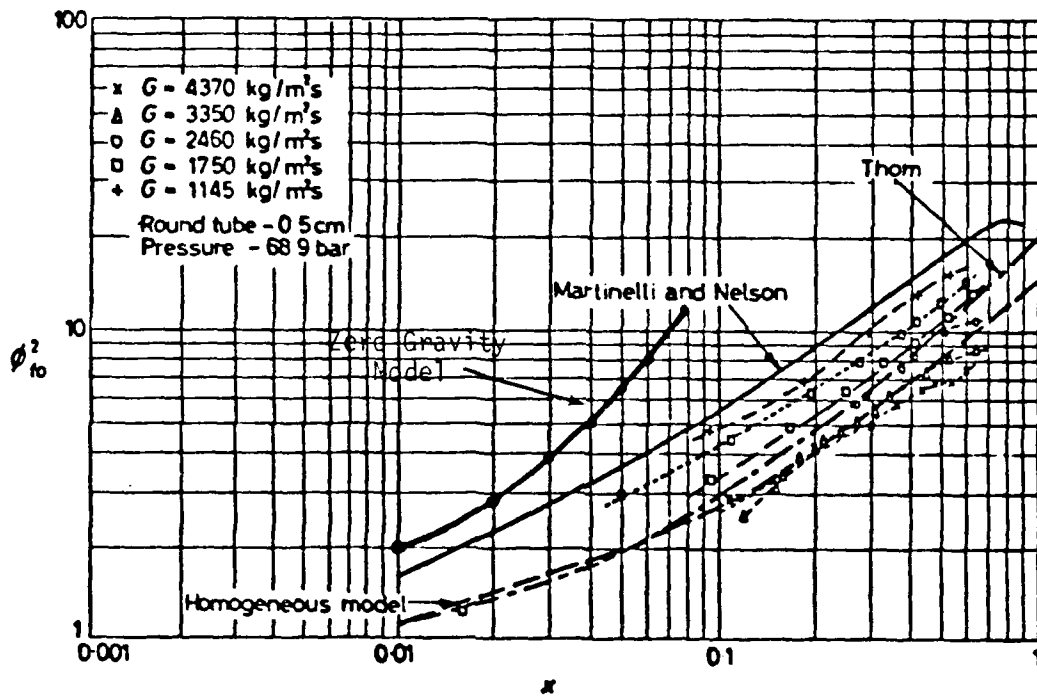
Figure 3.4 - Two-Phase Friction Multiplier for Steam-Water
at 68.9 bar - Reproduced from Ref. 67

When the mass flux increases, the slip between the phases is reduced which causes ϕ_o^2 to decrease and approach the homogeneous value. Under zero gravity conditions, there is no slip between the phases and such a trend is not expected to occur. The two-phase friction multiplier variation with mass flux is dictated by the relative properties of the phases.

The zero gravity tests performed for air/water mixtures in a 0.5 inch tube at atmospheric conditions, Ref. (54), are for mass flow rates of 96 and 186 Lbm/ft2/s. The predictions by the present model, HEM, and Lockhart-Martinelli for these conditions are shown in Figure 3.5. These results can be compared with data when published.

Ammonia requires considerably lower pumping power for equal heat removal in comparison to other refrigerants at 50-80°F which is the range of operating condition for the two-phase thermal management loops. Predictions of the two-phase friction multiplier for ammonia in a 1 inch tube at different pressures and mass flow rates are shown in Figures 3.6 and 3.7. Unlike the air/water flow, increasing mass flow rates results in increasing ϕ_o^2. Increasing system pressure results in decreasing two-phase friction multiplier.

As mentioned earlier, the void fractions predicted by the present model are slightly below the HEM predictions but can generally be approximated by the HEM relation, equation (3.45).

3.4 BUBBLY FLOW WITH NUCLEATION AT THE WALL

In a two-phase thermal transport loop, large amounts of heat are removed from the heating surface due to the latent heat of vaporization of liquid. Normally, single phase liquid enters the heating section and nucleation takes place at the wall. In comparison to a single phase loop, this process will reduce the pumping power and increase the heat transfer coefficients by up to two orders of magnitude.
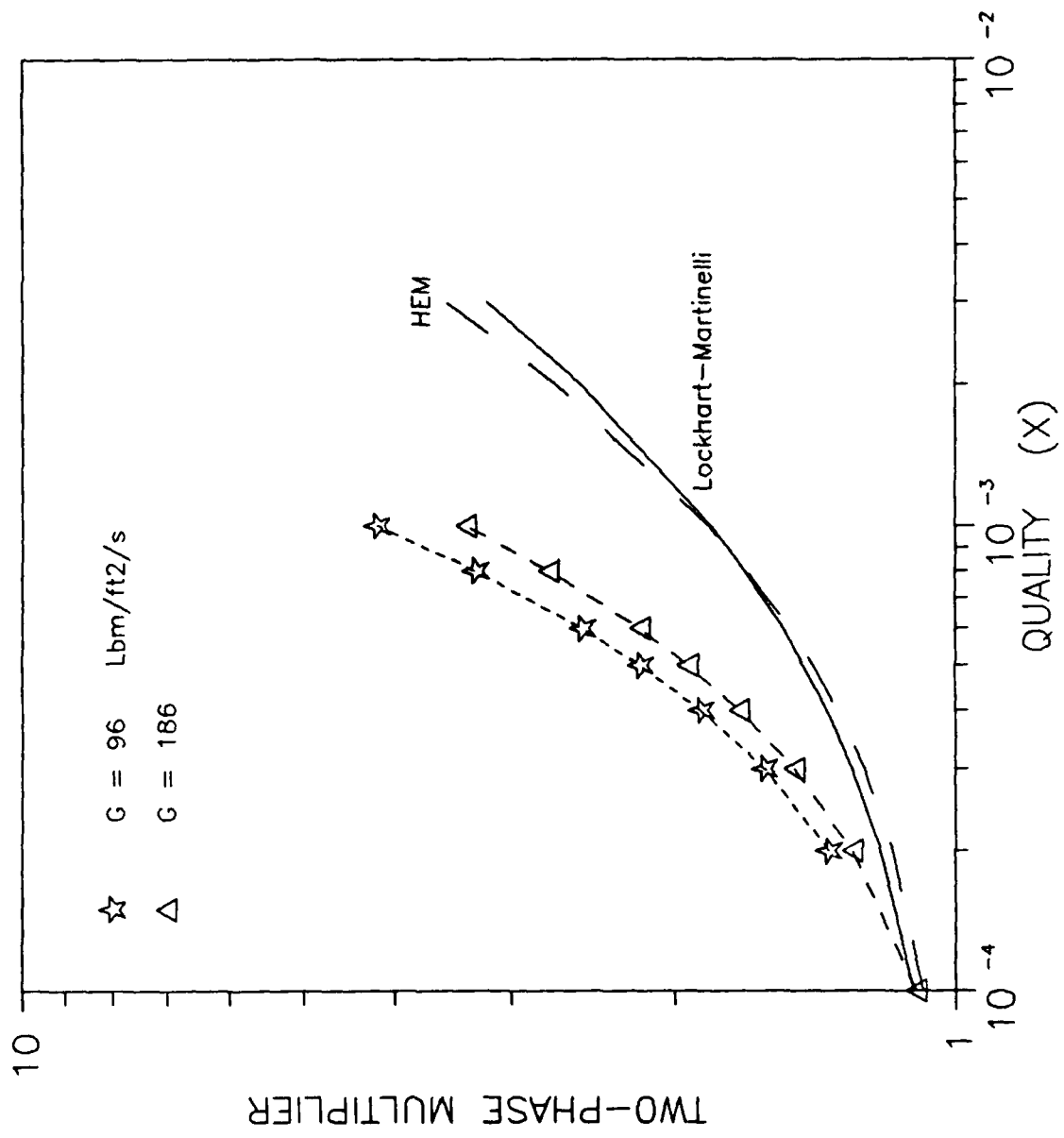
Figure 3.5 – Two-Phase Friction Multiplier vs. Quality
for Air/Water at 14.7 psi in a 0.5 inch Diameter Tube
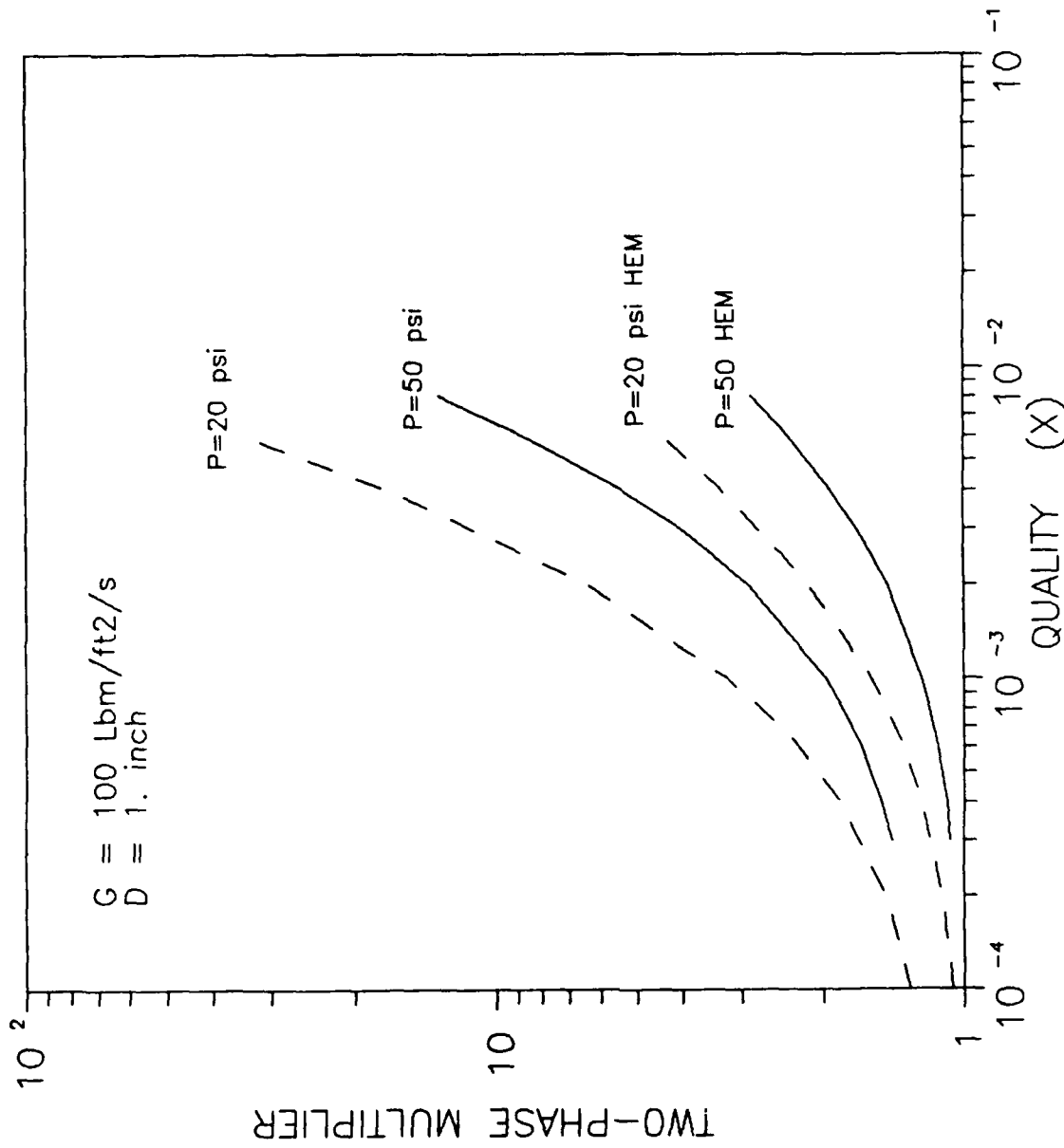
Figure 3.6 — Effect of Pressure on Two-Phase Friction Multiplier for Ammonia.
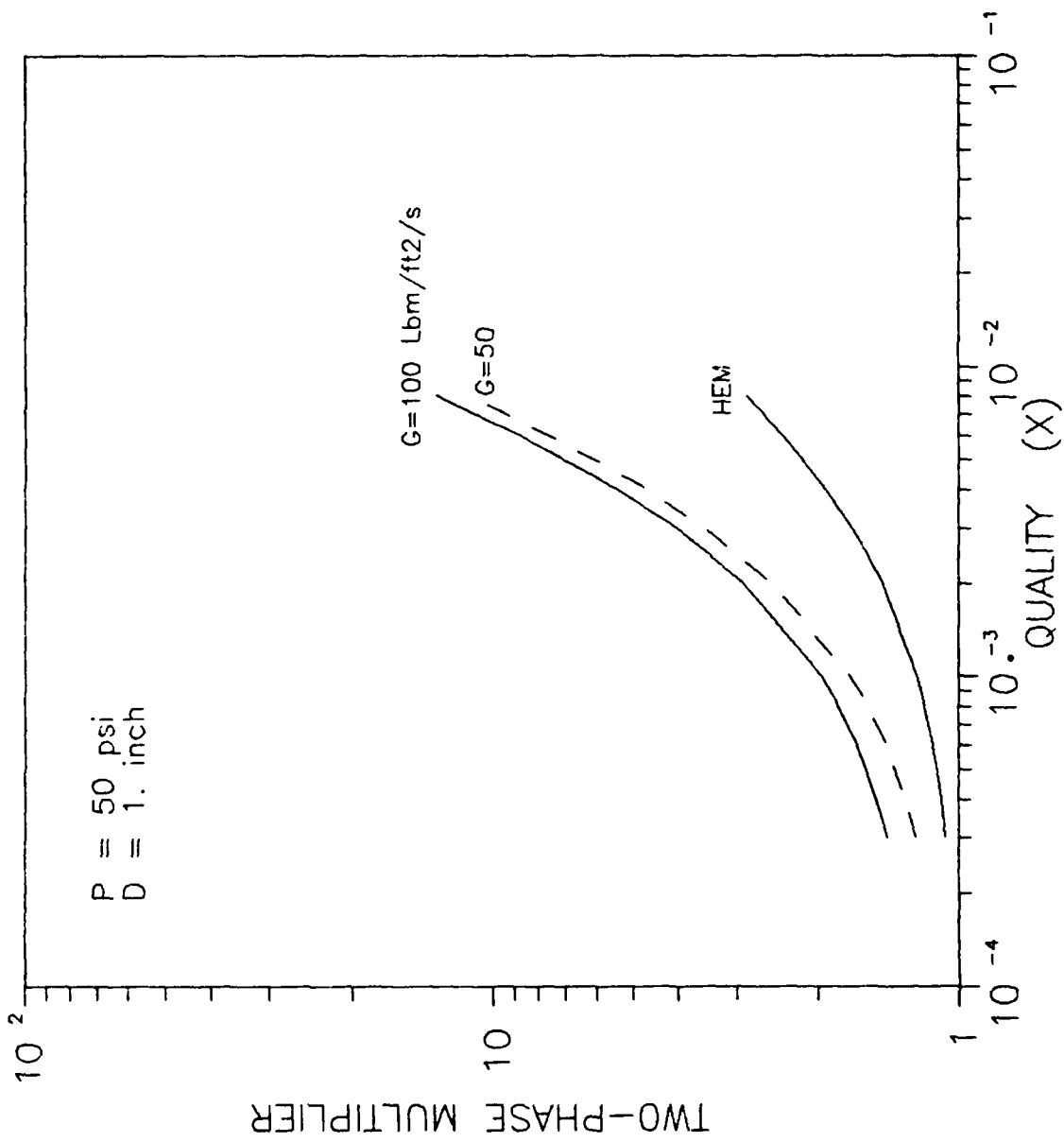
Figure 3.7 – Effect of Mass Flux on Two-phase Friction
Multiplier for Ammonia.

As mentioned earlier, the empirical models developed for two-phase friction multiplier and void-quality relation at earth gravity do not differentiate between adiabatic and diabatic conditions or different flow regimes. In order to see the effect of wall voidage on the pressure drop, the model developed for adiabatic conditions at zero gravity can be used and the effect of wall voidage can be incorporated through the boundary condition. This means that for a given wall heat flux and surface conditions, the void fraction at the wall should be evaluated. It should be noted that the adiabatic model did not include any mass or momentum transfer across the interface. This would obviously be a major assumption for diabatic two-phase flow of a single component fluid.

It is known that the number and size of the bubbles at the wall during the nucleate boiling process depend on a variety of parameters including the wall heat flux, fluid properties, surface condition, and mass flow rate (for convective boiling process). Therefore determination of the void fraction at the wall in terms of the above factors can not be easily accomplished. The approach adopted here is to estimate the void fraction for a specific condition, i.e. critical heat flux, and to correlate the void fraction at the wall in terms of the known parameters.

It is known that the number of active nucleation sites is proportional to the heat flux according to the following relation

$$N = D \, (\dot{q})^n$$

Empirical information on a wide variety of liquids and surfaces has shown that the range of variation of the exponent n is between 2 and 3. This does not imply that the heat transfer is independent of surface finish since the coefficient D is a function of the surface conditions. For a given surface with known cavity distribution it can be concluded that the void at the wall, α_w, is related to heat flux by the above relation

3-34

$$\alpha_W = E \; (\dot{q})^2$$

Therefore, if the critical heat flux and the corresponding void fraction at the wall can be determined, they can be used to find the void for any other heat flux by

$$\alpha_W = (\alpha_W)_{CHF} \; (\frac{\dot{q}}{\dot{q}_{CHF}})^2$$

where $\dot{q}_{CHF}$ and $(\alpha_W)_{CHF}$ are the critical heat flux and wall void fraction respectively.

It is generally agreed that the mechanism leading to critical heat flux (CHF) depends on the quality. At high qualities when the flow is annular CHF is due to dryout of the liquid film and should be modeled by balancing the evaporation and entrainment with droplet deposition. At low qualities, typical of bubbly flow conditions, CHF is a local phenomenon and is caused by build up of a bubbly layer at the wall, Ref. (57). As bubble nucleation increases, the lift and turbulent forces are insufficient to transport the bubbles to the regions of higher velocity. Therefore, the bubble layer will become thicker and at CHF when it has reached the maximum thickness the enthalpy transport with the core is limited. With this mechanism leading to the CHF condition the void fraction at the wall can be readily estimated.

If the average size of the bubbles attached to the wall is known, the local void fraction can be determined from the following relation

$$\alpha_W = \frac{(\text{Number of Bubbles}) \; (\text{Volume of a Bubble})}{\text{Total Volume}}$$

If the bubbles on the wall are separated by a distance of S, the number of bubbles along the tube is given by P_h/S, where P_h is the perimeter of

the tube. The above relation for spherical bubbles with average radius of r_c would therefore become

$$\alpha_W = \frac{(\pi D/S) (4/3 \pi r_c^3)}{\pi D S r_c} = \frac{\pi}{6} (\frac{r_c}{S})^2 \qquad (3.48)$$

The average size, r_c, does not affect the present analysis but if the radius at the bubble departure is r_d, it can be assumed that the average radius of the attached bubbles is $r_d/2$.

It is postulated that CHF occurs for the maximum void fraction at which individual bubbles can be maintained. Therefore, α_W can be estimated from the condition that the bubbles would be just touching one another, i.e. $S = 2 r_c$. The local wall void fraction at CHF from the above equation becomes $(\alpha_W)_{CHF} = 0.52$. According to Ref. ([57]), photographic studies of the bubbly layer have shown that the shape of the bubbles can be approximated by an ellipsoid with ratio of long to short axis of 3:1. With such bubbles just touching the void fraction at CHF becomes $(\alpha_W)_{CHF} = 0.82$ and the local wall void fraction will be

$$\alpha_W = 0.82 (\frac{\dot{q}}{\dot{q}_{CHF}})^2 \qquad (3.49)$$

The problem of establishing the critical heat flux under pool boiling condition at zero gravity has been studied extensively and reported among others in Refs. ([58]) ([59]) ([60]) ([61]). It is generally believed that the critical heat flux decreases with gravity as $g^{1/4}$. This corresponds to the earth gravity theories of critical heat flux and has been confirmed for gravity range of 0.01 to 1.0 g_0, ([58]) ([59]). However drop tower tests of Sherley ([62]) and tests with magnetic fluids, ([60]), have shown that such a dependence on gravity breaks down for $g < 0.1 \, g_0$ and the critical heat flux approaches a value corresponding to 0.5 to 0.7 of the earth gravity

CHF. Based on the existing data, it can be concluded that no satisfactory conclusion regarding the pool boiling CHF at zero gravity can be drawn. There is practically no information available on the critical heat flux under two-phase convective boiling conditions. The study reported in Ref. (63) has shown that the effect of buoyancy on critical heat flux at earth gravity decreases with increasing pressure, inlet velocity, and subcooling. It can be assumed that the effect of gravity on decreasing the critical heat flux would be much smaller than the pool boiling case, since liquid drag will cause the bubbles to depart in convective boiling conditions. Recent modeling efforts for earth gravity forced convective critical heat flux are reviewed in Ref. (64) and results of several experimental studies are shown in Ref. (65).

In the absence of a correlation for the critical heat flux, the effect of wall voidage can be qualitatively shown for different heat fluxes. Using equation (3.49) for q/q_{CHF} of 0.05 and 0.15 the void fraction at the wall would be 0.002 and 0.018, respectively. The model developed for the adiabatic conditions was used for refrigerant 11 with wall void fraction of zero, 0.002, and 0.018. The results are shown in Figure 3.8 and it shows less than 15% increase in the two-phase friction multiplier for q/q_{CHF} of 0.15 and negligible increase for q/q_{CHF} of 0.05. Since the proposed two-phase loops for the spacecraft cooling systems are expected to operate at low power levels (~1 W/cm2), the effect of wall voidage would be small unless the critical heat fluxes for the operating conditions are found to be smaller than 5 W/cm2.
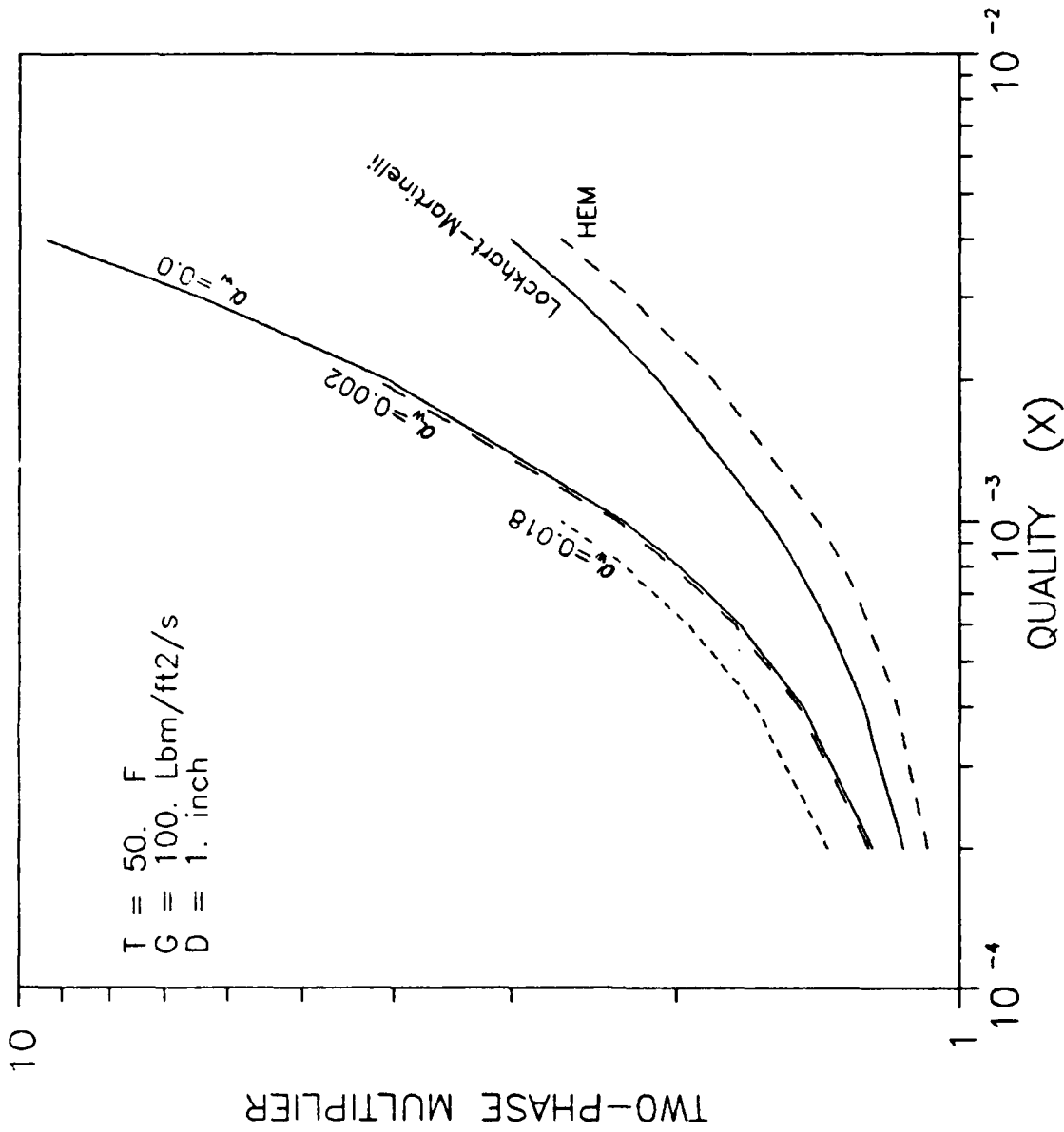
Figure 3.8 — Effect of Wall Voidage on Two-Phase Friction Multiplier for Refrigerant 11.

3-38

Section 4

ANALYSIS OF ANNULAR FLOW

It is generally accepted that under annular flow conditions, a significant fraction of liquid may be entrained as droplets in the gas core. There is continuous interchange of mass and momentum between the liquid film and the gas core. The predictive capability of a phenomenologically based annular flow model rests on the relations used to define the interfacial friction factor and the entrainment fraction.

In this section, a one-dimensional steady state annular flow is presented. The model uses the triangular relationship proposed by Hewitt (31). By using the experimental results discussed in Section 2, empirical relations for the interfacial friction factors and entrainment fraction are obtained. The resulting model provides a method for evaluating the two-phase friction multiplier and void fraction under annular flow conditions in the absence of buoyancy.

4.1 ONE-DIMENSIONAL STEADY-STATE ANNULAR FLOW MODEL

Consider a horizontal steady fully developed annular flow as shown in Figure 4.1. Assuming that the core can be considered as a homogeneous mixture of gas and entrained liquid, the mean core density is given by

$$\rho_C = \frac{w_C}{w_G} \rho_G = \rho_G \left(1 + \frac{1-x}{x} e\right) \qquad (4.1)$$

where e is the entrainment fraction and w_C is the mass flow rate in the gas core

$$w_C = w_G + e \, w_\ell \qquad (4.2)$$
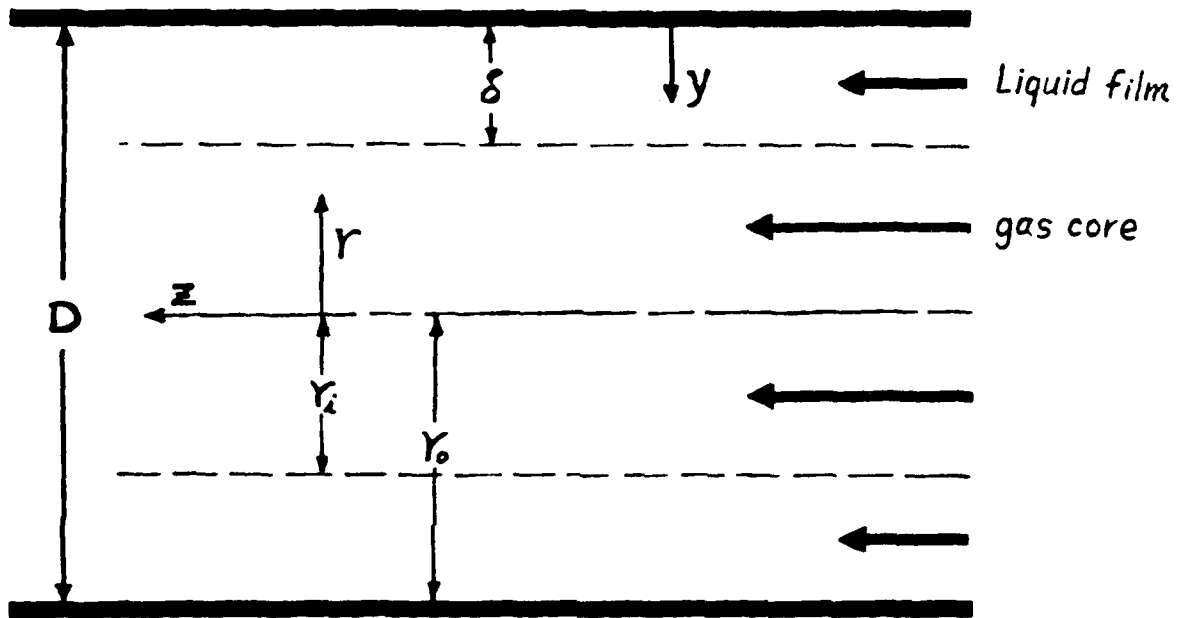
Figure 4.1   Annular Flow Model

It is also assumed that the ratio of the mass flux in the core to mass flux within the liquid film is constant, i.e.

$$K = \frac{\dfrac{\rho_G \, q_G + e \, \rho_L \, q_L}{\alpha_c}}{\dfrac{(1-e) \, \rho_L \, q_L}{(1-\alpha_c)}} \qquad (4.3)$$

where α_c is the ratio of the core cross-sectional area to the total cross sectional area of the tube

$$\alpha_c = (1 - 2\frac{\delta}{D})^2 \qquad (4.4)$$

Equation 4.3 can be solved for the entrainment fraction which results in the following equation

$$e = \left[\frac{1 - \alpha_c}{1 + (K-1)\,\alpha_c} \right] \left[\frac{K\,\alpha_c}{1 - \alpha_c} - \frac{\rho_G \, q_G}{\rho_L \, q_L} \right] \qquad (4.5)$$

The mean core velocity is given by:

$$U_c = \frac{1}{\rho_c \alpha_c} \, G \, (x + (1-x)e) \qquad (4.6)$$

The relation between the actual void fraction α_v (when entrainment is considered) and α_c can be expressed as:

$$\alpha_v = \frac{\alpha_c - e}{1-e} \qquad (4.7)$$

4-3

The definition of the interfacial friction factor can be written as:

$$f_i = \frac{\tau_i}{\frac{1}{2} \rho_c U_c^2} \tag{4.8}$$

A force balance on the gas core in the z direction gives (see Figure 4.1):

$$\tau_i = -\frac{r_i}{2} \left\{ \frac{\partial P}{\partial z} + \left(\frac{r_o}{r_i}\right)^2 \frac{\partial}{\partial z} \left(G^2 \left(\frac{r_o}{r_i}\right)^2 \frac{x^2}{\rho_g}\right) \right\} \tag{4.9}$$

Since fully developed flow is considered, (4.9) is simplified to:

$$\tau_i = -\frac{r_i}{2} \frac{\partial P}{\partial z} \tag{4.10}$$

Note that

$$\frac{r_i}{2} = \frac{D-2\delta}{4} = \frac{D}{4} \left(1 - 2\frac{\delta}{D}\right) = \frac{D}{4} \sqrt{\alpha_c} \tag{4.11}$$

which yields from equation (4.10)

$$\frac{dP}{dz} = -\frac{4}{D\sqrt{\alpha_c}} \tau_i \tag{4.12}$$

The relation for the shear stress distribution in the liquid film given by Hewitt ([31]) is:

$$\tau(r) = \tau_i \left(\frac{r_i}{r}\right) + \frac{1}{2} \frac{dP}{dz} \left(\frac{r_i^2 - r^2}{r}\right) \tag{4.13}$$

4-4

Note that

$$\frac{r_i}{r} = \frac{\frac{D}{2} - \delta}{\frac{D}{2} - y}$$ (4.14)

and

$$\frac{r_i^2 - r^2}{r} = r_i \left(\frac{r_i}{r}\right) - r$$

$$= \left(\frac{D}{2} - \delta\right) \left(\frac{\frac{D}{2} - \delta}{\frac{D}{2} - y}\right) - \left(\frac{D}{2} - y\right)$$

$$= \left(\frac{D}{2} - y\right) \left[\left(\frac{\frac{D}{2} - \delta}{\frac{D}{2} - y}\right)^2 - 1\right]$$ (4.15)

Equation (4.13) can be written as:

$$\tau(y) = \tau_i \left(\frac{1 - 2\frac{\delta}{D}}{1 - 2\frac{y}{D}}\right) + \frac{1}{z}\frac{dP}{dz}\left(\frac{D}{z} - y\right) \left[\left(\frac{1 - 2\frac{\delta}{D}}{1 - 2\frac{y}{D}}\right)^2 - 1\right]$$ (4.16)

The shear stress in the liquid film is assumed to be given by the relation:

$$\tau = (\mu_\ell + \epsilon \, \rho_\ell) \frac{du}{dy}$$

4-5

Thus

$$\frac{du}{dy} = \frac{\tau}{\mu_\ell + \epsilon \, \rho_\ell} \qquad (4.17)$$

where ϵ is an assumed given turbulent eddy diffusivity correlation. With the above relation, the film thickness and thus the two-phase multiplier and void fraction can be determined as follows.

Integrating (4.17) from $y = 0$ to y results in $u(y)$ which can be used to calculate the total liquid film mass flow rate by:

$$\dot{m}_\ell = \int_0^\delta \pi(D-2y) \, \rho_\ell \, u(y) \, dy \qquad (4.18)$$

For each guessed value of δ, the calculated $\dot{m}_\ell$ can be compared with the actual liquid film mass flow rate:

$$\dot{m}_\ell = \frac{\pi}{4} D^2 G \, (1-x)(1-e) \qquad (4.19)$$

When the two values for $\dot{m}$ are equal, the film thickness is obtained.

The Martinelli's parameter X_{tt} is defined in 2.5.3 and is writen as

$$X_{tt} = \left(\frac{\rho_\ell \, f_\ell \, q_\ell}{\rho_G \, f_G \, \rho_G}\right)^{1/2} \qquad (4.20)$$

The two-phase multiplier ϕ_f^2 defined in 2.5.2 is given by

$$\phi_f^2 = \frac{(\frac{dP}{dz})_F}{(\frac{dP}{dz})_f} \qquad (4.21)$$

4.2 NON-DIMENSIONALIZATION OF EQUATIONS

The interfacial friction factor in (4.6) can be expressed as:

$$\tau_i = \frac{1}{2} f_i \rho_c u_c^2$$

or

$$\tau_i^* = \frac{\tau_i}{G^2/\rho_G} = \frac{f_i}{2} \frac{\rho_G}{G^2} \frac{G^2 (x+e(1-x))^2}{\rho_G (1+e \frac{1-x}{x})\alpha_c^2}$$

$$= \frac{f_i}{2} \frac{x(x+e(1-x))}{\alpha_c^2}$$

Using

$$\tau_i^* = \frac{f_i}{2} \frac{x(x+e(1-x))}{(1-2a)^4} \qquad (4.22)$$

where

$$a = \frac{\delta}{D}$$

Similarly, dividing (4.16) by $\frac{G^2}{\rho_G}$ gives

$$\tau^* = \tau_i^* \left(\frac{1-2a}{1-2\frac{y}{D}}\right) + \frac{1}{2} \left(\frac{\frac{dP}{dz}}{G^2/\rho_G}\right) \frac{D}{2} \left(1-2\frac{y}{D}\right) \left[\left(\frac{1-2a}{1-2\frac{y}{D}}\right)^2 - 1\right] \qquad (4.23)$$

Letting

$$\eta \equiv \frac{y}{\delta} \quad \text{and} \quad \left(\frac{dP}{dz}\right)^* \equiv \frac{\left(\frac{dP}{dz}\right)}{\frac{G^2}{\rho_G D}} \qquad (4.24)$$

(4.23) becomes

$$\tau^* = \tau_i^* \left(\frac{1-2a}{1-2\eta a}\right) + \frac{1}{4} \left(\frac{dP}{dz}\right)^* (1-2a\eta) \left[\left(\frac{1-2a}{1-2a\eta}\right)^2 - 1\right] \qquad (4.25)$$

A similar procedure for (4.12) results in

$$\left(\frac{dP}{dz}\right)^* = - \frac{4}{\sqrt{\alpha_c}} \tau_i^* \qquad (4.26)$$

Defining

$$u^* \equiv \frac{u}{\frac{G}{\rho_G}} \qquad (4.27)$$

(4.17) can be written as:

$$\frac{G}{\rho_G \delta} \frac{du^*}{d\eta} = \frac{G^2}{\rho_G \mu_\ell} \left(\frac{\tau^*}{1 + \frac{\epsilon}{\nu_\ell}}\right)$$

4-8

Therefore

$$\frac{du^*}{dn} = Re_\ell \ a \ \frac{\tau^*}{1 + \frac{\epsilon}{\nu_\ell}} \qquad (4.28)$$

where

$$Re_\ell = \frac{GD}{\mu_\ell}$$

From (4.18) we have

$$\frac{d\dot{m}_\ell}{dy} = \pi \ (D-2y) \ \rho_\ell \ u(y)$$

Defining

$$\dot{M} \equiv \frac{4\dot{m}_\ell}{\pi D^2 G} \qquad (4.29)$$

and using (4.27) and (4.29) yields

$$\frac{d\dot{M}}{dn} = 4a(1-2an) \ \gamma u^* \qquad (4.30)$$

where

$$\gamma \equiv \frac{\rho_\ell}{\rho_w}$$

Using (4.19) and (4.29) results in

$$\dot{M} = (1-x) \ (1-e) \qquad (4.31)$$

The two-phase multiplier in (4.21) can be related to the nondimensional quantities as follows.

$$\left(\frac{dP}{dz}\right)_f = \frac{2f_\ell}{D} \frac{G^2 (1-x)^2}{\rho_\ell} \tag{4.32}$$

Using (4.21), equation (4.24) can be written as

$$\phi_f^2 = \frac{\left(\frac{dP}{dz}\right)^* \frac{G^2}{\rho_G D}}{-\frac{2f_\ell}{D} \frac{G^2 (1-x)^2}{\rho_\ell}}$$

$$= -\frac{\gamma \left(\frac{dP}{dz}\right)^*}{2f_\ell (1-x)^2} \tag{4.33}$$

4.3 PROCEDURE FOR CALCULATING THE FILM THICKNESS, TWO-PHASE MULTIPLIER, AND VOID FRACTION

From the above results and the given correlations for the interfacial friction, f_i, and the turbulent eddy diffusivity, ε, of the liquid film, the film thickness can be obtained by iteration as described below.

(1) Given flow conditions G, x and fluid properties.

(2) Choose values for dimensionless liquid film thickness, a.

(3) Use the correlation for the interfacial friction factor, f_i, and (4.22) to calculate τ_i^*.

(6) Use (4.4) and (4.26) to calculate $\left(\frac{dP}{dz}\right)^*$

(5) Use the relation for eddy diffusivity and (4.25) to integrate (4.28) from $n = 0$ to $n = 1$ to obtain u^* for different n values.

4-10

(6) Use the result of step 5 and (4.30) to calculate $\frac{d\dot{M}}{d\eta}$ and integrate from $\eta = 0$ to to $\eta = 1$ to obtain the liquid film mass flow rate, $\dot{M}$.

(7) Compare the result of step 6 with equation (4.31). If the values are equal then the chosen value of a is correct; otherwise, a new value of a is chosen and the same procedure is repeated.

(8) With a correct value of a, the Martinelli parameter, X_{tt}, void fraction, α_v, and the two-phase friction multiplier, ϕ_f^2, can be obtained from equations (4.20), (4.7), and (4.33).

4.4 INTERFACIAL FRICTION, ENTRAINMENT RATE, AND EDDY DIFFUSIVITY CORRELATIONS

As mentioned earlier, the accuracy of the physically based annular flow models rests on the correlations used for the interfacial friction and entrainment rate. Wallis, Ref. (68), suggests the following relation for the interfacial friction factor:

$$f_i = f_s \left(1 + 300 \frac{\delta}{D}\right)$$

where f_s is the single-phase friction factor for the gas flowing alone in the tube with the total core flow rate. Wallis uses a value of 0.005 for f_s. Whalley and Hewitt, Ref. (69), use the following relation for the interfacial friction factor:

$$f_i = f_s \left[1 + 24 \left(\frac{\rho_L}{\rho_G}\right)^{1/3} \frac{\delta}{D} \right] \tag{4.34}$$

Different models for entrainment rate have been proposed but no satisfactory correlation is presently available.

4-11

For calculation of the velocity profile in the liquid film, Ref. (31) uses Deissler's relation, while Levy, (70) uses the mixing length approach. The model described in Section 4.3 was used to predict the two-phase friction multiplier and cross-sectional average void fraction for the conditions tested with L-45/water. Different relations for the interfacial friction, entrainment fraction, and eddy diffusivity were tested, and the following relations were found to result in best agreement.

Interfacial Friction Factor:

An exponential variation with the film thickness was found to result in better agreement than the generally used linear relation

$$f_i = 0.005 \ e^{\frac{\varepsilon}{D}} \tag{4.35}$$

Entrainment Fraction:

Although a constant ratio of mass flux between the core and liquid film is not physically correct, it was found that the constant K in equation (4.3) is a weak function of the film thickness and flow rates. A value of K = 0.95 was used in equation (4.5) to obtain the entrainment fraction.

Eddy Diffusivity:

The following non-dimensional turbulent eddy diffusivity was used in the present model.

$$\frac{\varepsilon}{\nu_\ell} = 0.16 \left(y^+ \left(1 - \frac{y^+}{y_0{}^+}\right)\right)^2 \left(1 - e^{-\left(\frac{0.16y^+ \left(1 - \frac{y^+}{y_0{}^+}\right)}{20}\right)}\right)$$

where

$$y^+ \equiv \left(\frac{y}{D}\right) \left(\frac{GD}{\mu_\ell}\right) \left(\frac{f_\ell}{2}\right)^{1/2}$$

and

$$y_0{}^+ = \frac{\delta G}{\mu_\ell} \left(\frac{f_\ell}{2}\right)^{1/2}$$

where f_ℓ is the single-phase friction factor for the simulating liquid alone and is discussed in 2.5.4.

4.5 COMPARISON WITH EXPERIMENTAL DATA

The calculated two-phase multipliers and the experimental data for L-45/water flow with annular flow mixing section are shown in Figure 4.2. The calculated void fractions and the experimental data for the same flow conditions are shown in Figure 4.3.

As expected, the predictions compare well with the experimental data since the empirical relations were developed from the same data base. However, the model does not result in good agreement with pressure drop data for nitrogen/water tests of Ref. (53). The interfacial friction and entrainment rates are empirically developed from the experiments with two equal density liquids. As will be discussed in Section 5, the method of simulating reduced gravities with two liquids for annular flow conditions is questionable. Although the model provides a general approach for predicting annular flow pressure drop and void fraction under reduced gravities, the empirical relations should be modified for use with gas-liquid flow in the absence of gravity.
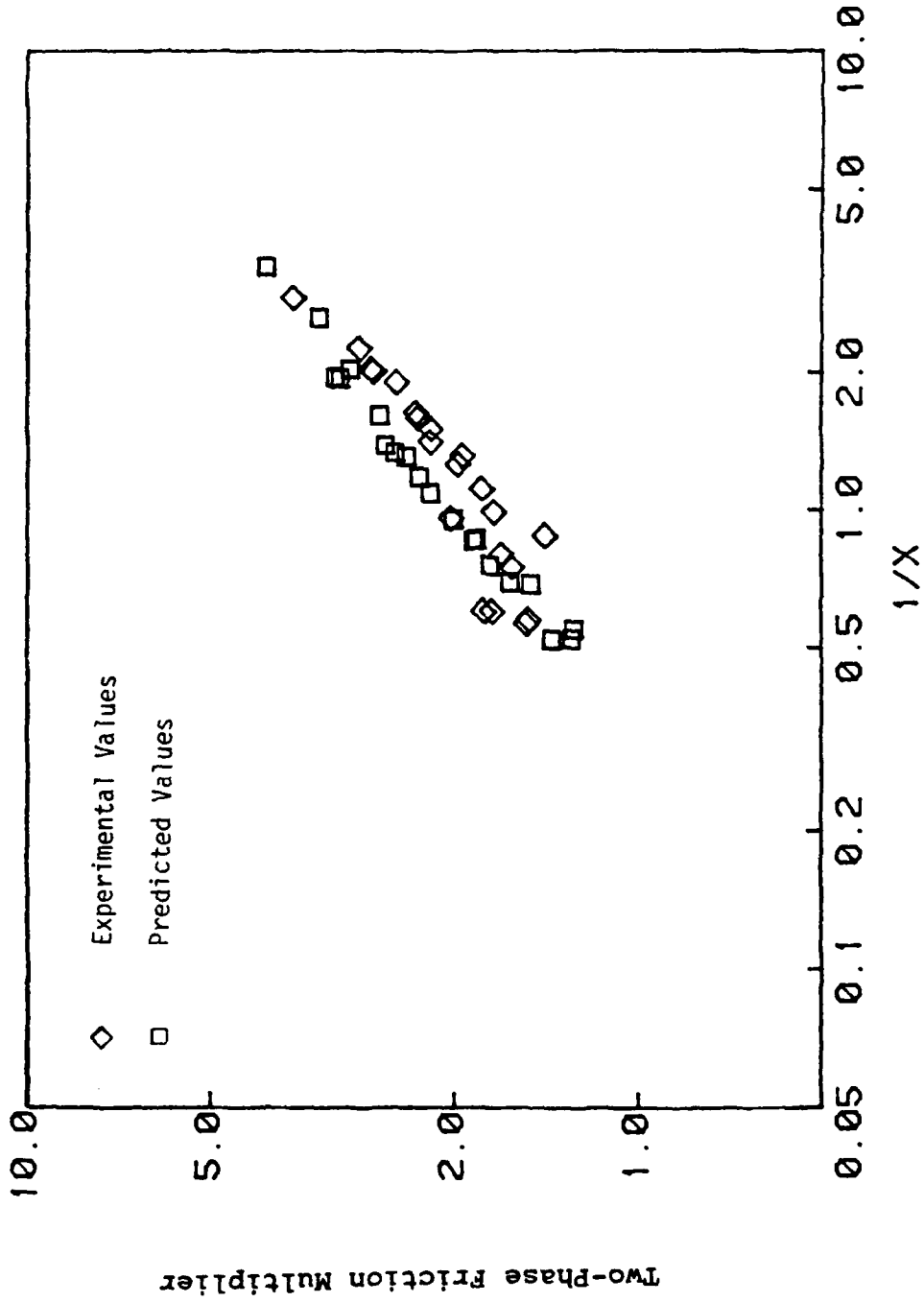
Figure 4.2   Comparison of the Predicted Values for the Two-Phase Friction
Multiplier With Experimental Values.
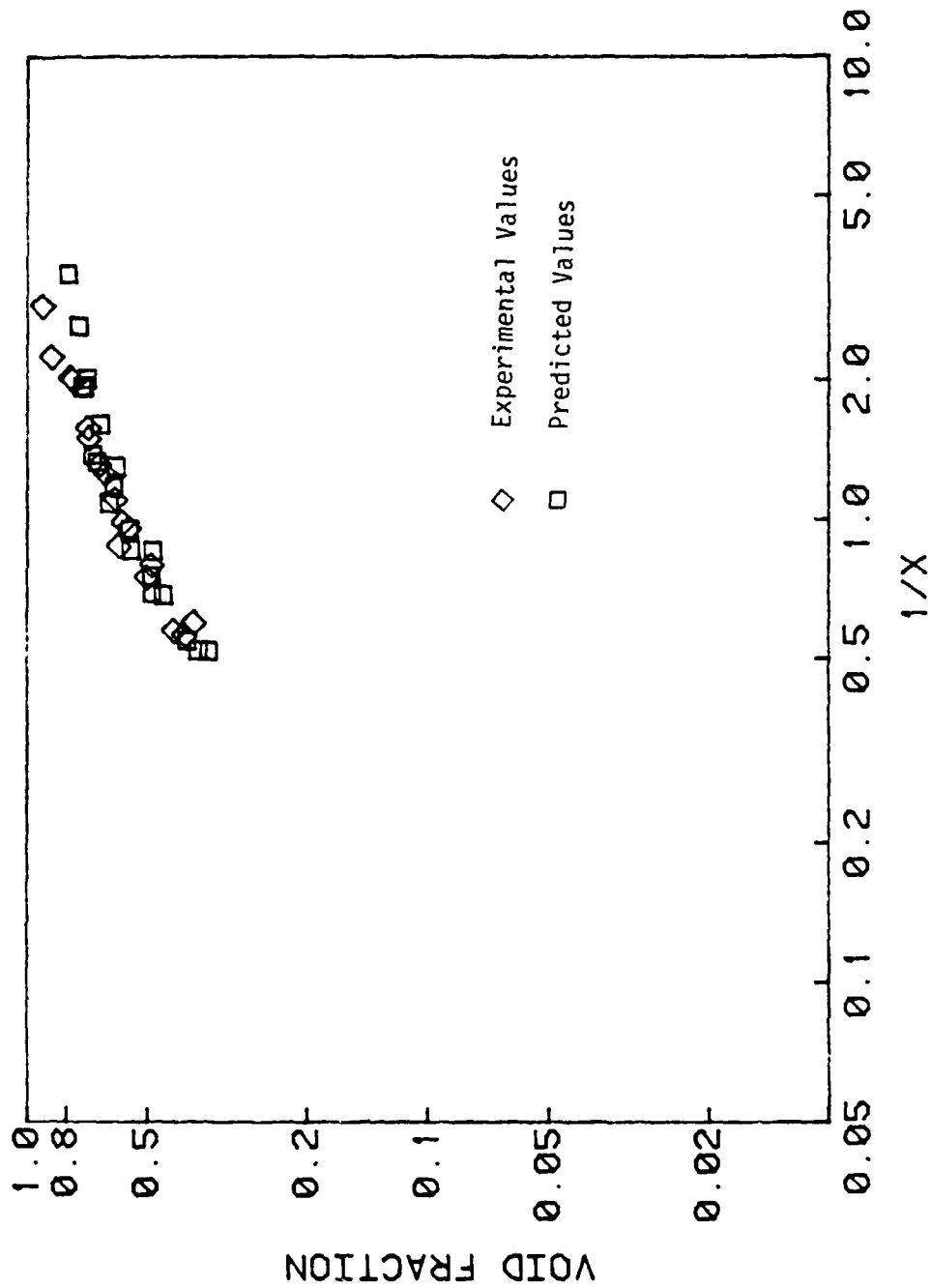
Figure 4.3   Comparison of the Predicted Values for the Void fraction with Experimental Values.

An attempt was made to modify the empirical relations. Density ratio was introduced in the interfacial friction relation to make it applicable to different fluid combinations. The same power of density ratio as used in Ref. (69), equation (4.34), was used. This modification made the predictions more reasonable, but the entrainment rates were considerably higher than expected and the resulting two-phase multipliers were higher than the measured values by a factor of two. This result should have been expected, since the correlation for entrainment rate is based on the data for two liquids which have a smaller interfacial tension than gas/liquid flows. Previous studies have shown that entrainment rate increases with decreasing surface tension. In addition, visual observation of our experiment had shown considerably higher entrainment than expected with gas/liquid systems. One could reduce the entrainment rate by the ratio of interfacial tensions or vary the constant K in equation 4.5 to improve the agreement with reduced gravity data. However, the limited amount of data does not justify such a *modification at this point. The above approach with the density correc-*tion introduced in the interfacial friction relation shows promising trends, but more reduced gravity gas/liquid data is needed to develop a useful correlation for entrainment.

Section 5

CONCLUSIONS AND RECOMMENDATIONS

1. In order to develop a better understanding of two-phase flow beha-
    vior under reduced gravity conditions and generate a data base for
    two-phase pressure drop and void-quality relation, an experimental
    program was developed to simulate these conditions at earth gra-
    vity. These tests provide data for long duration steady state fully
    developed two-phase flow conditions.

2. The simulation of zero gravity by using two equal density liquids
    works well if care is taken in selecting the liquids with proper-
    ties which represent the gas/liquid system. The wetting capability
    of the liquids as well as the relative viscosities and surface ten-
    sions are particularly important.

3. A test matrix was selected to result in turbulent flow conditions
    which have more practical applications than laminar flow. The simu-
    lation of zero gravity two-phase flow under turbulent conditions is
    more appropriate for bubbly flow. This is due to the fact that in a
    two liquid annular flow condition, the liquid representing the gas
    phase travels at a velocity which is not greatly different from the
    velocity of the other phase. However in a gas/liquid annular flow,
    the phases travel at considerably different velocities due to den-
    sity differences. Therefore, the two liquid annular flow simula-
    tion can only provide a qualitative representation of the actual
    condition by eliminating the buoyancy effects.

4. The test results showed that the pressure drop and void-quality
    relation can be closely predicted by the Homogeneous Equilibrium
    Model (HEM). However, it is believed that such a result is due to
    the equal densities of the fluids rather than an inherent condition

5-1

in the absence of buoyancy. The two types of mixing sections produced the same void fraction and pressure drops which means that for fully established flow the method of introducing the phases does not affect the flow patterns.

5. The model developed for adiabatic bubbly flow resulted in two-phase friction multipliers which were considerably larger than earth gravity models. There is no data presently available for bubbly flow at zero gravity. However, the data from airplane trajectory tests for other flow patterns have shown approximately 80% to 120% higher pressure drops than equivalent conditions at earth gravity. The model developed for bubbly flow resulted in pressure drops which were 10% to 120% higher than predicted by HEM. The void fraction predicted by this model is very close to HEM prediction.

6. The model proposed for bubbly flow with nucleation requires the critical heat flux for evaluation of the pressure drop and void fraction. This model results in higher two-phase friction multipliers than predicted under a similar adiabatic condition. However, the increase would only be significant at high heat fluxes which are unlikely as long as bubbly flow exists.

7. The annular flow model was based on a phenomenological approach and results in a good agreement with the data. However, since the empirical relations used for the interfacial friction and the entrainment rate are based on the data from the equal density liquids, they can not be extended to gas/liquid flow in zero gravity. The model provides a general approach for predicting annular flow pressure drop and void fraction. Attempts to generalize the empirical relations for gas/liquid flow at reduced gravities showed promising trends but more tests are needed to develop relations for the interfacial friction and entrainment rates.

8. Study of the convective boiling phenomenon has shown that the mechanism of two-phase heat transfer should not be affected by the

gravity level. For equal mass flow rate and void fraction, the earth gravity results for heat transfer coefficient can be used. However, since the available correlations are generally expressed in terms of mass flux and quality, a void-quality relation from the earth gravity data is implicitly utilized in these models. Therefore, if the heat transfer rates for the given mass flux and void fraction are not available, the correlations developed from the earth gravity data should be modified to account for differences in the void fraction.

Based on the results of the present study and the review of the existing and ongoing efforts in reduced gravity two-phase flow, the following recommendations for future studies are made:

o   The bubbly flow model should be evaluated by comparing the model to data from zero gravity gas/liquid flow. The empirical parameters in this model are based on limited data and should be modified, if needed, when data from true zero gravity tests for different fluids become available.

o   The empirical relations for the interfacial friction and entrainment rate in the annular flow model should be re-examined when more zero gravity data becomes available.

o   There is a great need for experimental data with adiabatic gas/liquid two-phase flow to establish the basic parameters needed for engineering designs. Obviously, fully developed long duration tests will be preferable, but airplane trajectory tests can also be used in the absence of such data. It should be noted that a few isolated points will not be sufficient, and systematic testing for a wide range of mass flow rates and qualities with tests for confirming the repeatability of the measurements is needed. This data is particularly important for establishing the flow regime maps and developing the constitutive relations for annular flow conditions.

5-3

o   The heat transfer correlations developed for earth gravity con-
    ditions should be modified and expressed in terms of void fraction
    rather than flow quality. These correlations can then be used for
    reduced gravity conditions.

o   The boundaries of the boiling regimes, i.e., the Net Vapor
    Generation (NVG) point, Departure from Nucleate Boiling (DNB or
    critical heat flux), and the minimum film boiling temperature are
    dependent on the gravity level. There is no useful data or models
    for prediction of these parameters in reduced gravity conditions.
    Knowledge of the heat transfer boundaries is of great importance
    for design of any system which operates under convective boiling
    conditions.

REFERENCES

1. T. Mahefkey, "Military Spacecraft Thermal Management: The Evolving Requirements and Challenges," AIAA Paper 82-0827, June 1982.

2. A. A. Fowle et al., "A Pumped, Two-Phase Flow Heat Transport System for Orbiting Instrument Payload," AIAA 16th Thermophysics Conference, June 1981, AIAA-81-1075.

3. S. Ollendorf, F. A. Costello, "A Pumped Two-Phase Cooling System for Spacecraft," 13th Intersociety Conference on Environmental Systems, SAE 831099, July 1983.

4. G. Hetsroni, Handbook of Multiphase Systems, Hemisphere Publishing, 1982.

5. R. Siegel and C. M. Usiskin, "A Photographic Study of Boiling in the Absence of Gravity," J. Heat Trans. Vol. 81, No. 3, 1959.

6. C. M. Usiskin and R. Siegel, "An Experimental Study of Boiling in Reduced and Zero Gravity Fields," J. Heat Trans., Vol. 83, No. 3, 1961.

7. R. Siegel and E. G. Keshock, "Effects of Reduced Gravity on Nucleate Boiling Bubble Dynamics in Saturated Water," AIChE. J., Vol. 10, No. 4, 1964.

8. T. H. Cochran et al., "Experimental Investigation of Nucleate Boiling Bubble Dynamics in Normal and Zero Gravities," NASA-LeRC, TND-4301, 1968.

9. E. Oker and H. Merte, "Transient Boiling Heat Transfer in Saturated Liquid Nitrogen and F-113 at Stanford and Zero Gravity - Final Report," NASA-20228, 1973.

10. Y. A. Kirichenko and A. I. Charkin, "Studies of Liquid Boiling in Imitated Reduced Gravity Fields," 4th International Heat Transfer Conference, Versailles, France, Vol. 6, 1970.

11. S. S. Papell and O. C. Faber, "Zero and Reduced Gravity Simulation on a Magnetic-Colloid Pool-Boiling System," NASA TND-3288, 1966.

12. Y. A. Kirichenko and B. I. Verkin, "Simulation of Zero and Reduced Gravity Fields for Heat Transfer Investigations Under Boiling," Dopovidi AN UKSSR, Ser. A(7), 1968.

13. G. Malcotsis, "The Mechanism of Bubble Detachment from a Wall at Zero and Negative Gravity," J. Fluid Mech., Vol. 77, 1976.

14. N. Bakhru and J. H. Lienhard, "Boiling From Small Cylinders," Int. J. Heat Mass Transfer, Vol. 15, 1972.

15. R. Siegel, Effects of Reduced Gravity on Heat Transient Advances in Heat Transfer, Academic Press, Vol. 4, 1967.

16. J. A. Stark et al., "Low G Fluid Behavior Technology Summaries," NASA CR-134746, December 1974.

17. Z. I. Anotoniak, "Two-Phase Alkali - Metal Experiments in Reduced Gravity," Battelle Pacific Northwest Laboratory, PNL-5906, June 1986.

18. T. H. Cochran et al., "Forced Convection Boiling Near Inception in Zero Gravity," NASA TN D-5612, January 1970.

19. J. C. Feldmanis, "Pressure and Temperature Changes in Closed Loop Forced Convection Boiling and Condensing Processes Under Zero Gravity Conditions," Proc. Inst. Environ. Sci., April 1966.

20. A. A. Fowle et al., "A Pumped, Two-Phase Flow Heat Transport System for Orbiting Instrument Payload," AIAA 16th Thermophysics Conference, June 1981, AIAA-81-1075.

21. S. Ollendorf, F. A. Costello, "A Pumped Two-Phase Cooling System for Spacecraft," 13th Intersociety Conference on Environmental Systems, SAE 831099, July 1983.

22. T. W. Lovell, "Liquid Vapor Flow Regime Transitions for Use in Design of Heat Transfer Loops in Spacecraft - An Investigation of Two-Phase Flow in Zero Gravity," Air Force Wright Aeronautical Laboratories Report No. AFWAL-TR-85-3021, 1985.

23. A. E. Dukler, Personal Communication, December 12, 1986. University of Houston.

24. W. J. Krotiuk et al., "Thermal Hydraulic Assessment Report for the Multimegawatt Space Nuclear Power Program," Battelle Pacific Northwest Laboratory, Draft Report PNL 6061, Vols. 1 & 2, October 1986.

25. Jet Propulsion Laboratory, "Conceptual Design Studies in Support of the SP-100 Program," JPL-9960-157, 1984.

26. General Electric, Space System Division, "SP-100 Ground Engineering System (GES) Baseline System Definition and Characterization Study," Final Report, Vol. 1, 85 SD54268, August 1985.

27. W. J. Krotiuk, Personal Communication, December 15, 1986, Battelle Pacific Northwest Laboratory.

28. B. F. North and M. E. Hill, "Conceptual Design of Two-Phase Fluid Mechanics and Heat Transfer for Spacelab," NASA CR-159810, 1980.

29. D. C. Hustvedt and R. L. Oonk, "Preliminary Design of Flight Hardware for Two-Phase Fluid Research," NASA CR-168072, February 1982.

30. J. R. Schuster, "Liquid Vapor Flow Regimes in Microgravity Experiments," Paper Presented at the NASA In-Space Research, Technology, and Engineering Workshop, October 8-10, 1985, Williamsburg, Virginia.

31. G. F. Hewitt, "Analysis of Annular Two Phase Flow: Application of the Dukler Analysis to Vertical Upward Flow in a Tube," Report AERE-R3680, UKAEA, Harwell, 1961.

32. W. M. Kays and A. L. London, Compact Heat Exchangers, 2nd Edition, McGraw-Hill, 1964.

33. R. C. Lockhart and R. C. Martinelli, "Proposed Correlation of Data for Isothermal Two-Phase Two-Component Flow in Pipes," Chem. Eng. Prog., 45, 39, 1949.

34. S. K. Wang, "Three-Dimensional Turbulence Structure Measurements in Air/Water Two-Phase Flow," PhD. Thesis, Rensselear Polytechnic Institute, Troy, New York, August 1985.

35. A. Serizawa, I. Kataoka and I. Michiyoshi, "Turbulence Structure of Air-Water Bubbly Flow," Int. J. Multiphase Flow, 2, pp 221-233, 1975.

36. G. Magnus, Poggendorffs Ann. Phys. Chem., 88, 1, 1853.

37. S. I. Rubinow and J. B. Keller, "The Transverse Force on a Spinning Sphere Moving in a Viscous Fluid," J. Fluid Mech., 11, p 447, 1961.

38. P. G. Saffman, "The Lift on a Small Sphere in a Slow Shear Flow," J. Fluid Mech., 22, p 385, 1968.

39. P. G. Saffman, Corrigendum for Reference 38, J. Fluid Mech., 31, 624, 1968.

40. A. E. Dukler et al., "Pressure Drop and Hold-up in Two-phase Flow," Part A - "A Comparison of Existing Correlations," and Part B - "An Approach Through Similarity Analysis." Paper presented at A.I.Ch.E meeting held Chicago, Dec. 2-6. 1962, also A.I.Ch.E.J.10(1) 38-51, 1964.

41. S. Levy, "Prediction of Two-Phase Pressure Drop and Density Distribution From Mixing Length Theory," J. Heat Transfer, 137, p 163, 1963.

42. S. G. Bankoff, "A Variable Density Single-Fluid Model for Two-phase Flow with Particular Reference to Steam-water Flow," Trans. ASME, Ser. C 82, 265-272.

43. Sullivan, Houze, Buenger and Theofanous, "Turbulence in Two-phase Flows," U.E.C.D., C.S.W.I., Paris, June 12-14, 1978.

44. M. Lance et al., "Turbulent Structure of a Co-currrent Air-Water Bubbly Flow," Proc. of the ANS/ASME/NAC Int. Topical Meeting on Nuclear Reactor Thermal-Hydraulics, Saratoga, NY, Oct. 5-8, 1980.

45. A. Serizawa, K. Tsuda and I. Michiyoshi, "Real Time Measurement of Two-Phase Flow Turbulence Using a Dual-Sensor Anemometry," IUTAM Symposium on Measuring Techniques in Gas-Liquid Two-Phase Flows, Nancy, France, July 5-8, 1983.

46. Y. Sato and K. Sekoguchi, "Liquid Velocity Distribution in Two-Phase Bubble Flow," Int. J. Multiphase Flow, Vol. 2, 1975.

47. D. B. Spalding, J. Appl. Mech., Vol. 28, pp 455-457, 1961.

48. H. Reichardt, ZAMM, Vol. 31, p 208, 1951.

49. J. Laufer, "The Structure of Turbulence in Fully Developed Pipe Flow," NACA Rep. 1273, 1954.

50. D. Malnes, "Slip Ratios and Friction Factors in the Bubble Flow Region in Vertical Tubes," KR-100, Institutt for Atomenergi, Kjelles, Norway, 1966.

51. "SIGSTAT", Significant Statistics, Provo, Utah.

52. D. B. Heppner, et al., "Zero-G Experiments in Two-Phase Fluid Flow Regimes," ASME Paper 75-ENAS-24, 1975.

53. J. Cuta, Personal Communication, September 18, 1987, Battelle Pacific Northwest Laboratory.

54. A. E. Dukler et al., "Gas Liquid Flow at Microgravity Conditions: Flow Patterns and Their Transitions," ASME Winter Annual Meeting, Dec. 13-18, 1987, Boston.

55. J. R. S. Thom, "Prediction of Pressure Drop During Forced Circulation Boiling Water," Int. J. Heat Mass Transfer, 7, 709-724, 1964.

56. C. J. Baroczy, "A Systematic Correlation for Two-Phase Pressure Drop," A.I.Ch.E. reprint No 37, paper presented at 8th Nat. Heat Transfer Conf. Los Angeles, August 1965.

57. J. Weisman and B. S. Pei, "Prediction of Critical Heat Flux in Flow Boiling at Low Qualities, Int. J. Heat Mass Transfer, Vol. 26, pp 1463-1477, 1983.

58. R. Siegel and J. R. Howell, "Critical Heat Flux for Saturated Pool Boiling from Horizontal and Vertical Wires in Reduced Gravity," NASA-LeRC TND-3123, Dec. 1965.

59. C. M. Usiskin and R. Siegel, "An Experimental Study of Boiling in Reduced and Zero Gravity Fields," J. Heat Transfer, 83, 243, 1961.

60. D. N. Lyon et al., "Peak Nucleate Boiling Fluxes for Liquid Oxygen on a Flat Horizontal Platinum Surface at Buoyancies Corresponding to Accelerations Between -0.03 and $1g_e$," A.I.Ch.E.J. 11, 773, 1965.

61. N. Bakhru and J. H. Lienhard, "Boiling from Small Cylinders," Int. J. Heat Mass Transfer, Vol. 15, 1972.

62. J. E. Sherley, "Nucleate Boiling Heat Transfer Data for Liquid Hydrogen at Standard and Zero Gravity," in Advances in Cryogenic Engineering, (K. D. Timmerhaus, ed.) Vol. 8, p 495, Plenum, New York, 1963.

63. S. S. Papell et al., "Buoyancy Effects on Critical Heat Flux of Forced Convective Boiling in Vertical Flow," NASA TN D-3672, October 1966.

64. D. C. Groenveld et al., "Prediction of Critical Heat Flux (CHF) for Non-Aqueous Fluids in Forced Convective Boiling," Int. Heat Transfer Conference, San Francisco, Sept. 1986.

65. W. M. Shah, "A Generalized Graphical Method for Predicting CHF in Uniformly Heated Vertical Tubes," Int. J. Heat Mass Transfer, Vol. 23, pp 557-568, 1979.

66. R. C. Martinelli and D. B. Nelson, "Prediction of Pressure Drop During Forced Circulation Boiling of Water," Trans. ASME, 7, 695, 1948.

67. J. G. Collier, <u>Convective Boiling and Condensation</u>, McGraw-Hill, 1972.

68. G. B. Wallis, "Annular Two-Phase Flow, Part 2 - Additional Effects," <u>J. Basic Eng.</u>, Vol. 92, 1970.

69. P. B. Whalley and G. F. Hewitt, "The Correlation of Liquid Entrainment Fraction and Entrainment Rate in Annular Two-Phase Flow," Harwell Report, AERE-R9187, July 1978.

70. S. Levy and J. M. Healzer, "Prediction of Annular Liquid-Gas Flow with Entrainment - Cocurrent Vertical Pipe Flow with No Gravity," EPRI Report NP-1409, May 1980.

APPENDIX

WORKING PRINCIPLES OF THE AUBURN MODEL 1090 CAPACITANCE PROBE

A.1 SYSTEM DESCRIPTION

The Auburn Model 1090 capacitance probe is designed to measure the void
fraction for two-phase flow of fluids with considerably different
dielectric constants.   The probe system consists of two major com-
ponents: the sensor spool-piece and the electronics unit.

The sensor spool-piece has an array of six electrodes spaced equally
around its inner circumference and is installed as a part of the test
section. A flow liner, or protective coating, separates the electrodes
from the flow and provides an unobstructed flow path through the sensing
volume.

The electronics unit provides excitation to the sensor electrodes and
the average dielectric constant, or capacitance which is related to the
void fraction.

A.2 FUNCTIONAL DESCRIPTION

The Auburn 1090 operates by continuously measuring the relative
dielectric constant of the flow through the sensor.   The dielectric
constant of the two-phase mixture is a function of the dielectric
constants of the two components and the volumetric ratio (void
fraction), and can be written as

$$\varepsilon_A = \varepsilon_\ell (1 - \alpha_V) + \varepsilon_G \alpha_V$$

where

   ε_A = the average electric constant

A-1

ϵ_ℓ = the dielectric constant of the simulating liquid phase

ϵ_G = the dielectric constant of water (the simulating gas phase)

α_V = void fraction as defined in (4.7)

In order to have an accurate, uniform measurement, an electrically rotating sensor field is provided by sequentially switching the excitation from electrode to electrode. The opposing three electrodes, the receive electrodes, are switched concurrently (see Figure A.1). The switching rates provide electric field rotation at greater than 200 Hz, thus insuring accurate response in less than 5 milliseconds.

The excitation voltage applied on the sensor electrodes is provided by a high frequency oscillator. The measured current from receiving electrodes is amplified and processed by the electronics unit. The basic operational block diagram is shown in Figure A.2.
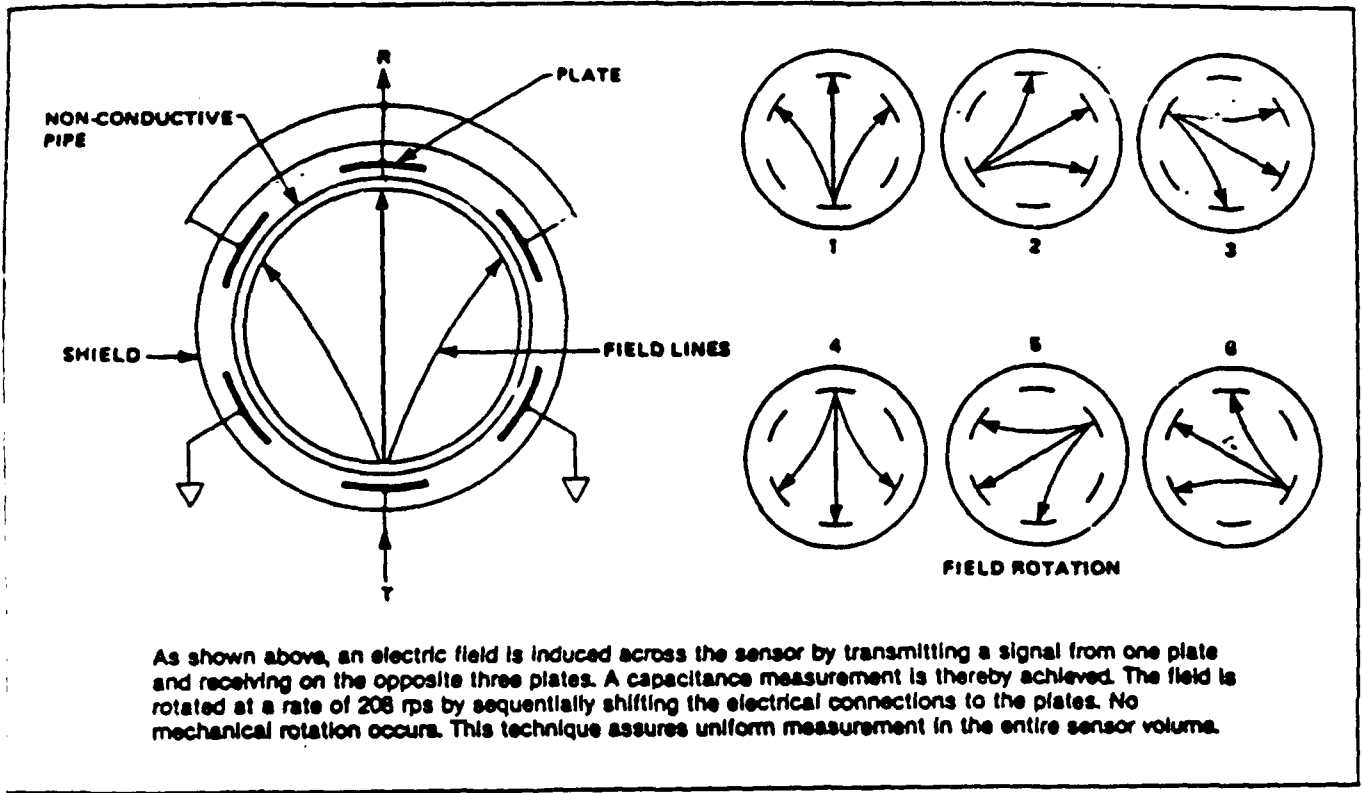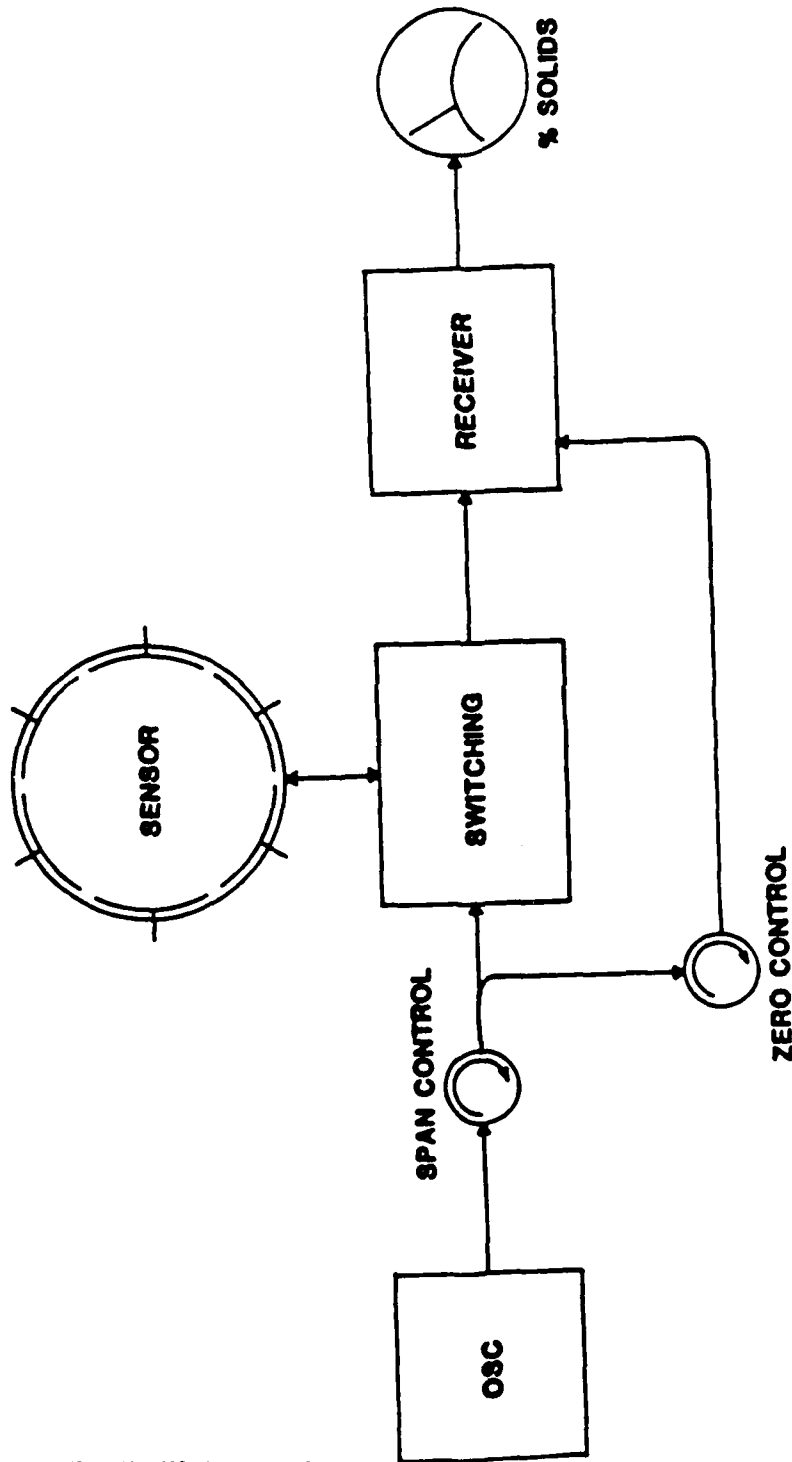
As shown above, an electric field is induced across the sensor by transmitting a signal from one plate and receiving on the opposite three plates. A capacitance measurement is thereby achieved. The field is rotated at a rate of 208 rps by sequentially shifting the electrical connections to the plates. No mechanical rotation occurs. This technique assures uniform measurement in the entire sensor volume.

Figure A.1   1090   Field Rotation

Figure A.2   1090 Block Diagram

END
DATE
FILMED

8-88

DTIC